Structural Engineering Report No. 145

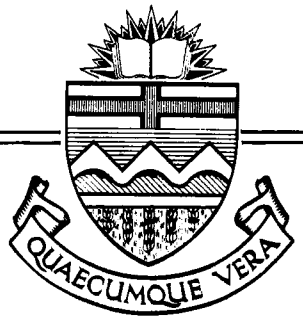


# CYCLIC AND STATIC BEHAVIOUR OF THIN PANEL STEEL PLATE SHEAR WALLS

by
E. W. TROMPOSCH
and
G. L. KULAK

April, 1987

# CYCLIC AND STATIC BEHAVIOUR OF THIN PANEL STEEL PLATE SHEAR WALLS

by

E.W. Tromposch

and

G.L. Kulak

Department of Civil Engineering

University of Alberta

Edmonton, Alberta

April, 1987

## ABSTRACT

The construction and testing of a single full scale steel plate shear wall test specimen is described herein. The 2.2 m by 5.5 m specimen consisted of two 3.25 mm thick steel panels in a configuration resembling a deep beam. The specimen, tested in a horizontal position, was subjected to both monotonic and cyclic loads applied at a single point at mid-specimen.

Measurements taken during the testing consisted of vertical deflections at the ends and at the centre of the specimen as well as strain measurements of the panels and of the boundary members. The buckle profile of one of the panels was also recorded on several occasions during the testing.

The specimen's load versus mid-point deflection hysteresis curve displayed a pinched, or S-shaped, behaviour. The specimen showed good ductility during monotonic loading with no significant deterioration prior to termination of the test. A comparison of the actual monotonic load versus deflection response with the response predicted using the inclined tension bar model showed very good correlation. Using the response predicted by the inclined tension bar model, a simple expression was developed that predicts the hysteresis behaviour of the steel plate shear wall test specimen. This expression can also be used to predict the hysteresis behaviour of other shear wall configurations which use thin panels.

## Acknowledgements

This report is based on the thesis submitted by Eric Werner Tromposch to the Faculty of Graduate Studies and Research at the University of Alberta in partial fulfillment of the requirements for the degree of Master of Science in Civil Engineering. During the period of his studies, he received financial support from the Alberta Regional Committee of the Canadian Institute of Steel Construction and from the Province of Alberta.

The project was sponsored by the American Iron and Steel Institute and was directed by an advisory committee consisting of J.W. Hotchkies, E.Y.L. Chien, R.M. Richard, and A.C. Kuentz.

The authors are grateful for the financial assistance received and acknowledge with thanks the helpful comments and direction provided by the advisory committee.

## Table of Contents

## List of Tables

## List of Figures

# 1. INTRODUCTION

## 1.1 General

The concept of using steel plate shear walls as the main lateral load resisting elements in a structure has been gaining acceptance around the world in recent years. Many structures in several countries have been constructed using this system. Several of these structures are located in seismically active regions with the potential for severe earthquakes. As far as is known, all of the existing structures have been built using either heavily stiffened or very thick steel panels, so that panel buckling would be prevented. The post-buckling strength of the shear wall panels was ignored.

The post-buckling strength of steel panels can be substantial, however, as initially reported by Wagner (1). The development of an inclined tension field in a steel plate shear wall provides considerable post-buckling strength, as has been shown by previous research on unstiffened steel plate shear walls at the University of Alberta (2,3). This research led to a simplified method for the analysis of the response of these panels by considering the tension field as the equivalent of a series of inclined tension bars. A conventional plane frame computer program can then be used to analyze the structure. The previous testing has shown that the thin unstiffened steel panels can be subjected to cyclic loads with deflections up to the

serviceability limit (h/400) without signs of degradation or deterioration (3).

The response of thin, unstiffened steel plate shear wall panels to cyclic loading beyond the proportional limit of the structure has not been examined to the same extent. Research in Japan has indicated that pinching of the hysteresis loops will occur when unstiffened panels are loaded cyclically (4,5). The effects of the frame stiffness were not included in any of these tests, however.

To examine properly the behaviour of the entire structural system, the influence of the framing members must be considered. The influence that axial loads in column members have on the in-plane load versus displacement behaviour of the system and the out-of-plane buckling behaviour of the panels should also be investigated. For these reasons, a further examination of the hysteresis behaviour of an unstiffened steel plate shear wall taking into account the above mentioned factors was considered necessary and is the basis for the experimental program conducted.

## 1.2 Objectives

The objectives of the testing program were as follows:

1. The examination of the hysteresis behaviour of a steel plate shear wall test specimen, consisting of thin unstiffened panels and typical structural members along the boundaries, subjected to a quasi-static, fully

reversed, cyclic load.

2. The examination of the validity of proposed theoretical hysteresis curves when applied to thin unstiffened shear wall panels.
3. The verification of the inclined tension bar model as a valid analytical method for determining the strength and stiffness of unstiffened steel plate shear wall panels.
4. The examination of the affects of conventional structural bolted connections and details on the behaviour of thin unstiffened steel plate shear wall panels.
5. The examination of the effects of applied column axial loads upon both the prebuckling of the shear wall panels and on the in-plane load versus displacement behaviour.

### 1.3 Outline of the Testing Program

A single full-scale unstiffened steel plate shear wall test specimen was constructed and tested. The symmetric specimen consisted of two adjacent panels with opposing tension fields in a configuration resembling a deep beam. The specimen was tested in a horizontal position, with a quasi-static, fully reversed, cyclical load applied vertically to the structure at the midpoint of the top column. An axial preload was also applied to the columns so that the loading would be more representative of the loads in a typical shear wall structure. Vertical deflections were measured at the mid-point and at the supports and were used

in the generation of hysteresis curves for the structure. Strain gauges mounted on the panels and on the boundary members were used to monitor the strains in these members. These strains were later used to calculate axial forces and moments. Comparison with theoretical values predicted by the analytical model was then possible.

# 2. REVIEW OF PREVIOUS RESEARCH

## 2.1 General Requirements for Structures in Seismic Regions

The response of a structure to a seismic event is dependent on many factors. The earthquake itself, the soil conditions present, the material properties of the members used, and the type of connections used all have an effect on the structural response. The hysteresis curve, developed experimentally by applying a quasi-static cyclic load in alternate directions, provides the member or frame material behaviour information needed when conducting a dynamic analysis. The area enclosed by the hysteresis loop is equal to the energy absorbed by the system. Systems that absorb a large amount of energy and exhibit sound and stable hysteresis loops have generally performed well in earthquakes.

Structural systems that perform well in seismic events generally also exhibit good ductility. A measure of the ductility of a system is defined as the ductility factor. This factor can be defined as either the maximum strain, rotation or displacement divided by the yield strain, rotation or displacement (6). The amount of ductility required for a given structure is difficult to determine because of the many factors involved. For structures subjected to strong seismic activity, Popov (6) has suggested that a displacement ductility factor in the order of six may be necessary. Good ductility, however, cannot

compensate for poor energy absorption; it merely changes the failure mode.

## 2.2 Cyclic Loading Behaviour of Common Structural Systems

When examining the cyclic loading response of a steel plate shear wall, a comparison with other commonly used systems will be useful. These too must all be compared with what is considered desirable behaviour. For frames, three types of structural systems are commonly considered when dealing with lateral load resistance. These are a moment resisting frame, a simply supported frame (continuous columns but simple beam-to-column connections) containing a core in which steel bracing (usually K- or X-bracing) is present, or a simply supported steel frame containing a vertical shear wall.

Moment resisting frames generally exhibit good hysteresis behaviour. Figure 2.1 is the hysteresis curve developed by a structural assemblage comprised of two half columns and two beams (6). The load versus displacement loops are sound and fully developed, showing excellent ductility. A displacement ductility factor in excess of ten is achieved. Because the columns are generally carrying large axial loads, the effect of the axial load acting through the displaced distance (P-$\delta$) causes the stiffness to decrease at large deflections. It is generally the contribution of the P-$\delta$ effects that causes the failure of moment resisting frames subjected to cyclic loading.

The second type of lateral load resisting system commonly used is diagonal bracing. It comes in many forms, but the two most typical configurations are K and X-bracing. Both of these systems exhibit a degenerating pinched loop behaviour when subjected to cyclic loads. Figure 2.2 is the hysteresis curve for the particular X-braced frame illustrated in the upper left corner of the figure (6). The pinched loops are the result of buckling of the yielded members before they can be recompressed. A recent innovation that improves the hysteresis performance of braced frames is to attach the diagonal brace to the beam a short distance away from the beam-to-column connection. The eccentrically braced frame, shown schematically in Figure 2.3, is designed so that the short link beam yields prior to the yielding or the buckling of the diagonal members (6). The hysteresis curves produced by cyclically loading this structure are fully developed and stable, as would be expected since only the short link beams are yielding.

shear walls are the final type of commonly used lateral load resisting system. Until recently, shear walls were exclusively made of reinforced concrete. The hysteresis performance of reinforced concrete shear walls varies greatly, depending on the configuration and the details used. Figure 2.4 illustrates the shear force versus shear distortion hysteresis loops for a simple reinforced concrete shear wall (7). The pinched loops in this case are caused by the yielding of the reinforcement. As load is applied in one

direction a permanent deformation remains in the reinforcement after unloading. When the load is then applied in the other direction, only the reinforcement is effective in resisting the applied moment prior to crack closure. This in turn results in a reduced stiffness prior to crack closure and causes the pinched loops. In this case, the shear distortion of 0.01 radians corresponds to a lateral deflection of about 20 mm. The rotational ductility factor in this case is in excess of 10. For shear walls, the rotational ductility factor is nearly equivalent to the displacement ductility factor. The hysteresis performance of concrete shear walls can be improved by linking slender shear walls with heavily reinforced coupling beams which act as the main energy absorbing units in the structure (8).

The concept of using a steel plate bounded by the beams and the columns of a structure to produce a steel plate shear wall has only recently gained acceptance. Research in this area is still continuing in an effort to fully understand the characteristics of this new structural system.

## 2.3 Previous Research on Steel Plate Shear Walls

The original concepts used in the design of steel plate shear walls date back to the work on tension fields done by Wagner (1) in the 1930's and then by Kuhn, et al. (9) in the 1950's. It was not until the late 1960's that steel plate shear walls were used in buildings. The Japanese appear to

have been the first to extensively design, test, and construct buildings using steel plate shear walls. The shear walls they designed were heavily stiffened to prevent buckling of the panels. The unstiffened steel plate shear wall was not considered a viable alternative for Japan. Recent research at the University of Alberta has demonstrated the considerable post-buckling strength of unstiffened steel plate shear wall panels (2,3).

### 2.3.1 Stiffened Steel Plate Shear Wall Research in Japan

In Japan, the stiffened steel plate shear wall has been used exclusively because of its superior hysteresis performance when compared to unstiffened panels. The extremely high seismic risk in Japan makes this a key factor in design. The first steel plate shear wall structures were designed on the basis that stresses in the panels be limited to the elastic range and that buckling of the panels not occur. The shear walls were assumed to carry only lateral loads and no vertical loads. The lateral resistance was assumed to derive totally from the shear resistance of the panels. The structures were analyzed, using a form of the Wagner model, with the stiffness characteristics then equated to an equivalent pair of diagonal braces (10). The expression developed for the area of the equivalent braces (both members) is given in equation 2.1.

$$A_b = \frac{w \; G \; H \; L_d}{\sin\theta \; E \; L} \qquad (2.1)$$

where:

$A_b$ = area of equivalent diagonal braces

$\theta$ = angle of inclination of the diagonal brace measured from the horizontal

H = panel height

w = plate thickness

$L_d$ = diagonal length

L = panel length

G = shear modulus of the panel

E = Young's modulus of the panel.

Because of the difficulty in obtaining information on Japanese research, it is unclear whether or not this analytical approximation was ever verified by physical testing.

Extensive research by Takahashi, et al. (4) on the hysteresis properties of stiffened steel plate panels demonstrated the large ductility available and the superior hysteresis properties of stiffened shear wall panels as compared to unstiffened panels. Figure 2.5 shows the hysteresis shear stress versus shear strain curve for an unreinforced shear wall panel 2100 mm by 900 mm by 2.3 mm thick, mounted on very stiff boundary members, and with idealized pinned connections. This arrangement produces hysteresis loop information which reflects the lateral

strength of the panel only if it is assumed that the very stiff boundary members did not yield. Figure 2.6 shows the hysteresis curve for a heavily reinforced panel of the same geometrical configuration as that illustrated in Figure 2.5. Note that the heavily stiffened panel displays a superior hysteresis curve, enclosing considerably more area and therefore absorbing more energy. The ductility of these specimens was very large. The maximum shear deformation was in the order of 0.1 radians for some of the specimens tested.

The principal recommendations of these researchers were that steel plate shear wall panels be designed so that elastic buckling does not occur and that when inelastic buckling occurs it does not extend across the entire panel. If these design recommendations are followed, the resulting shear wall panel would display sound, stable hysteresis loops.

Mimura and Akiyana (5) followed this work by developing general expressions for predicting the monotonic and the hysteresis behaviour of steel plate shear wall panels. They assumed in their derivation that the steel panels developed a tension field to resist the applied loads. The assumed inclination of the tension field was that developed by Wagner (1). The monotonic load versus deformation curve they developed is an elastic-plastic model that superimposes the frame and the plate stiffnesses. Figure 2.7 illustrates the concept. The notation ${}_fQ_u$, ${}_wQ_b$, ${}_wQ_y$, $Q_y$, and $Q_{ULT}$ represents

the ultimate frame load, the ultimate wall load, the wall yield load, the idealized system yield load, and the idealized system ultimate load, respectively.

Mimura and Akiyana then developed a theoretical hysteresis curve for a steel plate shear wall panel in the following way. If the shear buckling strength is greater than the shear yield strength (Von Mises), then the behaviour of the structure will assumed to be be similar to a conventional steel beam in bending. For cases where the shear buckling load is less than the shear yield load, the theoretical hysteresis curve shown in Figure 2.8 was developed. Line O-A-H represents the monotonic load versus deflection curve for the panel. If the panel loading is taken to a load like that at point B and is then unloaded, the unloading path would be parallel to the elastic curve to point C'. Applying load in the negative sense, the deflections would continue to be parallel to the elastic curve until shear buckling of the panel occurs at a point C. The deflection C-D is that required to develop the tension field. This distance is approximately one-half the distance O-C'. From point D, the curve follows a linear transition back to the point of negative yield at A'. The curve then repeats itself, with yielding to point E, unloading to point F and redevelopment of the tension field at point G. The distance F'-G', which is equal to F-G, is taken as the average of the distances O-F' and O-D'. From point G, a linear transition back to the point of last maximum load, B,

is assumed. For further cycles the hysteresis curves would follow the same form.

The reasons for assuming that it would require a deflection of one-half the permanent plastic deformation to redevelop the tension field are based on the assumptions of a tension field angle of 45 degrees, Poisson's ratio effectively equal to 0.5, and an initially unbuckled panel. If a panel is deflected a distance delta, $\delta$, and yielded, a plastic tensile principal stress, $\sigma$, will develop as well as a perpendicular compressive stress of magnitude $0.5\sigma$. Figure 2.9 illustrates this (5). Then a deformation of $0.5\delta$ ,the result of the difference between $\sigma$ and $0.5\sigma$, can be considered to correspond to the buckle deformation. When the load is applied in the opposite sense, a deformation of $0.5\delta$ beyond the the zero load permanent deformation, C', will result in the buckles cancelling each other and a tension field developing in the opposite sense.

In addition, the authors (5) conducted a series of tests on plate girders in an attempt to verify the analysis technique. The specimens chosen varied in configuration; the characteristics are described in Table 2.1 and illustrated in Figure 2.10. Typical hysteresis curves developed for the various specimens are also shown in Figure 2.10. The test behaviour seems to correlate well with the predicted behaviour. Unfortunately, the limited number of loading cycles prevents the examination of the stability of the hysteresis curve.

### 2.3.2 Steel Plate Shear Wall Use in the United States

The use of steel plate shear walls in the United States has also recently gained acceptance. The general design philosophy employed has been that buckling of the steel panels is not permitted. This is generally accomplished by using thick steel plates or stiffeners in regions of high stress. Structures are generally designed as vertical cantilevers or by using finite element programs (11). It does not appear that any experimental testing has been conducted. Several structures have been completed and appear to be functioning as intended after being designed in this manner. Thorburn, et al. (2) conducted a general review of the design of several of these structures and several of the structures built in Japan as well.

A recently developed application for steel plate shear walls is in the retrofitting of existing structures. The Charleston, South Carolina, Veterans Administration hospital is a documented recent example (12). The engineers chose to use four steel plate shear walls to increase the lateral load-carrying capacity of the existing reinforced concrete flat slab and column structure. The shear walls were made up of a series of subpanels and assembled inside the hospital. The shear panel assembly was connected to the concrete slabs and columns by means of drilled-in anchors. The subpanels had C-sections welded at the boundaries, in effect acting as stiffeners for the shear wall panels. A factor of safety of four against plate buckling was chosen. A finite element

program was used to analyze the shear wall panels.

### 2.3.3 Unstiffened Steel Plate Shear Walls

Research at the University of Alberta on the behaviour of steel plate shear walls has concentrated on the post-buckling strength of unstiffened panels. Thorburn, et al. (2) and Timler and Kulak (3) conducted both theoretical and experimental studies on the post-buckling behaviour of unstiffened steel plate shear walls and developed a simple plane frame model that predicted the behaviour.

Thorburn, et al. conducted a parametric study on the effects of different factors on the stiffness of unstiffened shear wall panels. The plane frame model used by Thorburn, et al.(Figure 2.11) consisted of a series of tensile bars inclined at an angle $\alpha$ from the vertical. The angle of inclination of the tension field is derived on the basis of a least work formulation. For a typical structure with continuous columns, simple beam-to-column connections, and a continuous steel plate, this angle is given by:

$$\alpha=\tan^{-1}\left[\frac{2/(w\,L)+1/A_c}{(2/(wL)+H/(180LI_c)+H/(LA_b))\tan\alpha+1/A_b}\right]^{1/3} \qquad (2.2)$$

where:

$\alpha$ = angle of the tension field with respect to the vertical

L = panel length

H = panel height

w = panel thickness

$A_c$ = column area

$A_b$ = beam area

$I_c$ = column moment of inertia.

Because $\tan\alpha$ appears within the radical of Equation 2.2, the solution is obtained iteratively. The buckling load of the thin, unstiffened panels is very low, so the initial prebuckling strength of the panels can be ignored. Either the results of the fabrication process or the axial shortening of the vertical shear wall stack as load is applied could produce buckling of the plates prior to any lateral load being applied. Ignoring the buckling strength of the panels allows the panels to be represented by the series of inclined tensile bars. The areas of the inclined tensile bars are all equal and are determined by dividing the dimension of the panel perpendicular to the tension field by the number of bars, then multiplying by the plate thickness. Since the bending capacity of the thin panels is very small, the ends of the bars can be assumed to be pinned. The beams in the model are assumed to be infinitely stiff if the panel being analyzed is a typical interior panel. This assumption is based on the observation that adjacent tension fields in the lower floors of actual structures are nearly equal, causing very little relative bending in the beam members. At the boundaries, the actual stiffnesses of the beams can be introduced into the model. The beam-to-column connections are pinned in the case

illustrated. Any particular case can be modelled, however.

The analytical technique used by Thorburn, et al. involved a conventional plane-frame-truss program. The elastic panel stiffness of several panel configurations was examined and compared in the study. The results of the parametric study conducted by Thorburn, et al. indicated that there was no single unique expression that could relate the stiffness of an unstiffened shear wall panel to the stiffness of an equivalent diagonal strut. It was found that the stiffnesses of the beams, the columns, and the plates all had an effect on the stiffness of the panel. It was generally determined that, for typical panel aspect ratios, panels could be divided into as few as five tensile members and still produce valid analytical results. A subdivision into ten members is usually chosen, however.

Timler and Kulak conducted an experimental program in an attempt to verify the inclined bar model. The specimen chosen by Timler and Kulak, shown in Figure 2.12 consisted of two adjacent panels with opposing tension fields. In Figure 2.12, the columns are those members positioned horizontally and the beams are those positioned vertically. This configuration eliminated the need for an external loading frame. The boundary members are joined by pinned connections at the corners. The member sizes used were representative of sizes found in typical building construction.

The testing of the Timler and Kulak specimen consisted of three statically applied cyclic loads in each direction, and then a final compressive load to failure. For the cyclic phase, the specimen was loaded to the maximum drift limit deflection (h/400) according to CSA S16.1 (13), in this case a deflection of 6.25 mm. The load versus deflection hysteresis for these cycles had linear accending and descending segments which indicates elastic behaviour. There was, however, a small permanent deformation observed at the end of each cycle. This was attributed to the method of measuring deflections and yielding of the hold-down devices. During this cyclic loading phase, the panel buckles changed orientation with a change in load orientation. The buckle profile was continually measured during this phase. No audible pop-throughs were noted when the buckle orientation changed. The maximum buckle amplitude was approximately 20 mm, an increase over the zero-load deflection of about 11 mm. These deflections were measured over a length of approximately 2600 mm.

The final compressive loading phase produced the load versus mid-point deflection curve shown in Figure 2.13. Also plotted is the predicted load versus deflection curve. The agreement between the two curves is quite good. The specimen was also extensively monitored by strain gauges on both panels and boundary members. Again the results were reasonably consistent with the predicted values. The maximum buckle amplitude upon completion was in the order of 40 mm.

Table 2.1 Dimensions and Properties of Specimens Tested by Mimura and Akiyana (5)

Geometry

| Test | n | $t_w$ (mm) | d (mm) | h (mm) | Flange | Stiffener |
|---|---|---|---|---|---|---|
| SW1 | 1 | 1.0 | 264.3 | 549.0 | 2L - 65x65x6 | 4L - 30x30x3 |
| SW2 | 2 | 1.0 | 460.2 | 550.0 | 2L - 65x65x6 | 4L - 30x30x3 |
| SW3 | 3 | 1.0 | 460.0 | 578.0 | 2L - 50x50x4 | 4L - 30x30x3 |
| SW4 | 2 | 1.6 | 599.0 | 599.0 | 2L - 75x75x9 | 4L - 40x40x3 |

Material Properties

| | Plate | | | | | Flange | | |
|---|---|---|---|---|---|---|---|---|
| Test | $\sigma_y$ MPa | $\sigma_s$ MPa | E MPa | $\epsilon_{st}$ X$10^3$ | $E_{st}$ MPa | $\sigma_y$ MPa | $\sigma_s$ MPa | E MPa |
| SW1 | 248 | 332 | 206000 | 19.0 | 1043 | 301 | 448 | 204000 |
| SW2 | 184 | 298 | 206000 | 6.0 | 2354 | 327 | 457 | 206000 |
| SW3 | 184 | 298 | 206000 | 6.0 | 2354 | 309 | 435 | 204000 |
| SW4 | 221 | 334 | 215800 | 22.0 | 2080 | 325 | 466 | 203600 |

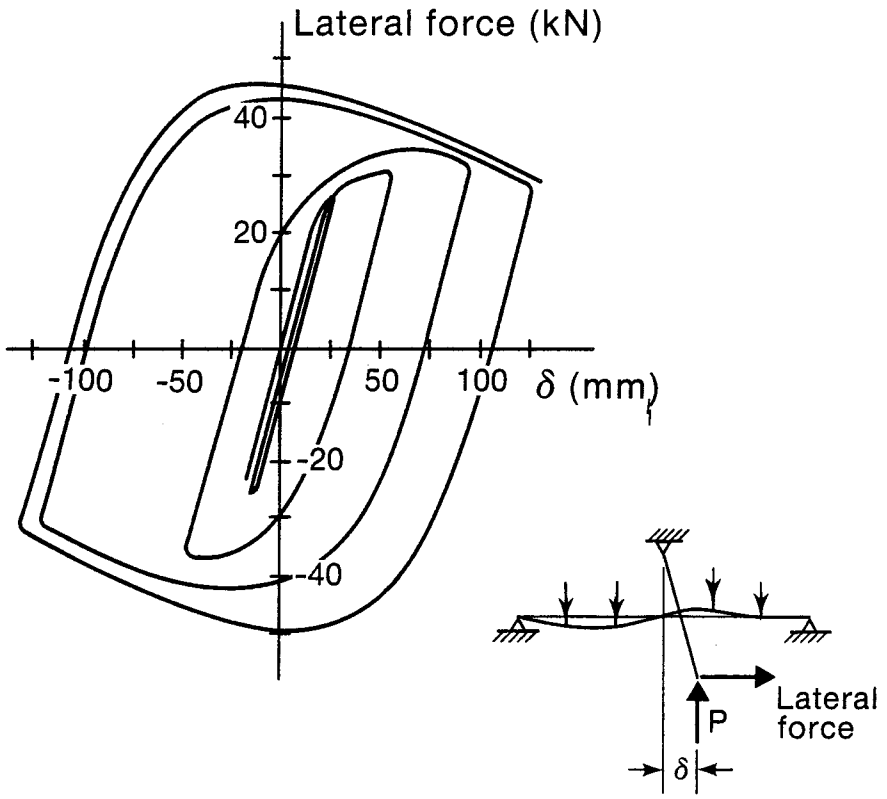


Figure 2.1 Hysteresis Behaviour of a Moment Resisting Frame (Reference 6)

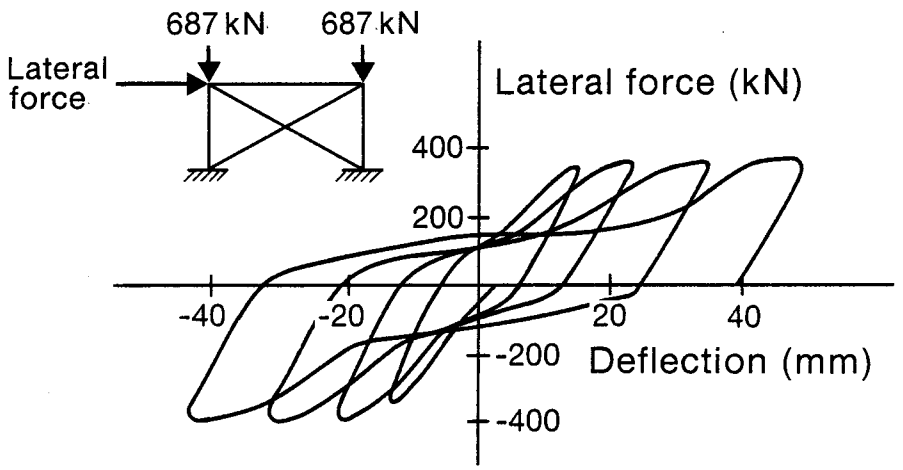


Figure 2.2 Hysteresis Behaviour of a Diagonally Braced Frame (Reference 6)

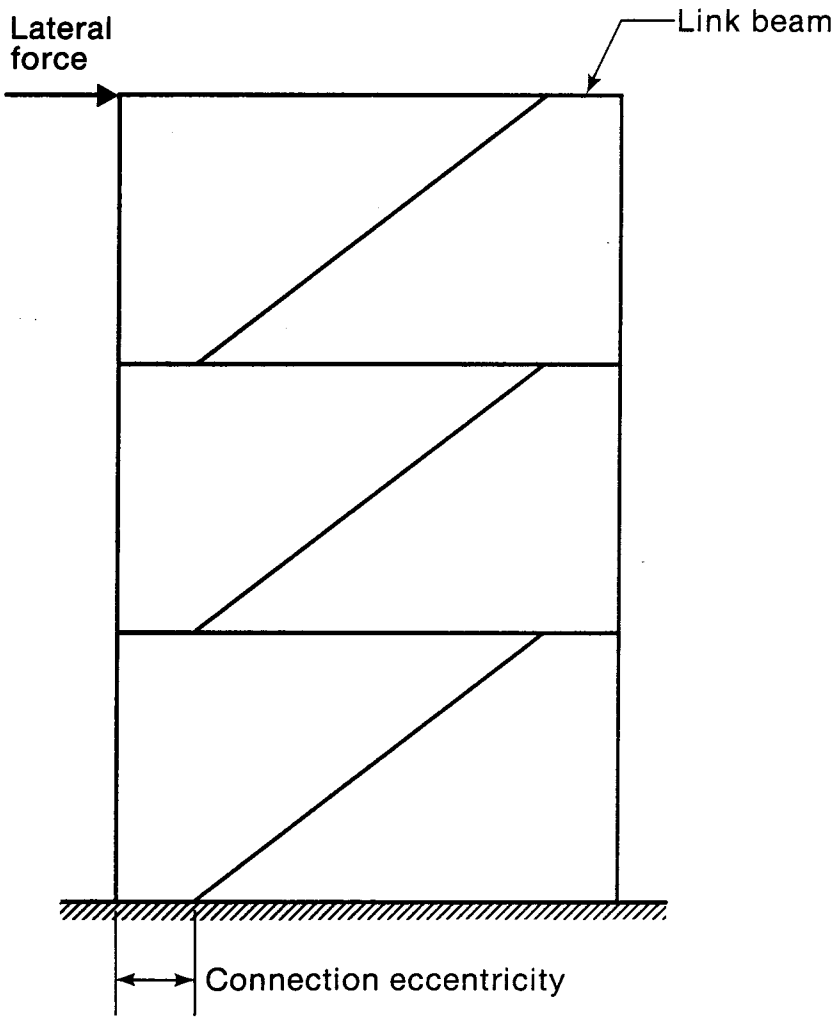


Figure 2.3 Eccentrically Braced Frame

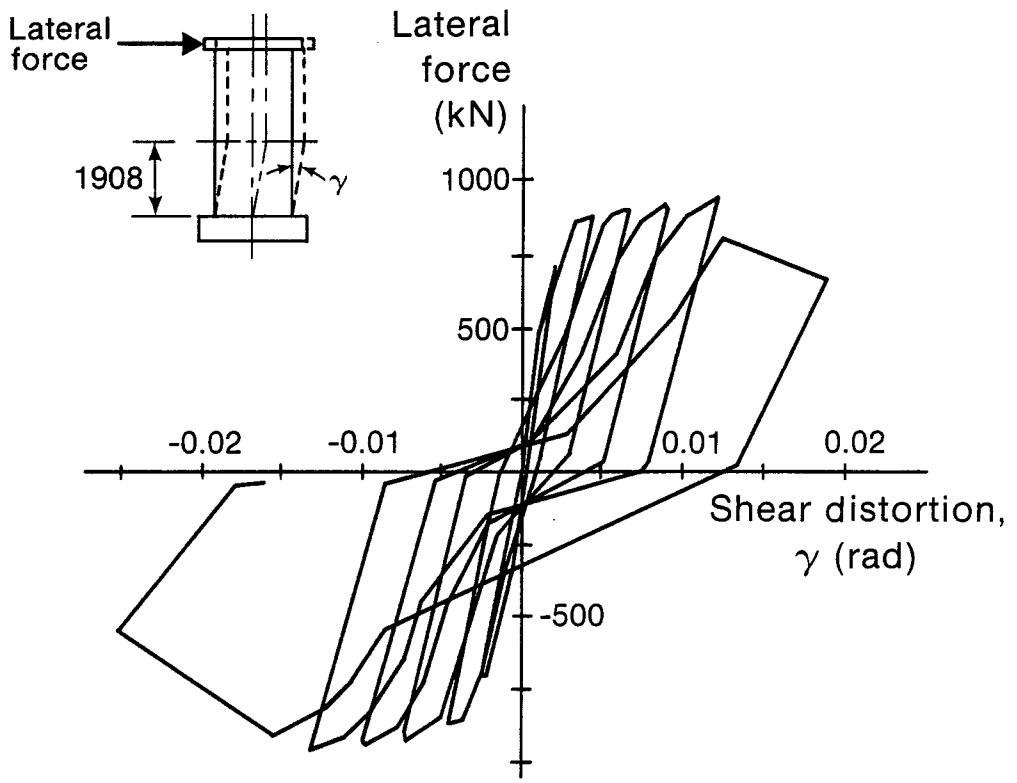


Figure 2.4 Hysteresis Behaviour of a Reinforced Concrete Shearwall (Reference 7)

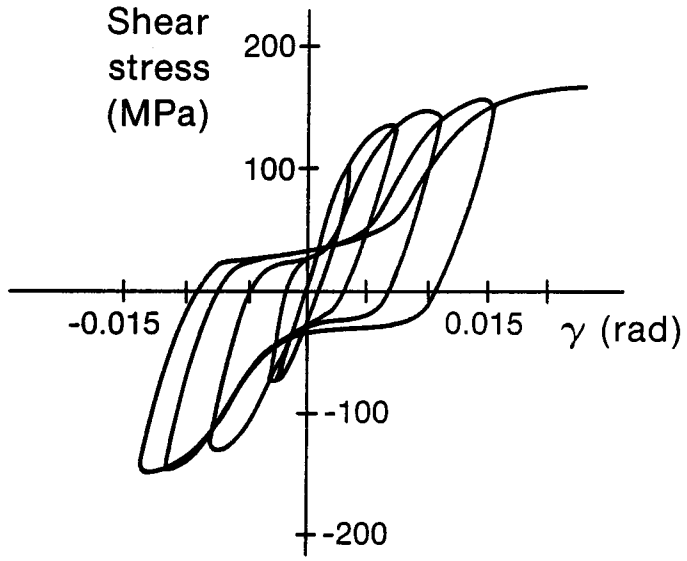


Figure 2.5 Hysteresis Behaviour of an Unstiffened Steel Plate Shearwall Panel (Reference 4)

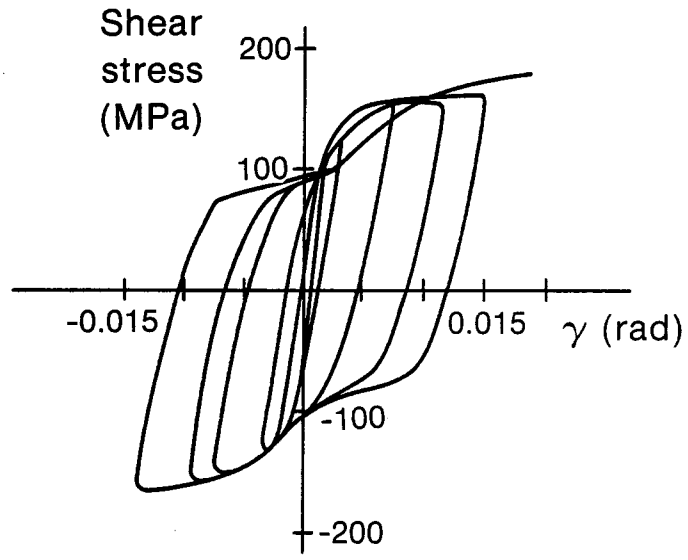


Figure 2.6 Hysteresis Behaviour of a Heavily Stiffened Steel Plate Shearwall Panel (Reference 4)

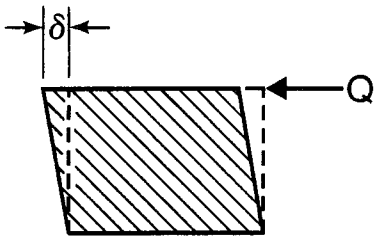


Panel deflection

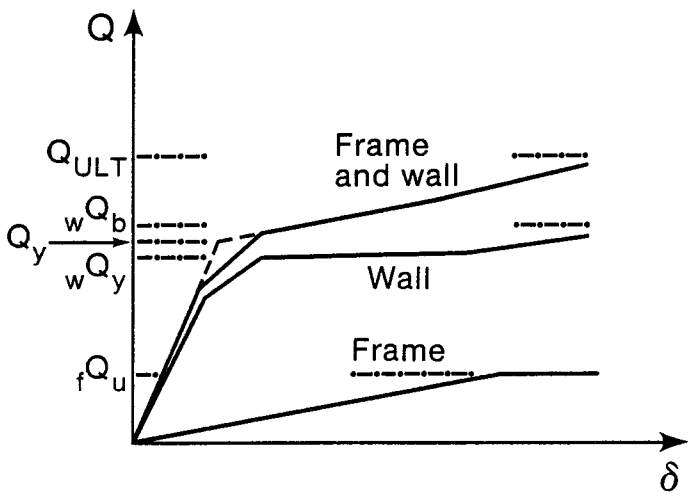


Figure 2.7 Load versus Deflection Behaviour
(Reference 5)

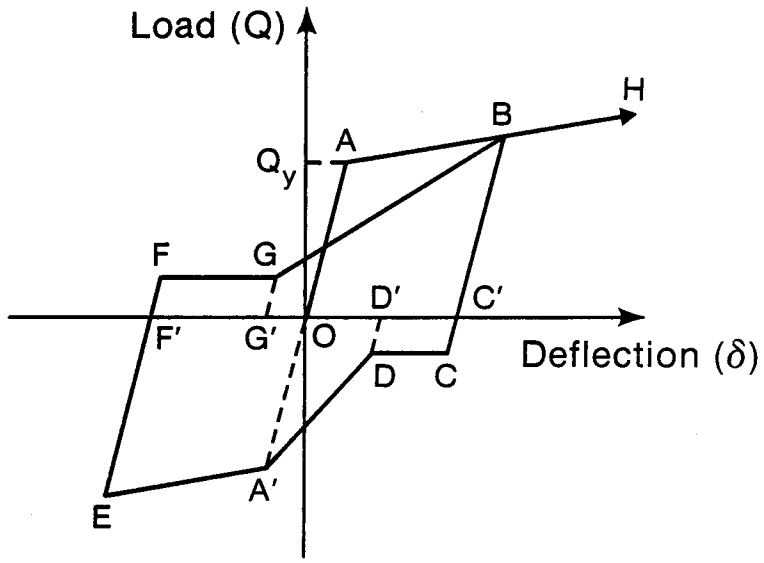


Figure 2.8 Theoretical Hysteresis Curve
(Reference 5)

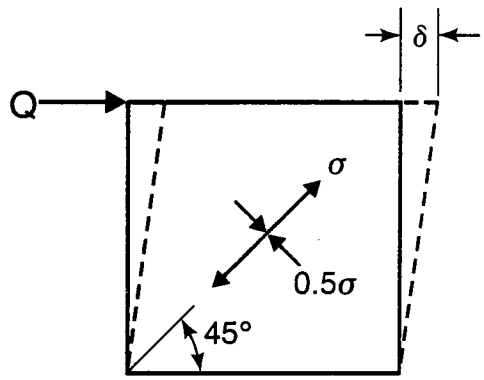


Figure 2.9 Idealized Panel Stress State
(Reference 5)

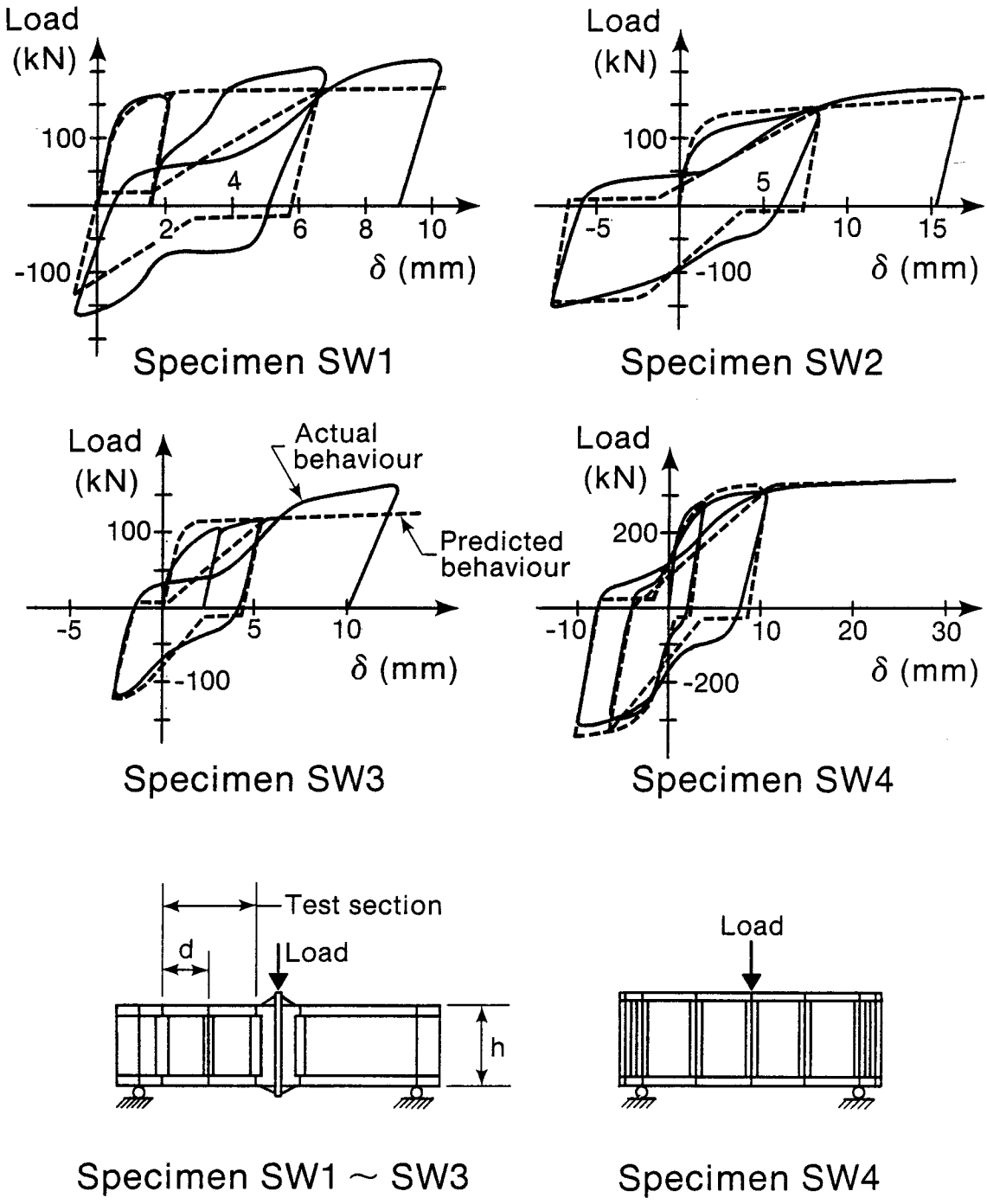


Figure 2.10 Test Specimens and their Hysteresis Behaviour
(Reference 5)

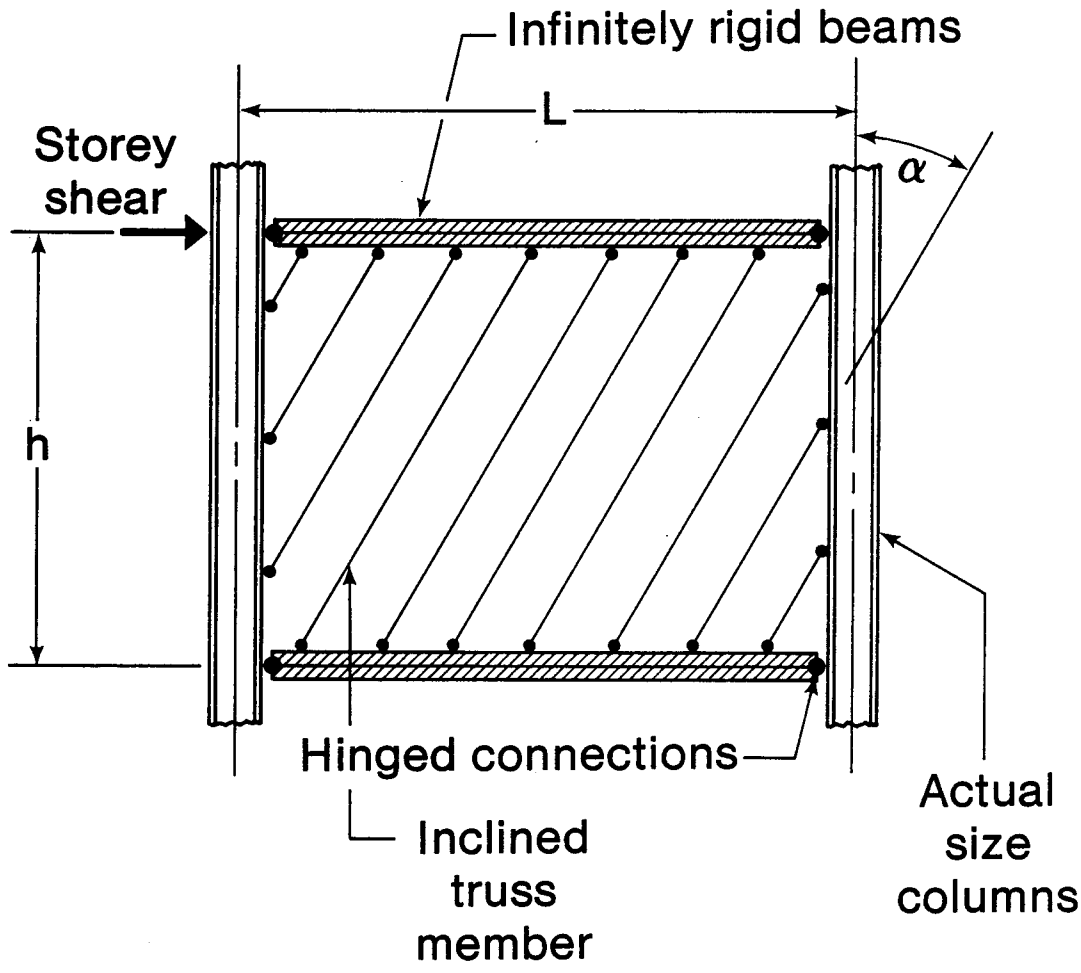


Figure 2.11 Plane Frame Model
(Reference 2)

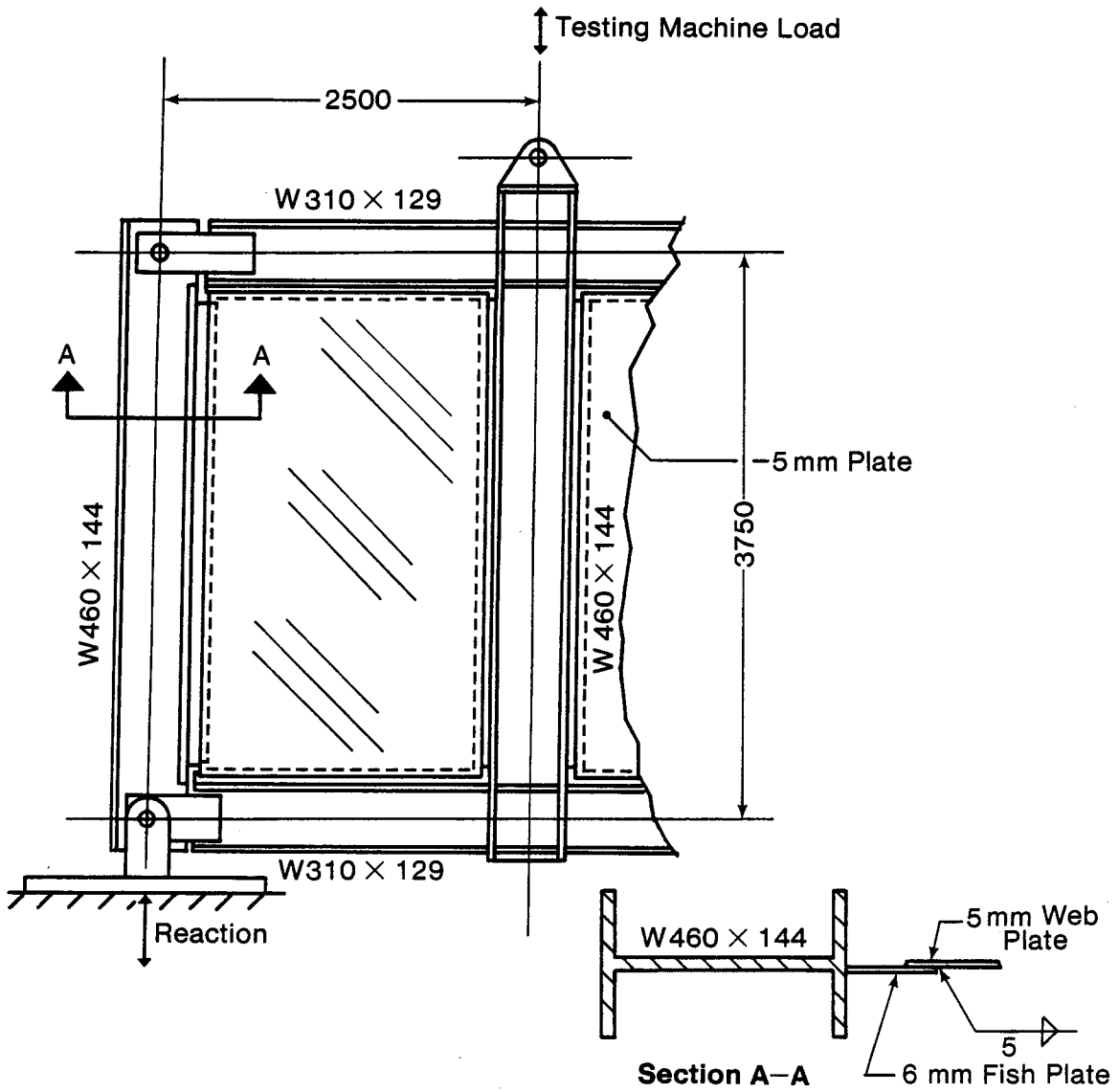


Figure 2.12 Test Specimen (Reference 3)

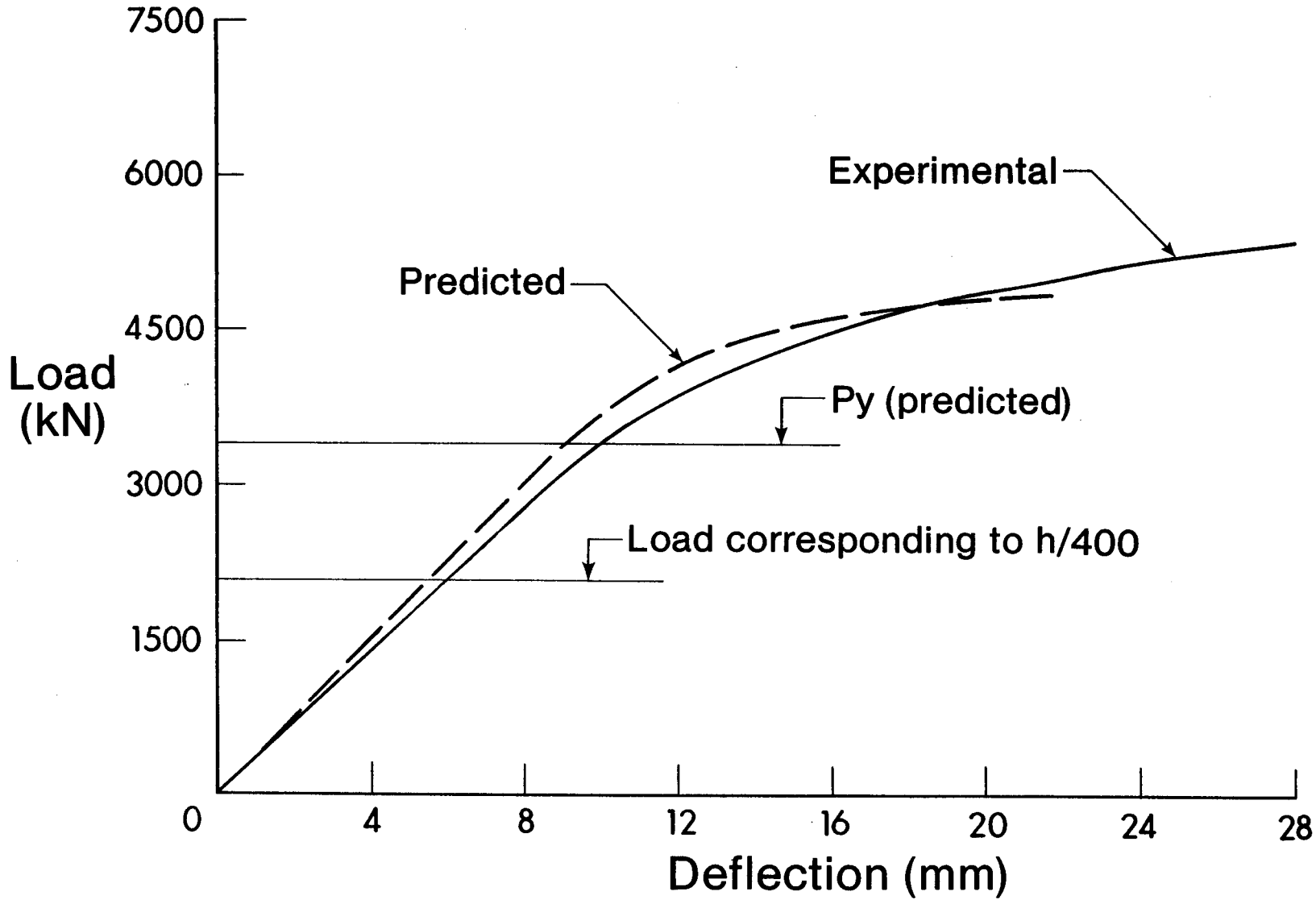


Figure 2.13 Load versus Deflection Curve (Reference 3)

# 3. EXPERIMENTAL STUDY

## 3.1 Design Considerations and Objectives

The analytical work of Thorburn, et al.(2) established that a relatively simple analysis procedure could be used to design steel plate shear walls if the concept of post buckling strength was accepted. The study reported by Timler and Kulak (3) verified the validity of the analytical model and provided information about the behaviour of the system under simulated wind loading. However, another verification of the inclined tension bar model was considered desirable and information on the cyclic response of an unstiffened steel plate shear wall was also needed.

The main objectives of the experimental study were to examine the hysteresis response of the specimen and to verify the analytical model proposed by Thorburn, et al. The specimen was to be subjected to a quasi-static, fully reversed cyclic load to failure in an approximation of seismic loading. The boundary members in this specimen were to be joined by bolted connections, unlike most previous studies (3,4,5), so that the influence of the typical structural connections could also be examined.

To accomplish these ojectives the specimen had to be designed with a number of considerations in mind. The test set up had to be simple, economical, as close to full-scale as possible, and constructed of typical building member sizes. It was felt that a full-scale specimen would provide

more accurate information on the performance of the details and the connections used. The bolted connections chosen were to be designed as bearing-type connections. The use of slip-resistant beam-to-column connections would have produced a connection with a more consistant force versus displacement characteristic, but it was felt that in a seismic event the connections could not be relied upon to be slip-resistant. Finally, in order to simulate the effects of gravity loads applied to the structure, the columns in the test specimen were to be axially preloaded.

Taking all of the requirements into consideration, it was decided that a specimen similar in configuration to the one tested by Timler and Kulak would be used. This arrangement eliminated the need for an external loading frame and simplified the test set-up considerably. The specimen resembles a deep plate girder, but either side of the symmetric specimen can be considered to be equivalent to a single storey shear wall structure.

### 3.2 Preliminary Analysis

The preliminary analysis process involved a trial and error examination of different member and plate thickness combinations. During the process, the capacity of the testing machine and other laboratory equipment had to be considered.

The initial restraint that had to be dealt with was the capacity of the testing machine and the loading yokes

available. The test required both tensile and compressive loads of large magnitudes. The final arrangement chosen had a maximum capacity of 4000 kN. This was governed by the hydraulic grips used to deliver the load to a tongue and clevis arrangement at the centreline of the specimen. This load capacity was still less than the absolute maximum capacity of the testing machine (6000 kN).

The restraint of the specimen also had to be considered. The reaction points would be required to provide tensile restraint in the order of 2000 kN per support. This required each reaction point to be secured to the laboratory floor by four high strength bolts. The locations where these bolts could be placed set limits on the storey height of the specimen. In order to load all four floor bolts equally, a storey height of 2200 mm was chosen.

Having set limits on the storey height and the maximum loads that could be applied to the system, an iterative process of examining alternatives was conducted. The various possible test configurations were analyzed using a modified plane-frame-truss program. This program had the capacity to take into account the effects of yielding on the various section properties. The configuration of the test specimen, however, was not identical to that of a shear wall in a conventional building. Timler and Kulak developed the following equation for the inclination of the tension field for the test case in which one beam member bends;

$$\alpha=\tan^{-1}\left[\frac{2/(w\ L)\ +\ 1/A_c\ +\ L/60HI_b}{(2/(wL)+H/(80LI_c)+H/(LA_b))\tan\alpha+17/16A_b}\right]^{1/3} \qquad (3.1)$$

in which all terms have been defined previously except

$I_b$= beam moment of inertia.

Using this program and the member arrangement shown in Figure 3.1, a final specimen configuration was chosen.

### 3.3 Specimen Design

The final specimen configuration chosen, shown in Figure 3.2, consisted of two panels arranged so that opposing tension fields would form. A storey height of 2200 mm and a bay width of 2750 mm made this specimen slightly smaller than the specimen tested by Timler and Kulak. The columns, positioned horizontally in this test arrangement, were the same size as used by Timler and Kulak (W310 x 129). The beams (W610 x 241), positioned vertically in the test set-up, were much larger than would be typically used. They were chosen so that a more uniform tension field would develop in the panels. The 3.25 mm thick panels were the thinnest hot-rolled plate readily available.

After the basic structural configuration was determined, the design of the remainder of the structure and the support devices was done according to CSA S16(13) and CSA W59(14).

The axial load applied to the columns was introduced using two 36 mm diameter threaded bars (of a type normally used to prestress concrete) per column, located adjacent to the web of each of the columns. The load applied to each bar was limited by the capacity of the jacks available in the laboratory (500kN). Bearing plates welded to the ends of the columns were used to transfer the force into the columns.

The top centre connection (Figure 3.3) located immediately below the load application point was designed for a maximum force of 4000 kN. The remainder of the connections (Figure 3.4) were designed for a maximum force of 2000 kN. The connections were made by first welding two clip plates per connection adjacent to the midpoint of the flanges of the columns. The clip plates were then bolted to the beam webs after matching holes had been drilled in each. The stiffeners, as shown in Figure 3.2, were designed based on the ultimate load applied to the connection. Each set of stiffeners had a slotted hole in its centre to permit the threaded bar to pass through. The slot permitted relative movement between the bar and the column to occur as the column deflected laterally while the bar remained straight.

The connection of the steel panels to the boundary members was achieved by using a fish plate arrangement, (Figure 3.5) similar to the one used by Timler and Kulak. The centre plane of the web plates panels and the centre planes of the boundary member webs were arranged so that they would be coincident. This arrangement produced an

eccentricity when the 5 mm fish plate was connected as shown in Figure 3.5. The welds between the web plate and the fish plate were designed so that the ultimate strength of the web plates could be achieved. At the corners, the fish plates were connected as shown in Figure 3.6, by means of a groove weld. A 6 mm backing plate was used. The three to five millimetre gap at the end of the horizontal fish plate was included based on the assumption that construction tolerances may not allow for a weld in this region.

### 3.4 Construction Procedure

The specimen was constructed entirely in the I. F. Morrison Structural Engineering Laboratory, this allowed for complete control of the assembly process. Construction procedures followed the recommendations in CSA S16.1-M84 (13) and CSA W59-82 (14). All welding was done by a qualified welder.

The construction sequence was as follows:

1. Weld stiffeners to columns.
2. Drill holes in clip plates and beam webs.
3. Weld clip plates to columns.
4. Weld bearing plates for preloading rods to columns.
5. Weld fish plates to beams and columns.
6. Assemble beams and columns.
7. Attach loading clevises.
8. Attach strain gauges to columns.

9. Apply 445 kN preload to columns.
10. Weld shear wall panels to fish plates.
11. Apply the remainder of the strain gauges.
12. Increase column compressive preload to 1023 kN.

Welding distortions caused several problems during the construction of the specimen. The welding of the clips to the columns caused the column flanges to curl toward the weld. This occurred between the stiffeners. The welding of the various components possibly caused the columns to develop a significant camber. This out-of-straightness required the two columns to be pulled together about 10 mm prior to bolt installation. The final welding induced problem occurred when the steel plates were installed. In the Timler and Kulak specimen, welding was done while the assembly was in the horizontal position. Because the web plates were not fully supported, some out-of-straightness was present after the welding was completed. To avoid this problem, the plates of this specimen were fully supported prior to welding. Consequently, as the welds cooled, tensile stresses were induced into the panels. At the time of the welding there were no strain gauges mounted on the panels. There were strain gauges mounted on the columns however. Figure 3.7 is a photograph of the assembled specimen. Note that both panels are very taut.

### 3.5 Data Acquisition

The data acquisition system consisted of both electronically measured and manually measured strains and displacements. Figure 3.8 illustrates the locations of the instrumentation. The electronic measurements were recorded on a computerized data acquisition system.

Locations 1 through 7 are sections where the strains in the boundary members were monitored. At these locations one uniaxial electrical resistance strain gauge was mounted on each flange tip and on each side of the web centre. This permitted the determination of axial loads and moments at these locations. At locations 8 through 16, two electrical resistance rosette strain gauges, one on each side of the panel, were used to measure the orientation and the magnitudes of the principal strains in the panel material. The strains in the threaded bars were measured by two uniaxial strain gauges per bar and were monitored during the test.

The vertical deflections were measured by linear variable differential transformers (LVDT's) at locations 17 through 22. At locations 20, 21, and 22, dial gauges were also installed as a manual check. At locations 17 and 18, rotation gauges were installed as well.

Lateral deflections of the panels were measured during this test on only a few occasions. This was accomplished by manually measuring the profile from a temporarily attached structural section used as a reference. The west panel

(orientation with respect to the testing machine) had a pair of lines marked on the south face, perpendicular to the expected tension field, so that the same profile could be measured on all occasions.

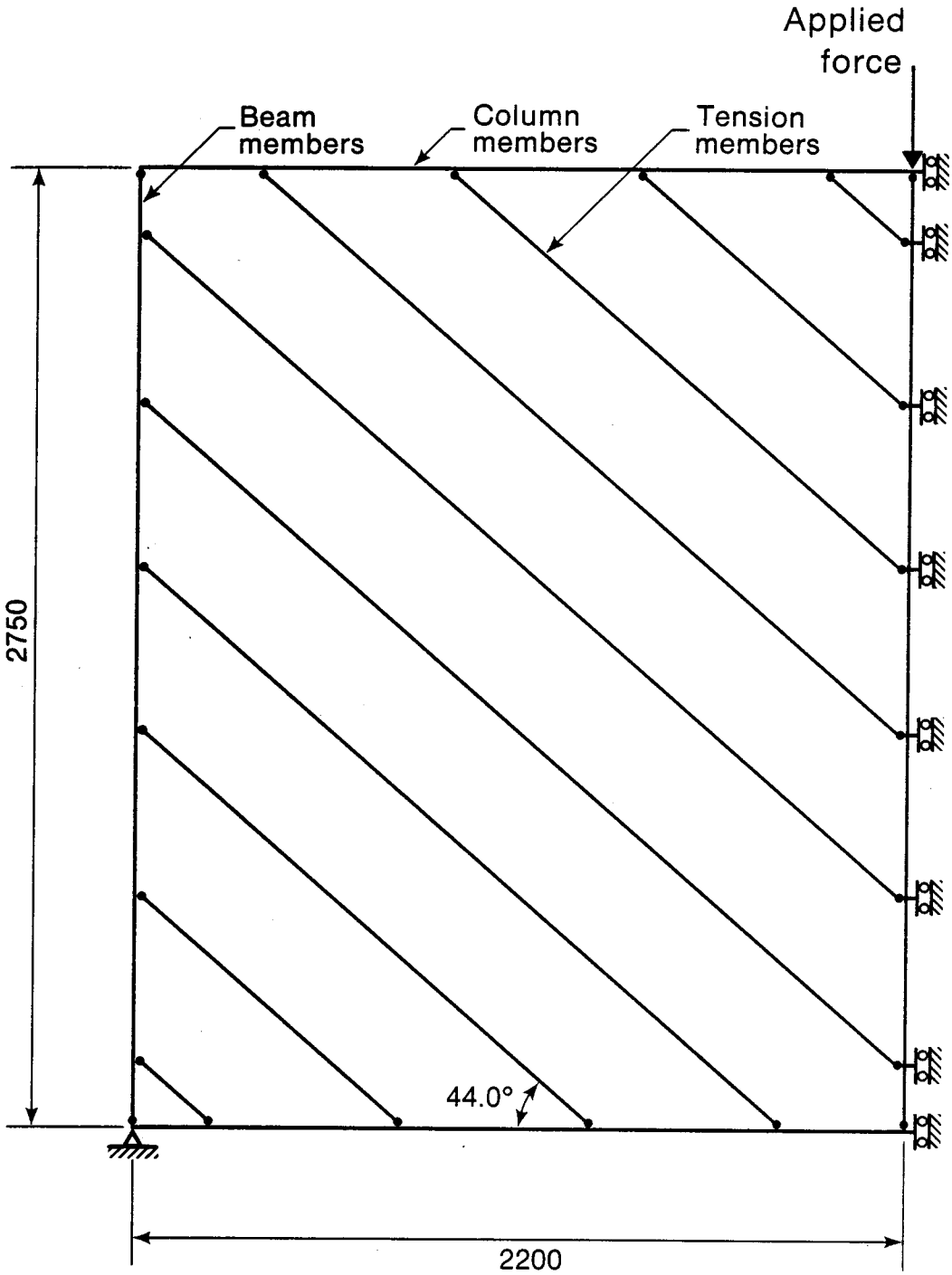


Figure 3.1 Plane Frame Model

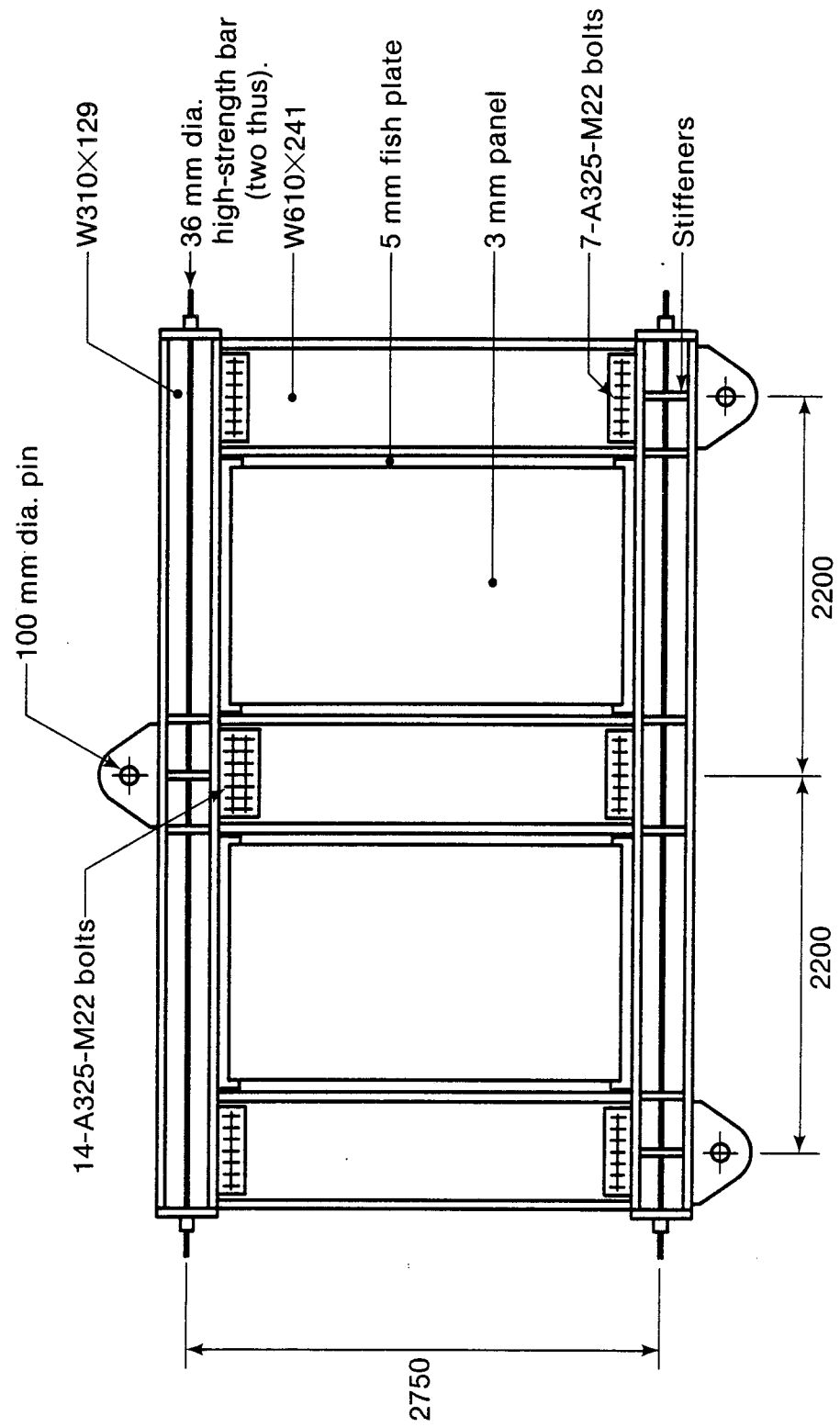


Figure 3.2 Test Specimen

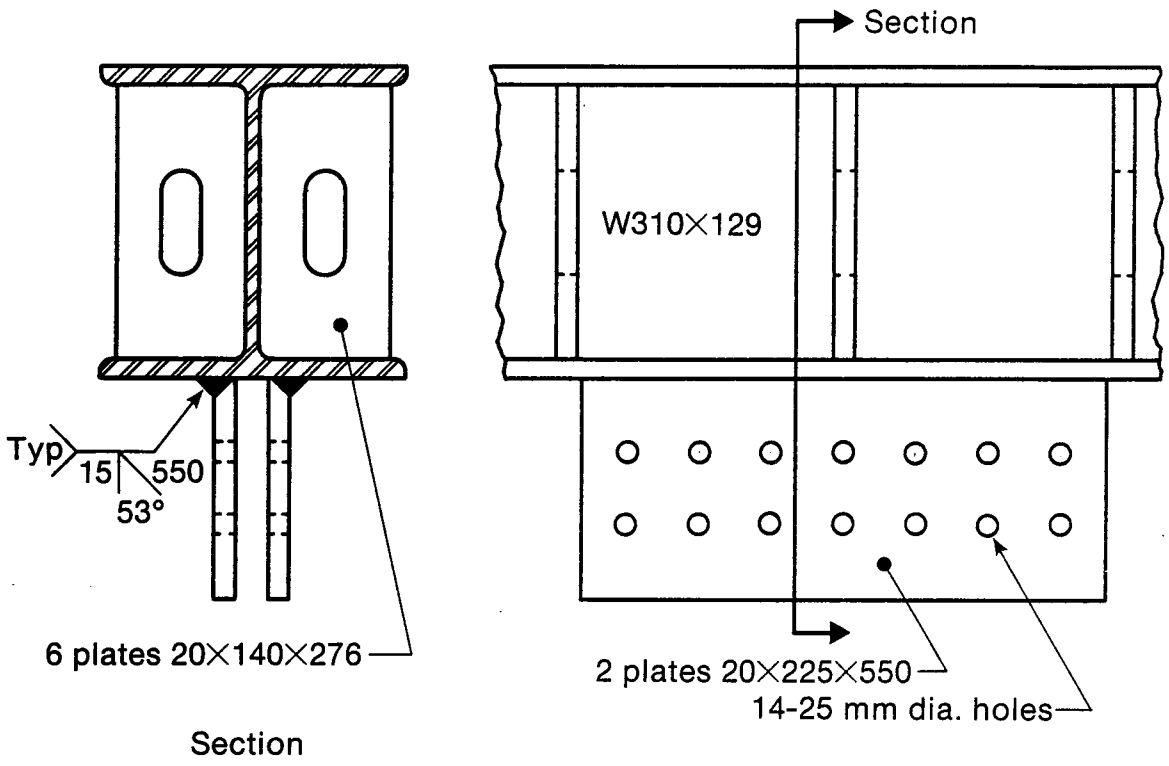


Figure 3.3 Top Centre Beam-to-Column Connection

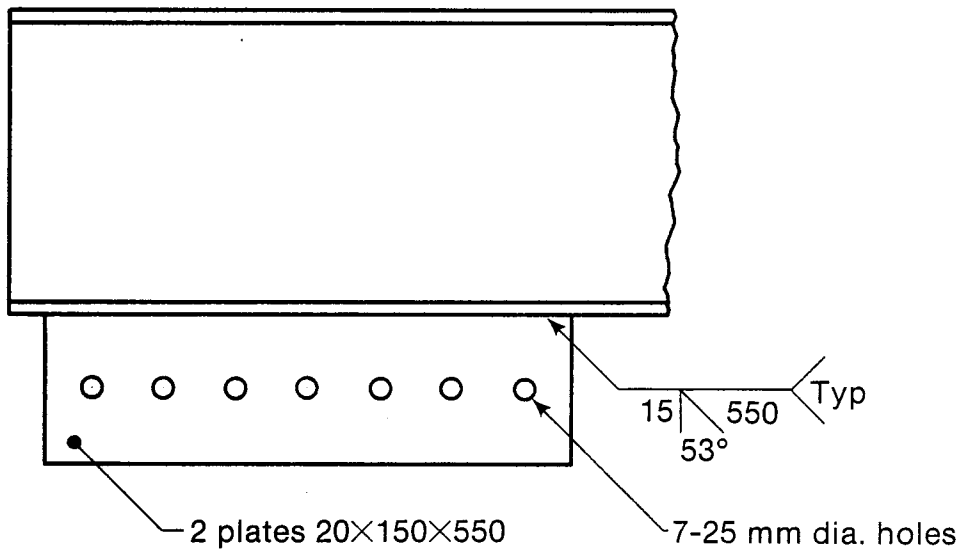


Figure 3.4 Typical Beam-to-Column Connection

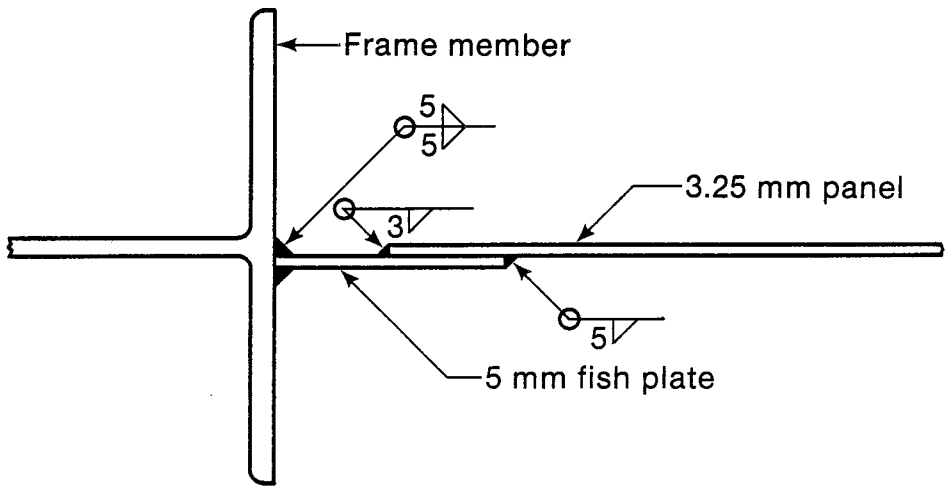


Figure 3.5 Fish Plate Connection Detail

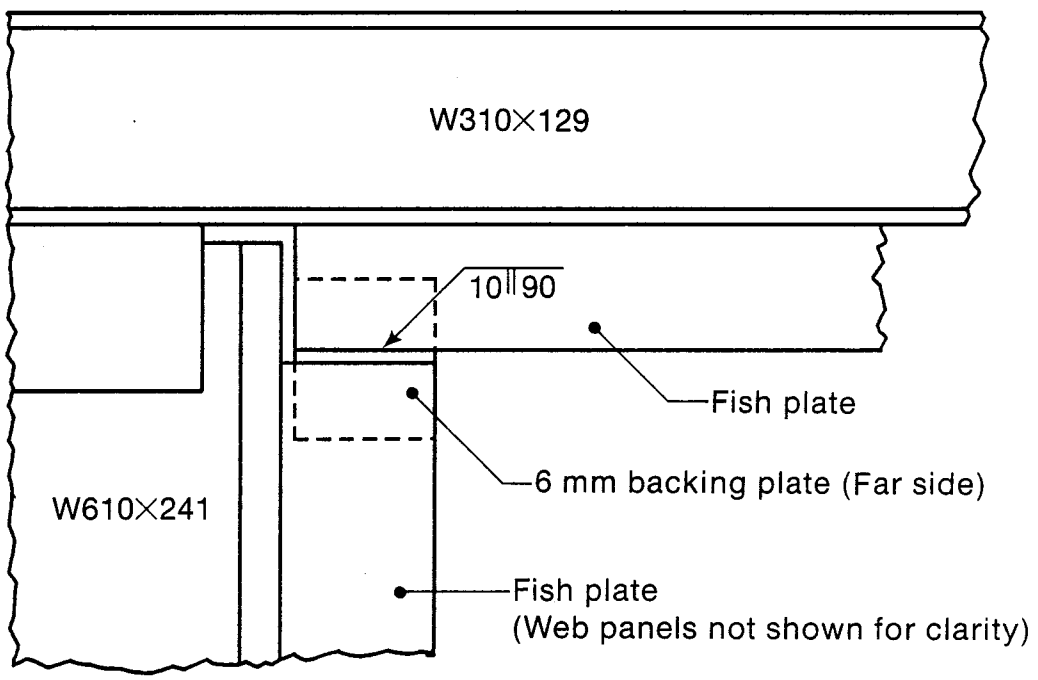


Figure 3.6 Fish Plate Corner Detail

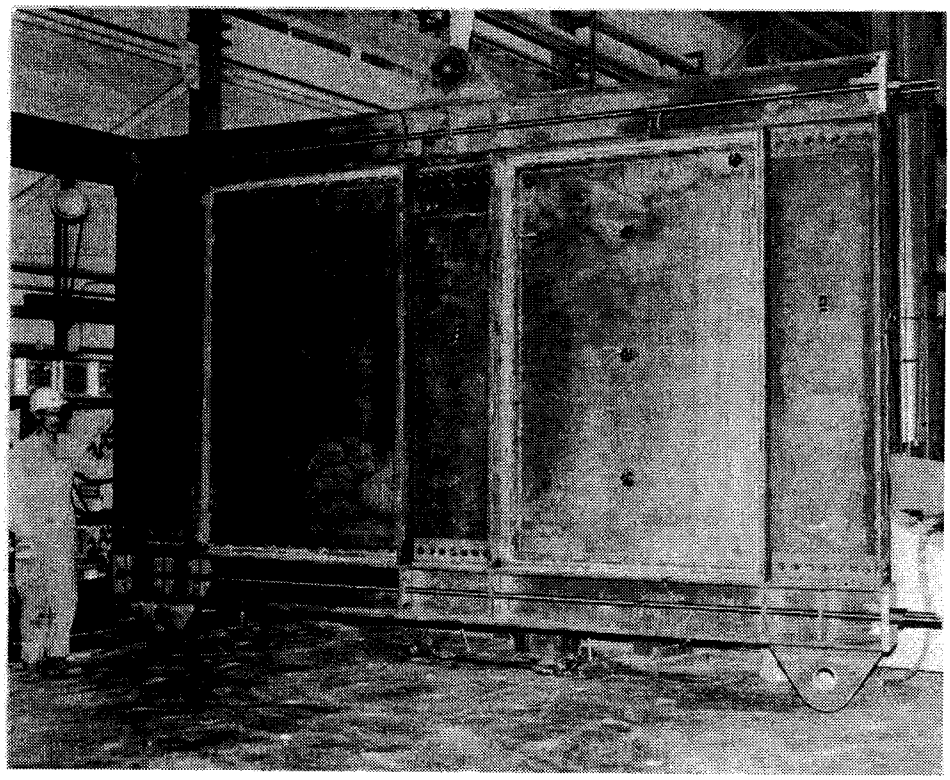

Figure 3.7 Assembled Structure

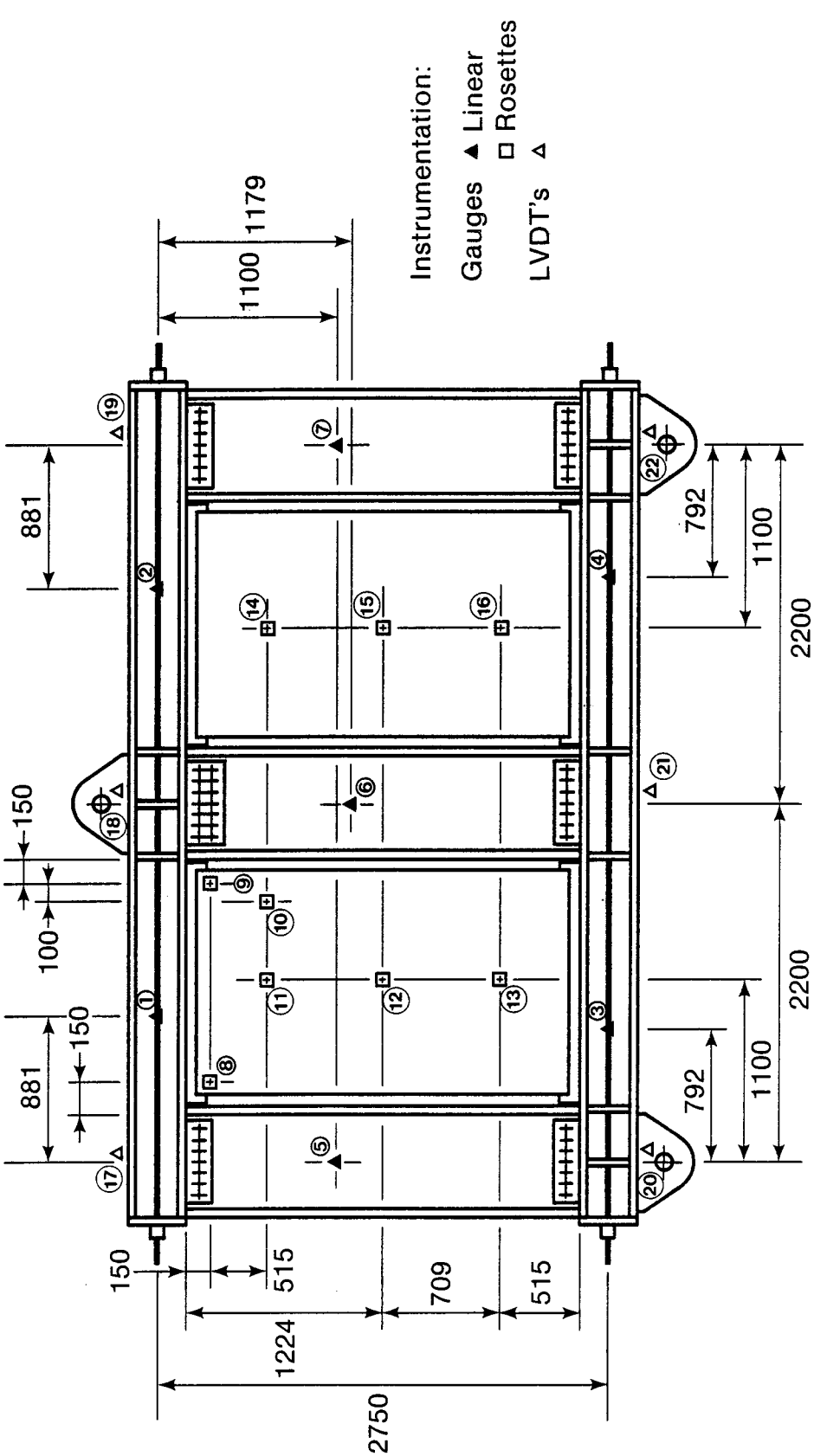


Figure 3.8 Instrumentation

# 4. ANCILLARY TESTS

To determine the material properties of the boundary members and the shear wall panels, a series of tests were conducted on coupons taken from this material. The coupons were taken from unused sections of members or from lengths of plate cut immediately adjacent to the material used in the shear wall specimen. Because the panel material was very thin, 3.25 mm, it was felt that there was a possibility that the panel material might not be isotropic. To examine this possibility, two sets of coupons were taken from the material in the assumed orthotropic directions. A stub column test was also performed on a length of column member, the W310x129 section.

## 4.1 Standards and Procedures

### 4.1.1 Tension Coupons

The general procedure followed in conducting the tension coupon tests is outlined in the American Society for Testing and Materials (ASTM) standard A370-77 (15). Tests to determine Poisson's ratio were conducted simultaneously with six of the panel coupon tests. These tests were carried out following the procedures described in the ASTM standard E132-61 (16). All of the coupons tested were of the same basic configuration, as outlined in ASTM standard A370-77, except for the coupons taken from the W610x241 beams. These coupons had a total length of 500 mm instead of the

conventional 450 mm length. The extra length was incorporated in the gripping sections of the specimens.

The instrumentation on the standard tension coupon test consisted of two uniaxial electrical resistance strain gauges mounted parallel to the direction of the applied force and located on opposite sides of the coupon at the geometric centre. These gauges were used to measure the strains in the specimen up to approximately 20 000 microstrain. Strains above this value were monitored by measuring the extension of two gauge points located 200 mm apart in the test region. The strains were also monitored continuously by an attached extensometer. This device was used to generate a continuous load versus deflection plot for the test. The strain output of the extensometer was also used as a check on the strain gauge values and the calculated strains. The instrumentation for the Poisson's ratio test consisted of two additional strain gauges, mounted on opposite sides of the coupon and perpendicular to the applied force. These gauges were immediately adjacent to the existing gauges used in the conventional tension coupon test. The applied load and the measured strains for all tests were recorded manually.

### 4.1.2 Stub Column Test

A stub column test was performed on a section cut from one of the W310x129 members. The procedure followed is outlined in the Guide to Stability Design Criteria for Metal

Structures (17). The instrumentation for the stub column test consisted of six strain gauges, three per flange, mounted at the centre of the column and parallel to the applied force. One gauge was placed 20 mm from each flange tip and one gauge was placed at the centre of each flange. Two Demec points were also placed on each flange at a 203 mm (eight inch) gauge length parallel to the applied force. Both the load and the strain in this test were electronically measured and stored.

## 4.2 Test Results

### 4.2.1 Panel Material

Fifteen coupons were taken from a section of steel plate cut from the same stock that later was used for the shear wall panels. The coupons were cut in two perpendicular directions. The coupons numbered 0.# (see Table 4.1) were representative of the material taken from the horizontal direction (with respect to the orientation of the shear wall specimen). The coupons numbered 90.# (see Table 4.2) were representative of material taken from the vertical direction.

The load versus deflection response in both of the perpendicular directions was elastic-plastic, exhibiting a definite yield plateau prior to strain hardening. This is the characteristic behaviour of a hot-rolled steel. Tables 4.1 and 4.2 list the results of the tension coupon tests.

Note that the material appears to be mildly orthotropic, with an average static yield strength of 232.4 MPa in the 0.# orientation and an average static yield strength of 252.6 MPa in the 90.# orientation. Coupon 0.7 was not included in the average because it was considered that the static yields were not maintained at a constant strain and some unloading occurred. Coupon 0.3 was taken from a region that appeared to be a flame affected zone. The results seem to indicate that the material properties in this zone were no different than the properties in the remainder of the plate. The average modulus of elasticity of the two series of tests were quite similar, with the difference being less than one standard deviation of either series.

During each of these series, three coupons were also tested to determine Poisson's ratio in the elastic range. The values in the 0.# direction are quite consistent while the values in the 90.# direction have a much higher standard deviation. Taking these material properties and trying to apply the standard orthotropic constitutive relationships does not produce an acceptable solution. The terms $\nu_{xy}E_y$ and $\nu_{yx}E_x$ are not equal. Since in most cases the material properties in the two directions are nearly equal, the assumption that the material behaviour is equivalent to an average of the two sets of values can be made. This valid assumption is also necessary because the plane frame model cannot accomodate an orthotropic material.

### 4.2.2 Beam Member Material

Five coupons (B1 through B5) were cut from the flange and two coupons (B6 and B7) were cut from the web of a W610x241 section obtained for coupons. The beam material was required to meet CSA Standard G40.21 300W. Table 4.3 lists the results of the coupon tests. The coupons cut from the flange exhibited a behaviour characteristic of a cold-worked material, with a very short or non-existant plastic region. The coupons taken from the flange tips (B1 and B3) had the shortest plastic region. This type of behaviour was to some extent expected since all of the members showed a large number of yield lines prior to the start of fabrication. The coupons taken from the web displayed the typical behaviour of a hot rolled material with a long yield plateau. The linearity of the stress versus strain curve in the elastic range was also affected by the possible cold working or by some remaining through-thickness residual stresses. The flange coupons displayed a non-linear stress versus strain curve at stresses far below the yield stress. The five point moving average procedure was used to determine the point at which the proportional limit occurred (18). The average stress at which non-linearity began to occur was 156 MPa. The stress versus strain curve from 156 MPa to yield could be idealized by a linear segment with a slope of 125 000 MPa. However, preliminary analysis of the structure indicated that the stress levels in these large members were not expected to exceed 156 MPa, even at maximum load. The

coupons taken from the web displayed a linear stress versus strain curve from zero load to yield.

### 4.2.3 Column Member Material

Five coupons from the flange (C1 through C5) and three coupons from the web (C6, C7, and C8) were taken from a length of column material (W310X129) obtained for testing. The column material was required to meet CSA Standard G40.21 300W. All of the coupons tested exhibited a yield plateau; the coupons taken from the web generally displayed a longer yield plateau than those coupons taken from the flanges. The stress versus strain curve for nearly all specimens became non-linear prior to reaching the yield plateau. Again, the five point moving average was used to determine the proportional limit. The average point at which non-linearity in the flanges occurred was 270 MPa. The average static yield stress for the same material was 335.4 MPa. The extent of the non-linearity in the stress versus strain curve between 270 MPa and 335 MPa in many cases was very small and not graphically apparent. The elastic modulus and the static yield for coupon C5 were not included in the average because upon closer examination it was found that the strain gauges were producing inconsistent results. This problem with the strain gauges also possibly identified a static yield much greater than the other specimens.

A stub column test conducted on a section of W310x129 produced a stress versus strain plot shown in Figure 4.1.

This curve also becomes non-linear prior to reaching the yield stress. The proportional limit in this case is approximately 120 MPa, much lower than found in the coupon tests. This is understandable because the residual stresses across the entire section are having an effect. The deviation from the linear however does not become apparent graphically until approximately 260 MPa and not significant until approximately 300 MPa. The value of the modulus of elasticity, 204 117 MPa, is quite comparable to the average value found from the tension coupon tests. The 0.2 percent offset yield strength value is about 355 MPa or approximately 20 MPa greater than the static yield strength found in the coupon tests. This discrepancy is believed to be the result of an insufficient time period allowed between the locking of the head of the testing machine and the recording of the test data.

The stress versus strain curve used in the plane frame analysis is assumed to be elastic-plastic with an elastic modulus equal to the average value found in the coupon tests (very close to the value found in the stub column test). The yield strength assumed is equal to the average value found in the coupon tests. The non-linearity in the stress versus strain curve can be ignored since, in the case of the coupons, the non-linearity is minor. The greater non-linearity recorded in the stub column test is only significant above a stress of about 290 MPa indicating that the initial residual stresses present were of low magnitude

on average. This further justifies the acceptability of the assumed elastic-plastic stress versus strain curve.

| Coupon | 0.1 | 0.2 | 0.3 | 0.4 | 0.5 | 0.6 | 0.7 | 0.8 | Mean | S.D. |
|---|---|---|---|---|---|---|---|---|---|---|
| E (MPa) | 205660 | 210510 | 207410 | 207296 | 206600 | 206550 | 206500 | 206540 | 207130 | 1466 |
| $\nu$ | - | - | - | 0.281 | - | - | 0.283 | 0.287 | 0.284 | 0.003 |
| $\sigma_y$ (MPa) | 230.8 | 234.6 | 233.0 | 235.4 | 226.7 | 230.3 | 218.0 | 235.9 | 232.4* | 3.31* |
| $\sigma_u$ (MPa) | 339.1 | 341.8 | 337.4 | 338.5 | 336.5 | 337.0 | 336.0 | 339.5 | 338.2 | 1.90 |
| $\epsilon_s$ | 21900 | 20200 | 21000 | 23100 | 20500 | 20000 | 20060 | 18000 | 20600 | 1500 |
| $\epsilon_u$ | 213200 | 199100 | 205800 | 203300 | 218200 | 206308 | 224900 | 209000 | 210000 | 8413 |
| $\epsilon_f$ | 300400 | 278900 | 294200 | 282500 | 318900 | 299900 | - | 286800 | 294500 | 13600 |

All strains given in Microstrain.
*-Coupon 0.7 not included. (see text)

Table 4.1 Plate Material Behaviour-Zero Degree Direction

| Coupon | 90.1 | 90.2 | 90.3 | 90.4 | 90.5 | 90.6 | 90.7 | Mean | S.D. |
|---|---|---|---|---|---|---|---|---|---|
| E (MPa) | 209241 | 207989 | 208629 | 205672 | 206630 | 208900 | 209269 | 208050 | 1393 |
| $\nu$ | - | - | - | 0.286 | 0.266 | 0.269 | - | 0.274 | 0.011 |
| $\sigma_y$ (MPa) | 257.0 | 254.6 | 247.3 | 247.1 | 252.8 | 254.1 | 255.3 | 252.6 | 3.90 |
| $\sigma_u$ (MPa) | 346.6 | 344.3 | 345.2 | 343.8 | 343.3 | 343.2 | 343.4 | 344.3 | 1.25 |
| $\epsilon_s$ | 27000 | 26000 | 27900 | 25000 | 29000 | 27000 | 28000 | 27100 | 1350 |
| $\epsilon_u$ | 195800 | 204900 | 200150 | 214400 | 207900 | 212670 | 211700 | 206800 | 6900 |
| $\epsilon_f$ | 278800 | 275800 | 282500 | 293300 | 281800 | 324800 | 298800 | 290800 | 17000 |

All strains given in Microstrain.

Table 4.2 Plate Material Behaviour-Ninety Degree Direction

| Coupon | B1 | B2 | B3 | B4 | B5 | B6 | B7 | Mean | S.D. |
|---|---|---|---|---|---|---|---|---|---|
| E (MPa) | 205330 | 203040 | 202840 | 204050 | 203720 | 202900 | 207800 | 204240 | 1800 |
| P.L. (MPa) | 200 | 185 | 113 | 130 | 150 | 308 | 300 | 156 (Flanges | 37 Only) |
| $\sigma_y$ (MPa) | 265.6 | 271.7 | 292.0 | 271.0 | 279.8 | 308.2 | 289.9 | 276.0 (Flanges | 10.3 Only) |
| $\sigma_u$ (MPa) | 457.7 | 466.3 | 455.3 | 462.7 | 465.0 | 471.3 | 471.3 | 464.2 | 6.2 |
| $\epsilon_s$ | 7000 | 9700 | 3400 | 8600 | 11700 | 20000 | 16000 | 8100 (Flanges | 3100 Only) |
| $\epsilon_u$ | 185500 | 180900 | 183200 | 179600 | 175200 | 178900 | 186000 | 181300 | 3900 |
| $\epsilon_f$ | 330300 | 324700 | 343800 | 350800 | 340500 | 315500 | 316300 | 331700 | 13800 |

P.L. is the proportional limit.
All strains given in Microstrain.
Coupons B1 to B5 taken from Flanges.
Coupons B6 and B7 taken from Web.

Table 4.3 Beam Material Behaviour

| Coupon | C1 | C2 | C3 | C4 | C5 | C6 | C7 | C8 | Mean | S.D. |
|---|---|---|---|---|---|---|---|---|---|---|
| E (MPa) | 200670 | 204775 | 209506 | 202650 | * | 200242 | 205170 | 200859 | 203400 | 3300 |
| P.L. (MPa) | 220 | 275 | 330 | 260 | * | 200 | 350 | 181 | 270 (Flanges | 46 Only) |
| $\sigma_y$ (MPa) | 338.4 | 331.9 | 337.0 | 328.4 | 346.5 | 335.1 | 339.8 | 337.4 | 336.8 | 5.4 |
| $\sigma_u$ (MPa) | 529.4 | 524.5 | 528.5 | 532.9 | 527.2 | 508.0 | 510.7 | 512.5 | 521.7 | 9.7 |
| $\epsilon_s$ | 11000 | 10700 | 10000 | 12600 | 11000 | 15600 | 20000 | 12400 | 11100 (Flanges | 950 Only) |
| $\epsilon_u$ | 159800 | 154700 | 141500 | 158400 | 167200 | 158500 | 152300 | 155000 | 155900 | 7350 |
| $\epsilon_f$ | 263500 | 258900 | 264000 | - | 272500 | 253400 | 245800 | 260000 | 259700 | 8450 |

P.L. is the proportional limit.
All strains given in Microstrain.
Coupons C1 to C5 taken from Flanges.
Coupons C6 to C8 taken from Web.
*-Strain gauge malfunction occurred.

Table 4.4 Column Material Behaviour

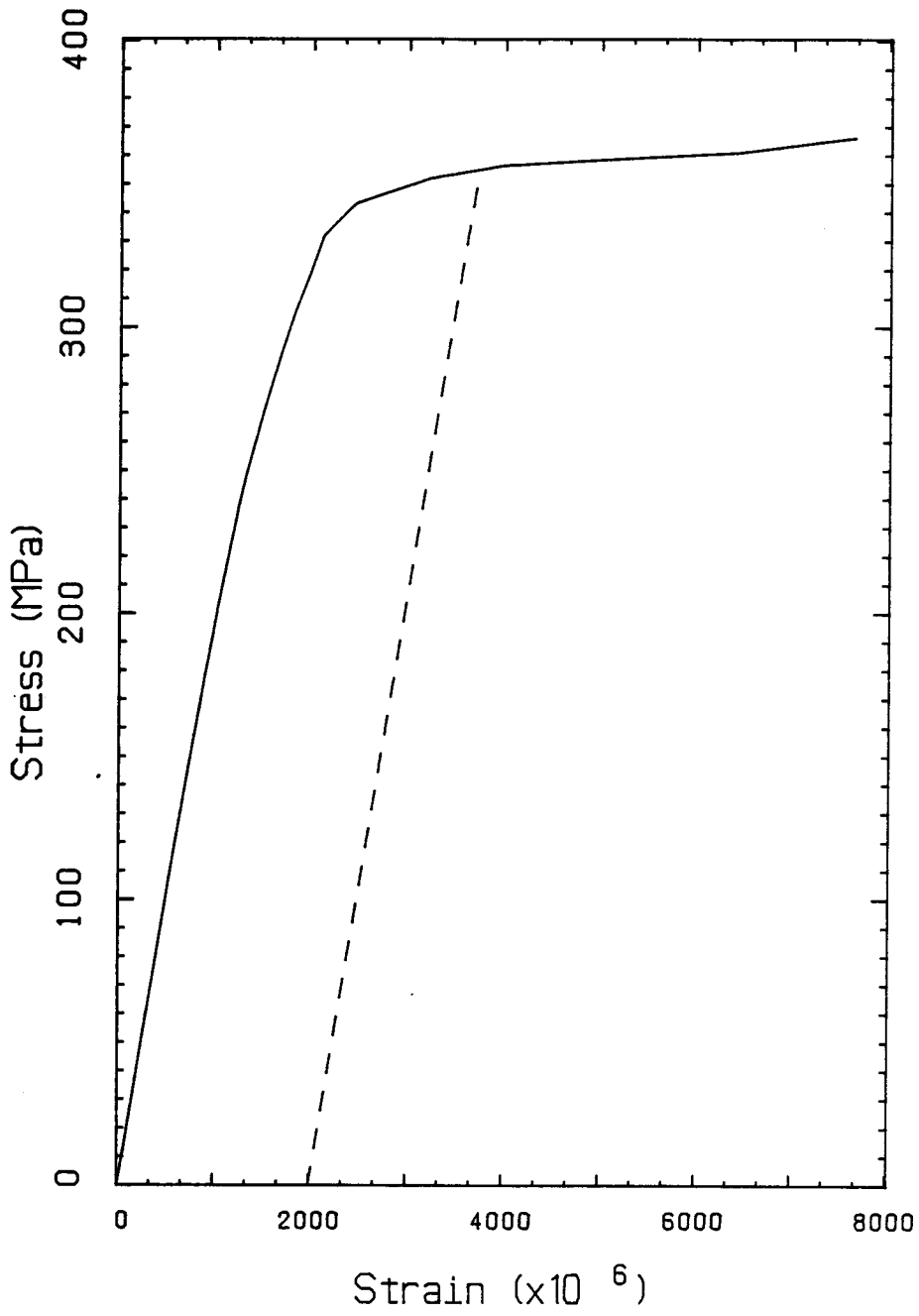


**Figure 4.1 Stress versus Strain Curve for W310 x 129 Stub Column**

# 5. SHEAR WALL TEST

## 5.1 General

After the fabrication of the steel plate shear wall test specimen had been completed, the specimen was positioned in the testing machine and secured to the support points by means of 100 mm diameter pins. The final column preload was then applied to the specimen before the support points were secured to the laboratory floor. This allowed axial shortening of the columns to occur without restraint. The test specimen was oriented in the testing machine in an east-west direction and it is this relative position in the testing machine (east or west) that will be used hereafter when referring to the panels. The outside top and bottom corners of the panels were those corners adjacent to the outside beams, located above the hold-down supports (See Figure 3.2). The inside top and bottom corners were those adjacent to the centre beam. The shear wall, vertical in an actual structure, was positioned horizontally in the testing machine. This permitted the loads to be applied vertically.

The testing of the shear wall specimen involved two loading phases, a cyclic loading phase and a monotonic loading phase. In referring to the applied loads in the cyclic loading phase, the sense of the load with respect to the testing machine will be used, that is, tensile or compressive. It should be kept in mind that the test attempted to simulate lateral loads applied to a vertical

shear wall and reference to loads as tensile or compressive is merely for convenience. During both of these loading phases the strains in the panels and the boundary members were monitored continually.

## 5.2 Cyclic Loading Test

### 5.2.1 Load History

It was intended originally that the specimen be loaded with a gradually increasing, fully reversed, cyclic load to failure. However, the specimen proved to be stronger and stiffer than predicted, causing parts of the loading system to reach their capacity before failure of the specimen could be attained in this manner. As a consequence, the maximum cyclical load applied was only about 67% of the ultimate load subsequently attained. After the cyclic loading sequence had been completed, the loading devices were then modified to accept only compressive loads from the testing machine. The final loading was then carried out in just one direction.

The applied cyclical loading sequence is illustrated in Figure 5.1. A total of 28 cycles was completed during this phase, with a maximum load of 4000 kN reached. Generally, during this phase at least two complete cycles to the same maximum deflection in both tension and compression were achieved. The drop in the maximum tensile load during cycle 19 was due to a problem with a support point.

This type of gradually increasing cyclic load is the scheme normally used to develop hysteresis loop data. Other arrangements, consisting of a few primary cycles of large magnitude followed by a gradually increasing cyclic load, have been proposed (19). Research by Malley and Popov (20) on shear links led those authors to conclude that the amount of energy dissipated by a system is independent of the load history. Considering this, it was felt that the typical loading sequence involving a gradually increasing load would be used. Also, structural systems that have displayed good hysteresis behaviour when subjected to gradually increasing cyclic loads in laboratory tests have performed well in actual earthquakes.

### 5.2.2 Hysteresis Behaviour

Figure 5.2 shows the load versus deformation response for all 28 cycles of loading. The behaviour of the structure will be described with respect to the various segments of this loading history.

Figure 5.3 is the load versus deflection plot for the first seven cycles. For the first four cycles the behaviour of the structure was nearly linear. No unusual behaviour was observed during these first four cycles, with only a few minor sounds as the orientation of the buckles changed. The fifth to seventh cycles produced a few major buckle changes (identified by very loud noises) and up to twelve minor ones. At a compressive load of 900 kN, during the fifth

cycle, it was observed that the central region of the east panel was carrying little or no load. The panel could be easily deflected out-of-plane in either direction with little effort. The strains in the system at this load level were recorded by the computerized data acquisition system.

By the seventh cycle, the loading and the unloading curves clearly were not identical, with some area now enclosed under the load versus deflection curve. The maximum tensile load for this cycle was 1931 kN. At this point in the test there were no physical signs of distress in the panels except for the presence of the panel buckles. These had a maximum amplitude of approximately 10 mm.

Figure 5.4 shows the load versus deflection curve for load cycles 8 through 14. The hysteresis curve for these cycles is beginning to show signs of deterioration. Pinching of the hysteresis loops, a consequence of yielded and buckled plate material not being immediately recompressed, resulted in a smaller enclosed area under the hysteresis curve and, therefore, a lower amount of energy absorbed by the system during successive cycles. During these cycles, the frequency of the buckle changes and the magnitude of the noises produced increased noticeably. It was also observed during these cycles that the bolted connections appeared to be slipping during each load reversal. This probably increased the deterioration of the hysteresis loops.

Cycle 9, in which a maximum load of 2200 kN was reached, produced the first physical signs of yielding.

Whitewash was observed flaking from both the fish plates and the panels at the top outside panel corners. During the eleventh compressive cycle, at a maximum load of 2500 kN, very sharp buckles formed at the top outside corners. Cycle thirteen, with a maximum cycle load of 2866 kN, produced the same buckles at the bottom inside corners. Yielding of the fish plates and the panels at all of the panel corners had extended considerably.

Prior to the completion of cycle 14, the deflections measured were less than the storey deflection limit (h/400 or 5.5 mm) prescribed in CSA Standard S16 (13). This deflection was, however, beyond the deflection (3 mm) where nonlinearity of the load versus deflection response was judged to have occurred.

Deterioration of the hysteresis loops continued for cycles 15 to 21, as shown in Figure 5.5. The magnitude of the buckles and the area of yielding of the plate continued to increase. The buckle changes were continuing to produce very loud pop-throughs during each load reversal. After cycle 21, several tears, up to 20 mm long, were noticed in the fish plates at the top outside and top inside corners of the panels.

The final seven cycles, shown in Figure 5.6, are marked by a change in the development of the hysteresis loops. The tension cycles continued to degenerate but the compression cycles appeared to have stabilized. The apparent stabilization of the compression cycles possibly resulted

because the same maximum compressive load was applied for all seven cycles. Behaviour during the tension cycles continued to show some degeneration because the maximum cycle load was still being increased. During these final seven cycles, several permanent crimps in the plates developed. These were caused by the large compression buckles. The tears in the fish plates had also extended slightly and were now generally in the order of 25 to 50 mm in length.

A review of the complete hysteresis curve for all 28 cycles, Figure 5.2, indicates from the general profile of the curves that the structure did not behave identically in both loading directions. The structure appears to have been stiffer when loaded in compression. A maximum deflection of over 17 mm was achieved during the final tension loading cycles, while the maximum compressive load applied during the cyclic phase produced a maximum deflection of only 13 mm. This difference in the behaviour of the specimen meant that the displacement ductility factor would depend on the loading orientation considered. If first yield is assumed to have occurred at a deflection between 2.5 and 3.0 mm (taken from observations of the hysteresis curve), then the deflection ductility factor at the maximum load levels reached in this test would vary from a minimum of 4.3 (compressive loading) to a maximum of 6.8 (tensile loading). These values are comparable to the deflection ductility value of 6 suggested by Popov (6) for structures in seismic

regions. It is likely that the specimen could have developed even higher ductility factors had the cyclic test not been limited to a maximum load of 4000 kN.

Figure 5.7 is a picture showing the south face of the west panel. The dark cross on the west panel was that portion of the panel not whitewashed in order to allow for the measurement of the profiles of the buckled shapes. The segments of the cross were perpendicular to the expected orientation of the tension fields. Also visible in Figure 5.7 are many of the permanent crimps that developed during the cyclic loading. Sharp buckles in the panel corners are clearly visible, but the finer yield lines are not. Figure 5.8 is a picture of the south face of the east panel. Again many of the permanent crimps and buckles are apparent, as well as the weld tear between the centre beam and the fish plate at the top inside panel corner.

### 5.2.3 Beam-to-Column Joint Rotations

The rotations of the top outside joints were monitored during the test by a pair of manually operated rotation measuring devices. The rotations recorded at these joints are plotted in Figure 5.9. The rotations measured at the two joints are quite similar, as expected, since the specimen was symmetrical about its centre. The lack of data below a load of 1900 kN was due to problems encountered with the rotation measuring devices. For loads higher than 1900 kN, measures were taken to correct the problems encountered.

Unfortunately these corrective procedures resulted in the loss of the neutral rotation position, that is, the original orientation of the joint prior to loading of the structure. This meant that only average rotations could be determined. Figure 5.9 is therefore the plot of the average load versus the average rotation.

### 5.3 Monotonic Loading Test

As noted earlier, the capacities of parts of the loading system limited the maximum cyclic load that could be applied to 4000 kN. The capacity of the testing machine, however, was 6000 kN. Therefore, following the application of the 28 cycles of load the loading arrangement was revised so that the full capacity of the testing machine could be used. It was possible to apply this load in only one sense, compression.

It was observed that the vertical deflection of the system had reached a relatively large value during the cyclic loading and it was considered that the continued presence of the prestressing rods (see Figure 3.2) could be expected to result in clearance problems prior to ultimate load. Therefore, the rods used to apply the compressive load to the columns were removed. This removal of axial load meant that the two phases of the test were not directly comparable, since the nature of the applied loads had changed somewhat.

Figure 5.10 is a plot of the monotonic load versus deflection curve. The initial portion of the response was obtained by plotting the peak compressive loads found during the cyclic loading test. Note that there appears to be a slight increase in strength when comparing the two curves at the point of the maximum cyclic load. This increase in capacity was probably due to the removal of the axial column loads prior to the start of the monotonic loading phase. This slight increase would tend to indicate that the effect of the axial column load acting through the displaced distance ($P - \delta$) had only a minor influence on the structural behaviour during the cyclic loading phase.

In the monotonic loading phase, the structure was loaded to the capacity of the testing machine, over 6000 kN. A maximum midpoint deflection in excess of 70 mm was reached. However, had the structure been loaded in tension, a joint failure probably would have occurred prior to reaching this maximum load. This is a possibility since the bearing capacity of the bolted connections were based on the structure having a maximum capacity of only 4000 kN. Nevertheless, the specimen displayed very good ductility.

At a load of 5200 kN, the top outside beam-to-column connections developed a series of inclined yield lines, Figure 5.11. Upon dismantling the specimen later, it was observed that these yield lines were caused by bearing of the bolts on the webs of the beams at locations approximately perpendicular to the yield lines. Figure 5.11

also shows that the columns are now bearing on the beams; initially, there had been a three to four millimetre gap between these two members.

After completion of the monotonic loading test, it was observed that the weld and plate tears in the fishplates had lengthened, but only to a minor extent. There were also a few new weld cracks observed. The major tears all occurred in the top panel corners. Three of the four tears were similar in configuration to the one shown in Figure 5.12. The figure is a photograph of the top outside corner of the west panel. The tear appears to have been caused by the backing plate, used in the connection of the two mutually perpendicular fishplates, shearing the fishplate. The length of this tear was approximately 55 mm. Two smaller cracks in the adjacent welds were also noted. Figure 5.13 shows the other weld tear that was observed. It occurred at the top inside corner of the west panel. In this case, it appears as if the tear was initiated by the incomplete square groove weld and then continued by developing the vertical tear in the fishplate. The length of the groove weld tear was approximately 40 mm and the vertical tear 25 mm. Another weld crack extended for 55 mm at the base of the panel-to-fishplate fillet weld. All of these corner fractures appear to have been caused by the very sharp buckles that occurred in these locations. These buckles appeared to be the result of joint slip and joint rotation.

Figure 5.14 is a photograph of the specimen following its removal from the testing machine. Note that the buckles are now clearly visible and that the orientation of the buckles and the orientation predicted by the dark cross is similar.

**5.4 Buckle Profiles**

Periodically, the profile of the west panel buckled shape was measured along the cross shown in Figure 5.14. The length along which the profiles were taken was 1.8 metres. A progression of the buckles which formed under compressive loading during the cyclic loading test is shown in Figure 5.15. The initial buckle profile was taken after the preload applied to the columns had been increased to 1023 kN. The buckled shape for the cyclic test phase consisted of a two wave length buckle that increased in amplitude with increased load. The profile of the buckle that occurred under tension loading was only recorded initially and at a load of 1500 kN. It is shown in Figure 5.16. Note that the amplitude of the buckles was similar to those measured at the same load level during the compression cycle.

The profile of the buckled shape developed during the monotonic loading test was measured on only one occasion, at the end of the test. The profile shown in Figure 5.17 is a three and one half wave length buckle. The point at which the buckled shape changed from the double wave length configuration was, unfortunately, not observed.

## 5.5 Strain Gauge Data

As described previously, strain gauges were mounted on the boundary members and on the panels. At gauge location 10,(Figure 3.6) one of the six strain gauges developed an electrical short early in the test. No data from this location was used. The gauges located at the top of the west panel were strongly influenced by their proximity to the boundary members and provided very erratic data. This data will also not be reported. The data from all of the boundary member gauges appears to have been quite consistant.

After examining the output from the strain gauges to verify that all of the gauges were functioning properly, the strains measured across the sections were used to determine an axial load and a moment at the section. These results will be discussed later and compared with predicted values.

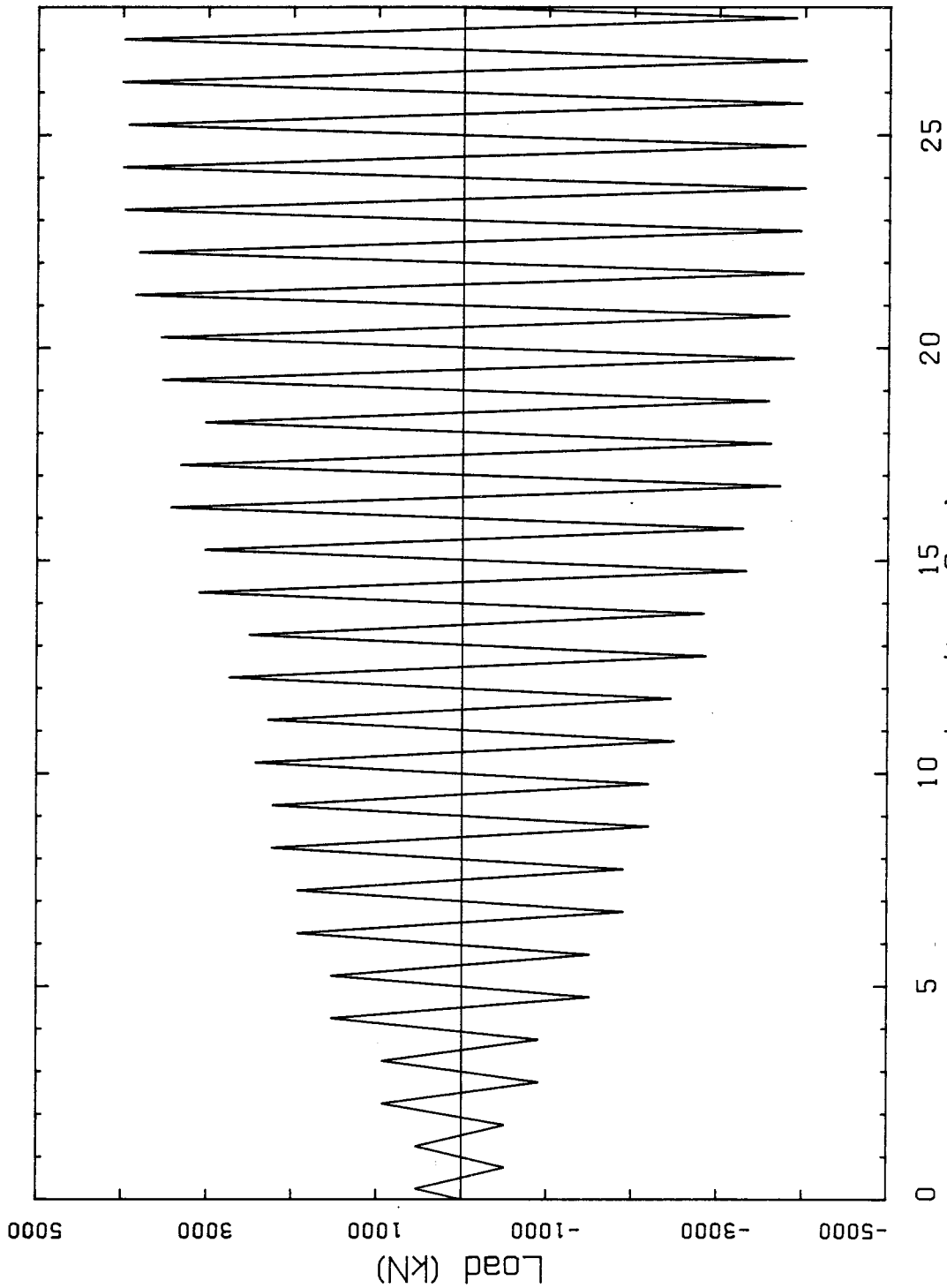


Figure 5.1 Cyclic Loading Sequence

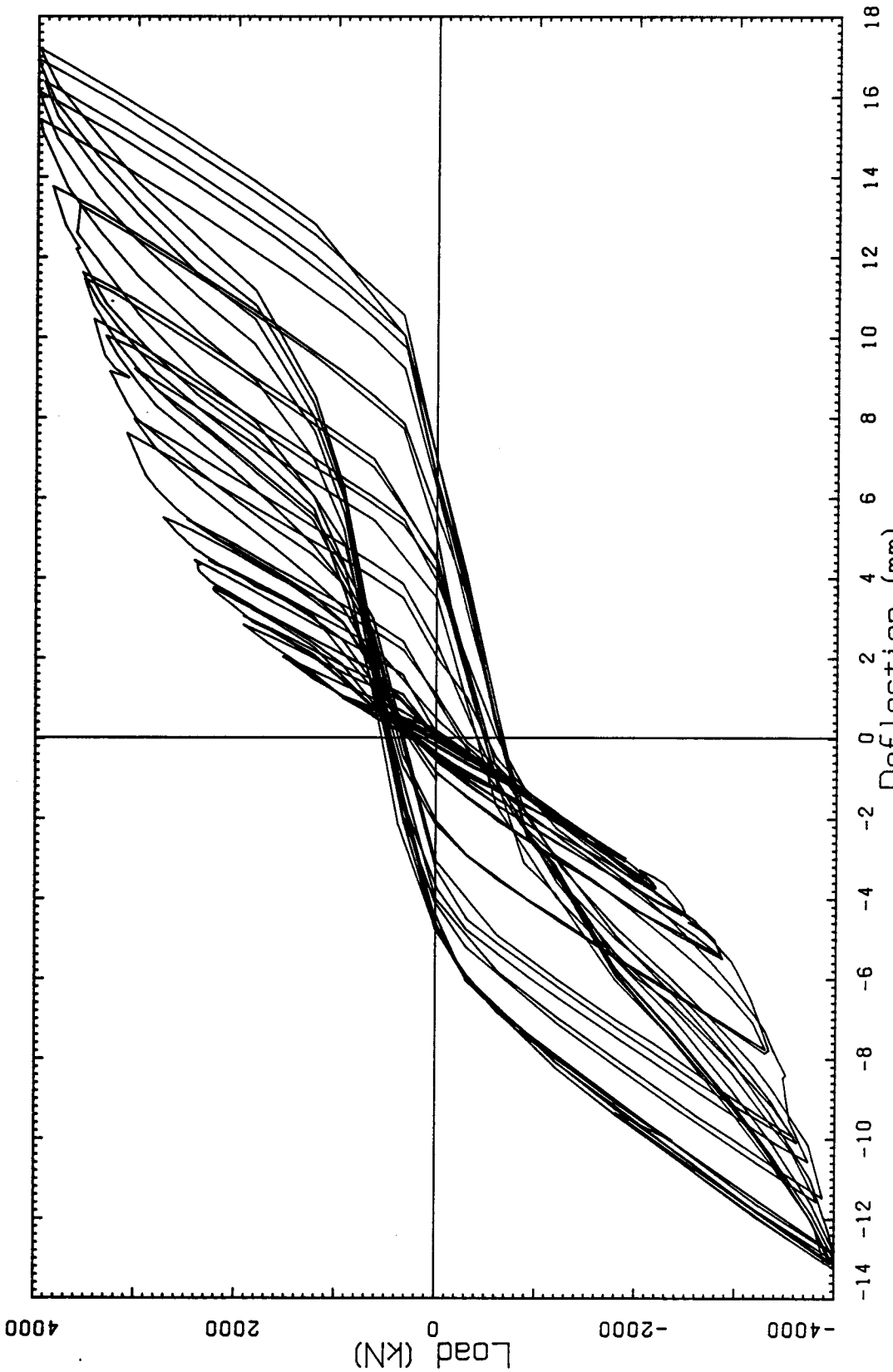


Figure 5.2 Complete Hysteresis Curve

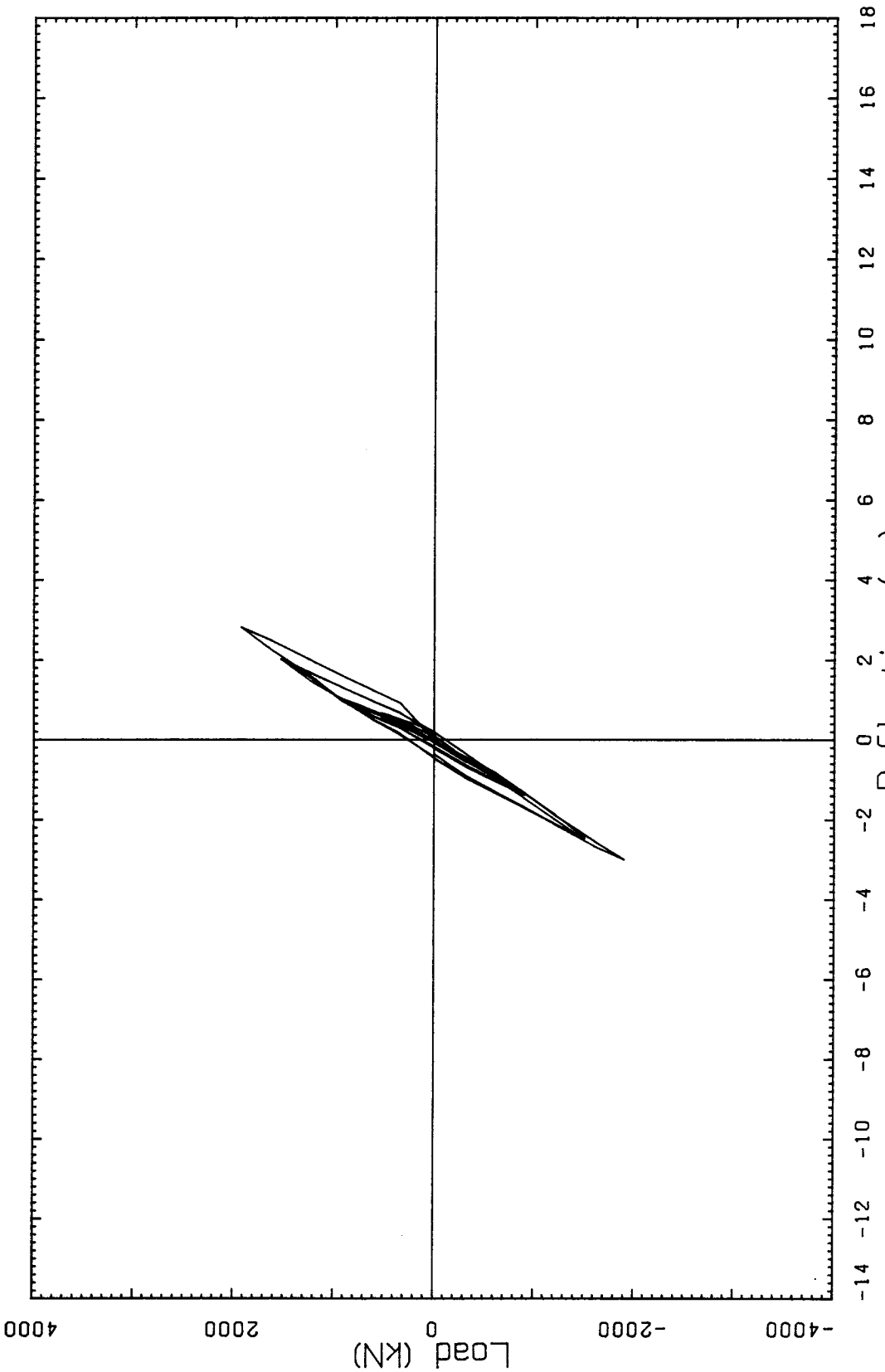


Figure 5.3 Hysteresis Curve - Cycles 1 to 7

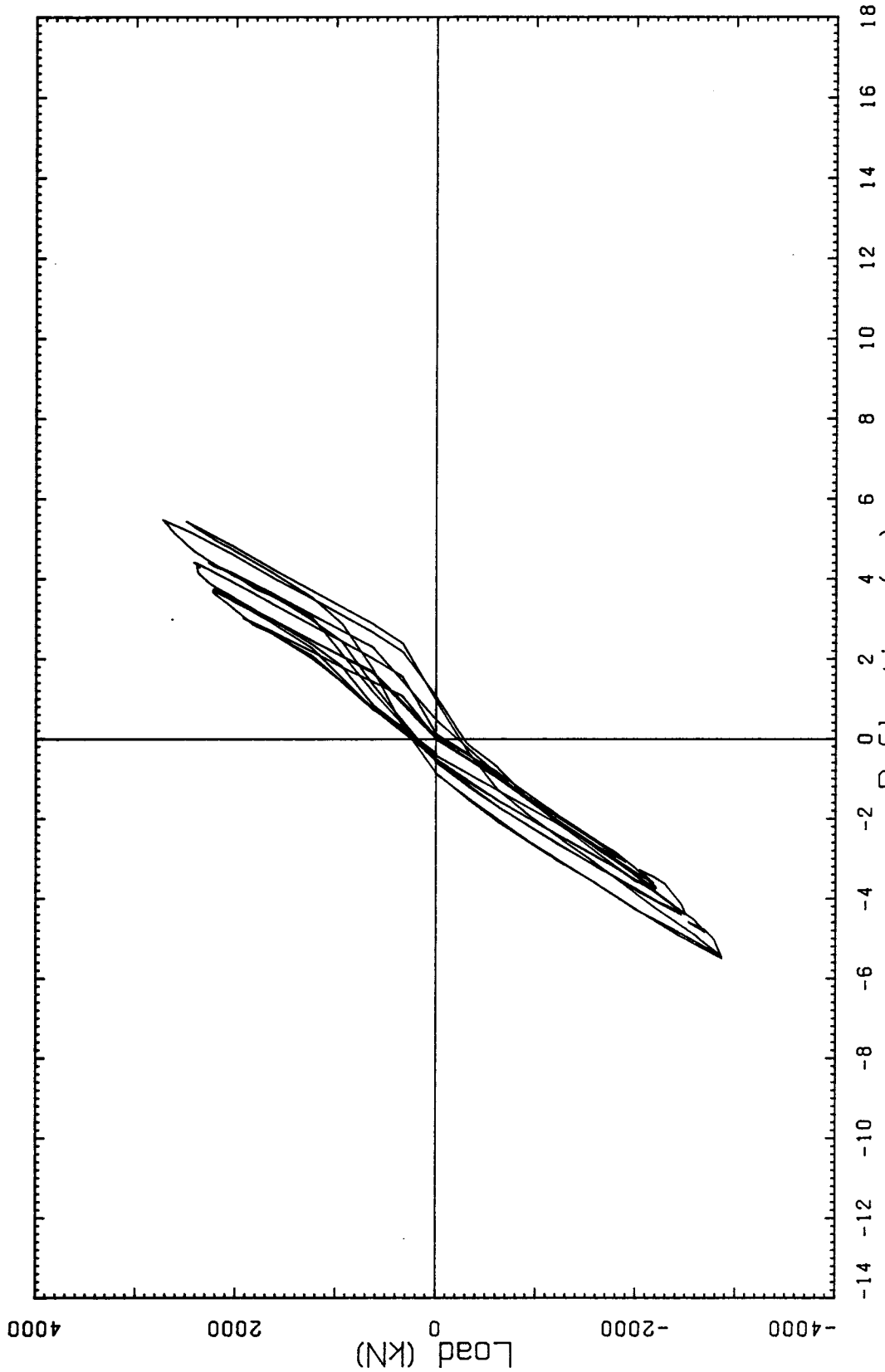


Figure 5.4 Hysteresis Curve - Cycles 8 to 14

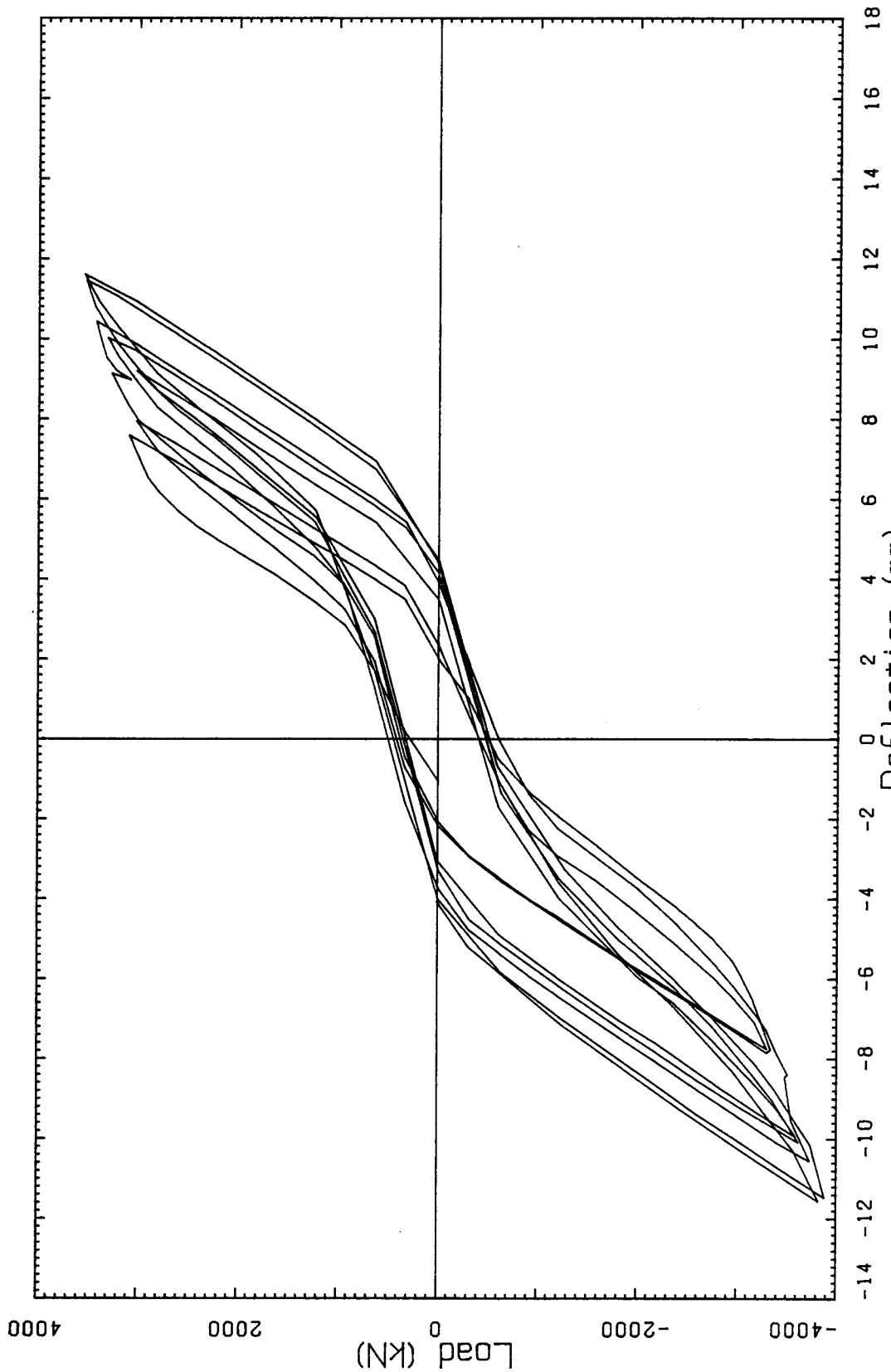


Figure 5.5 Hysteresis Curve - Cycles 15 to 21

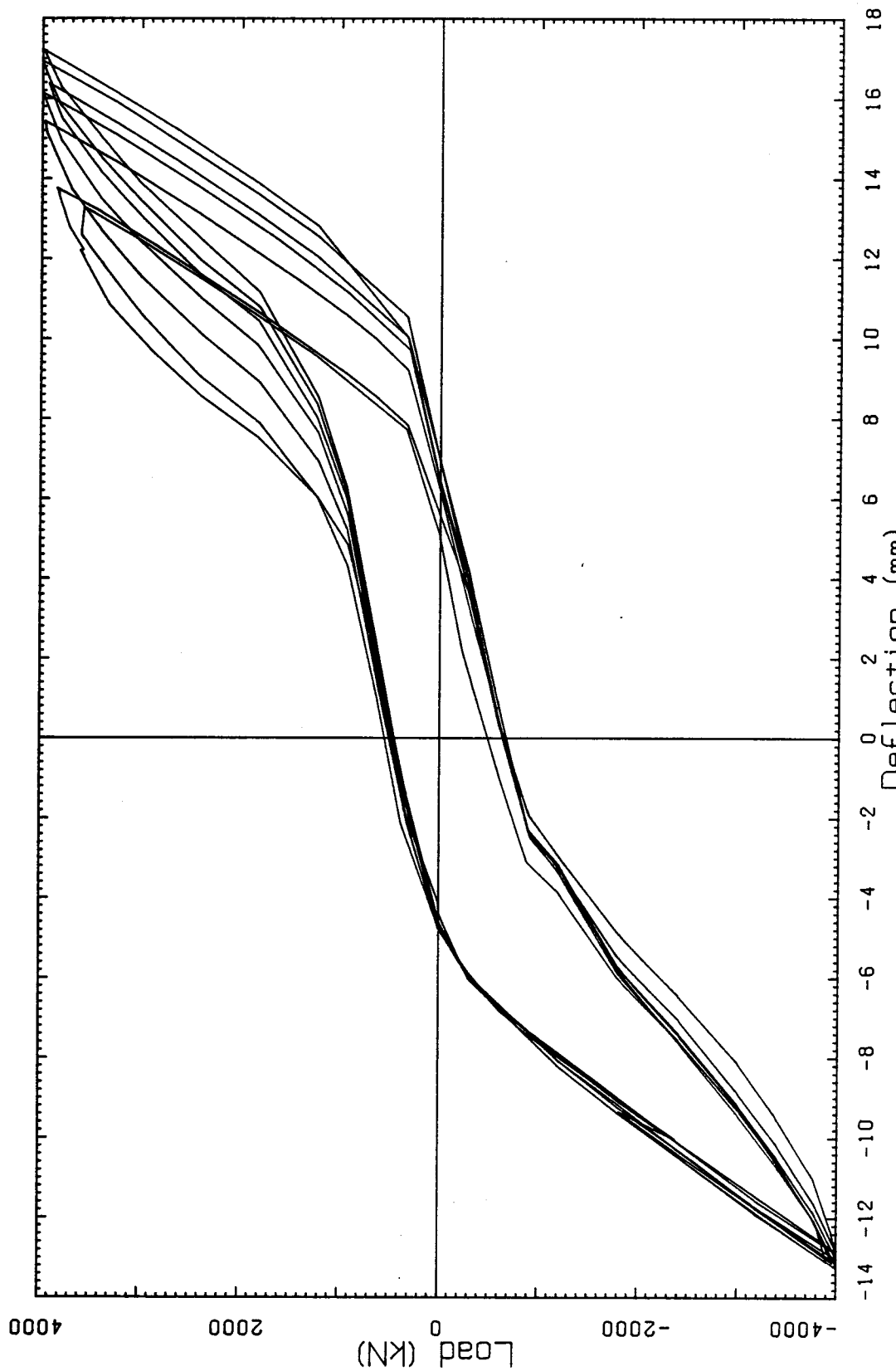


Figure 5.6 Hysteresis Curve - Cycles 22 to 28

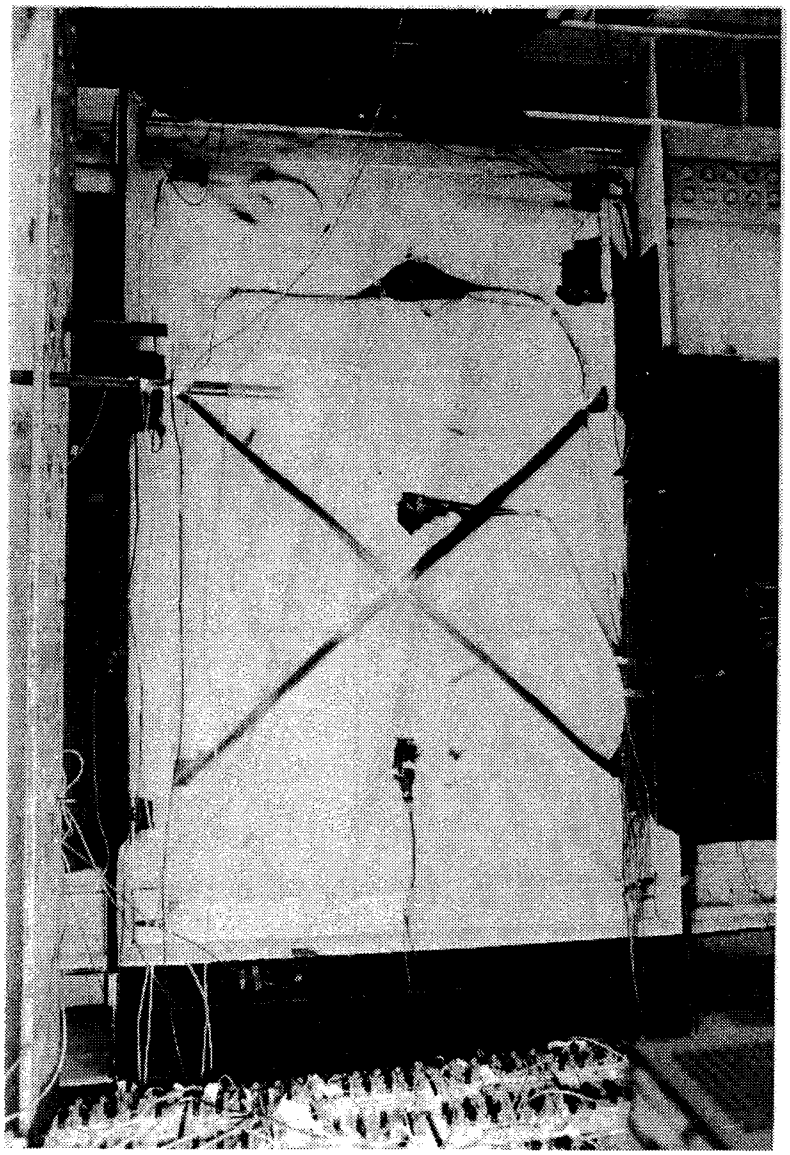

Figure 5.7 South Side of West Panel

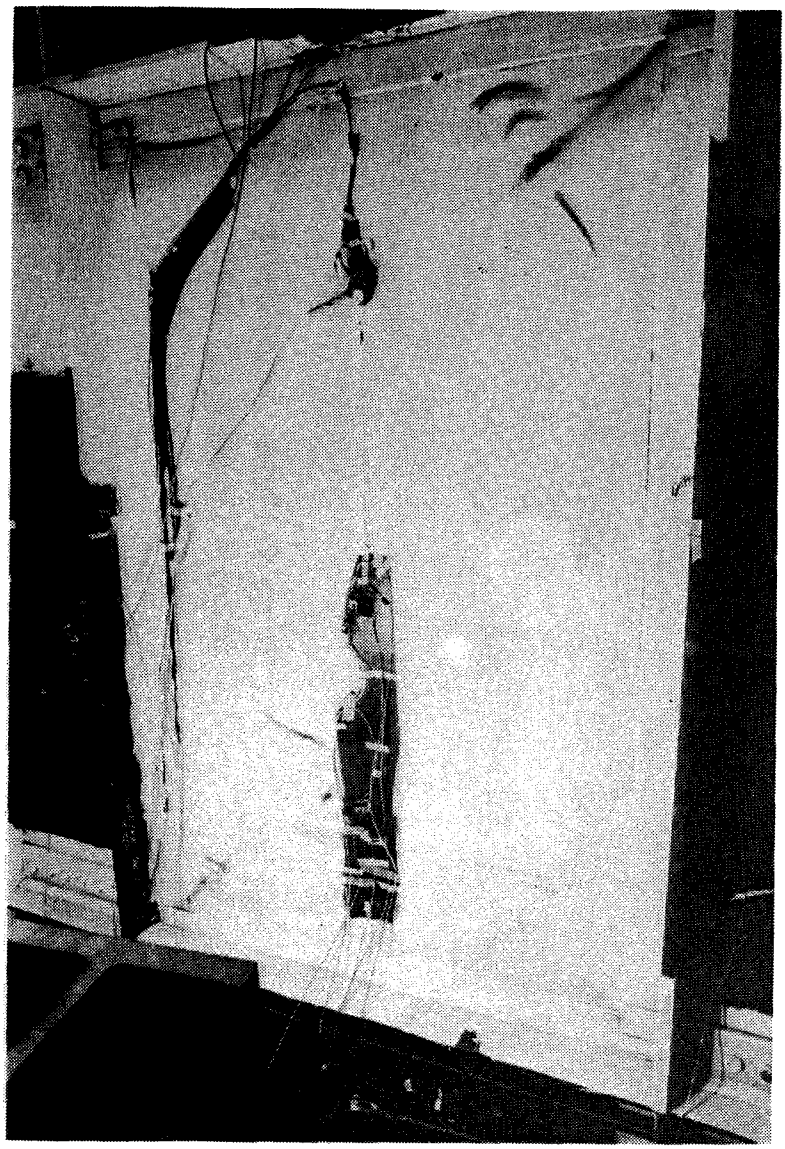

Figure 5.8 South Side of East Panel

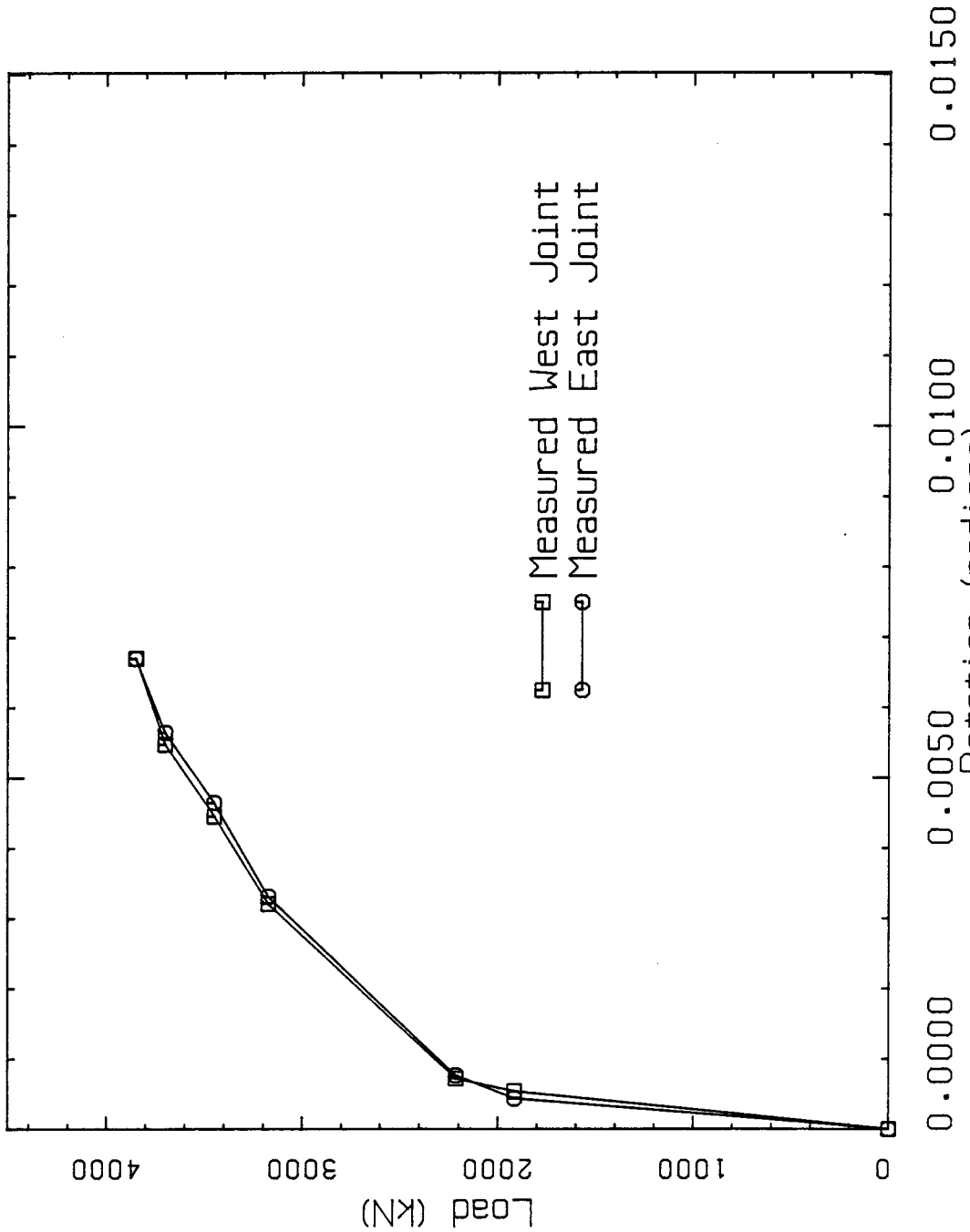


Figure 5.9 Observed Joint Rotations

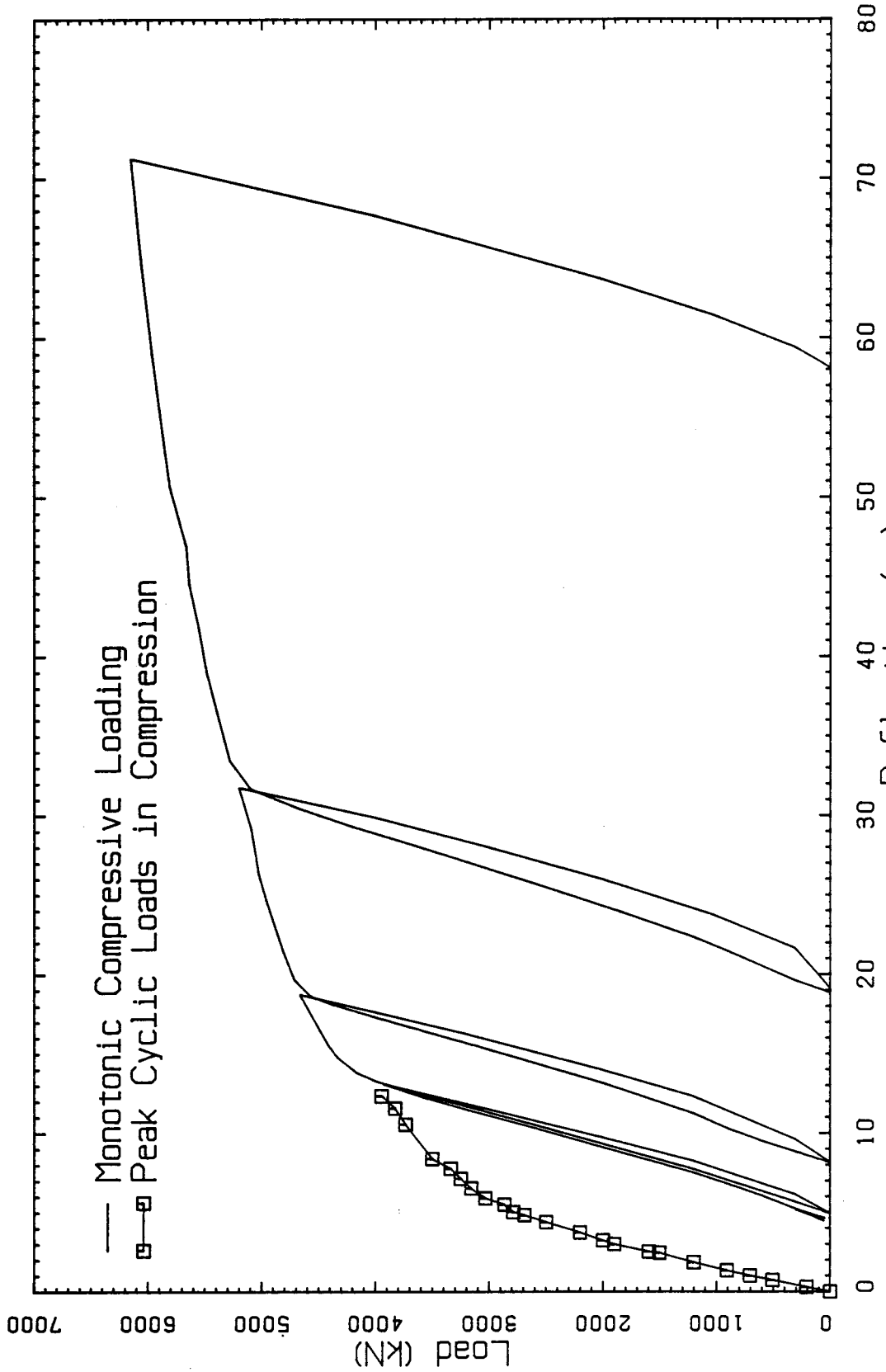


Figure 5.10 Monotonic Load versus Deflection Curve

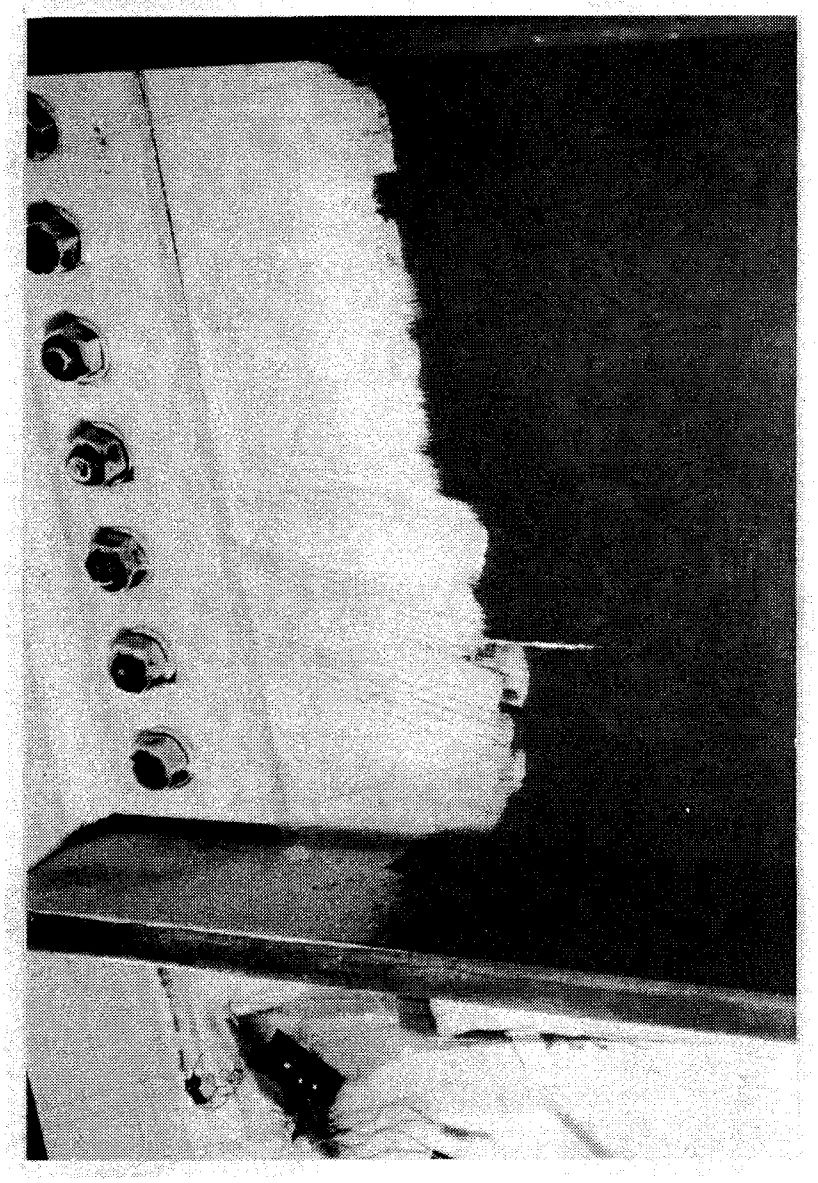

Figure 5.11 Top Outside Beam-to-Column Connection

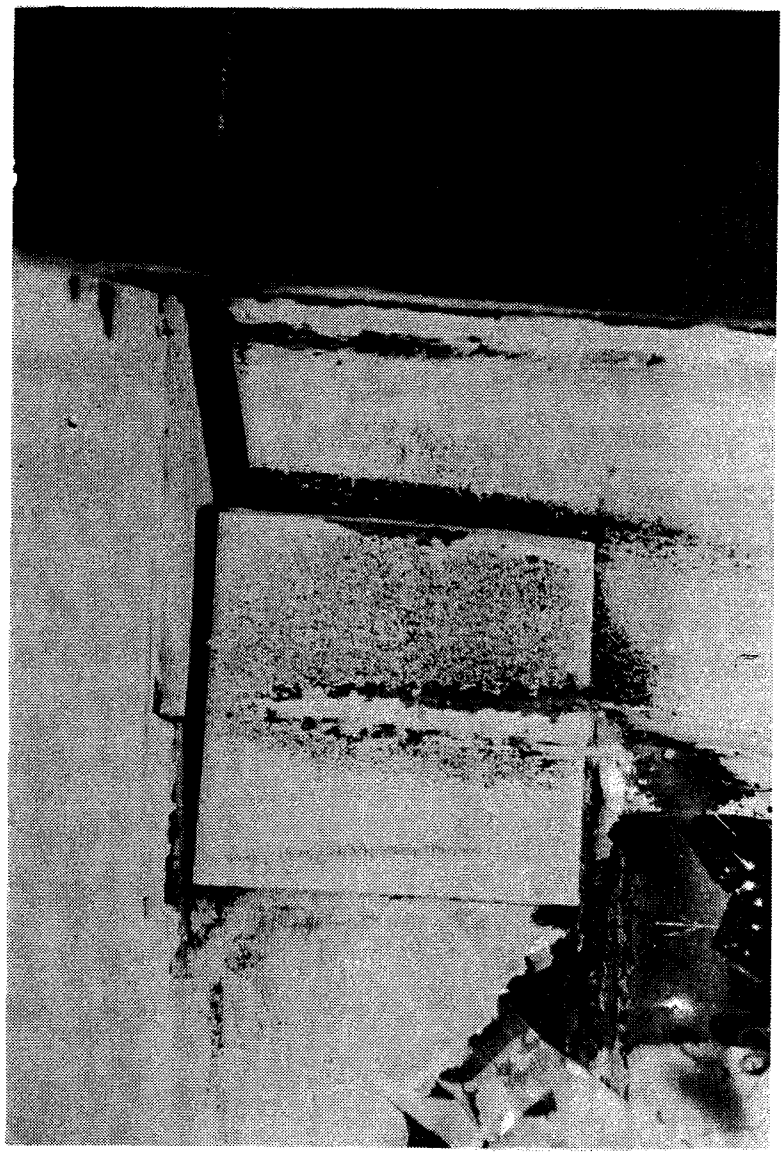

Figure 5.12 Fish Plate Tear in Top Panel Corner

Figure 5.13 Fish Plate Tear in Top Inside Panel Corner

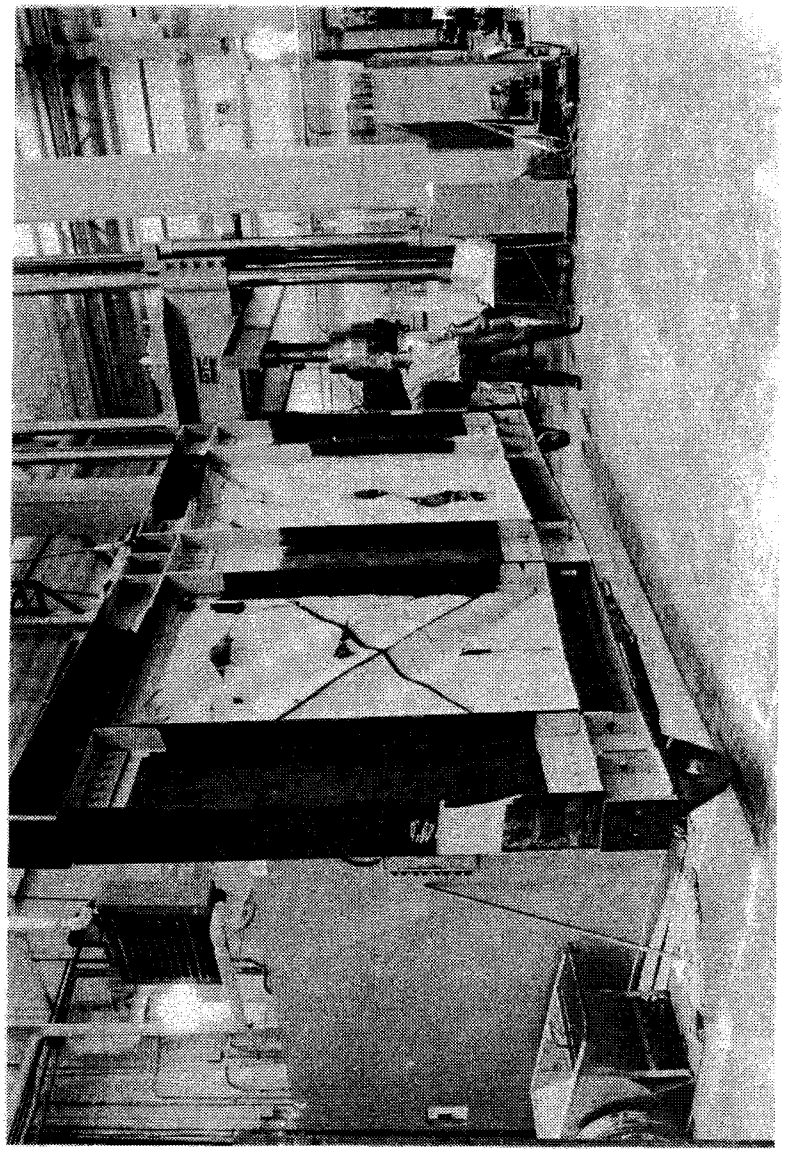

Figure 5.14 Specimen After Completion of Testing

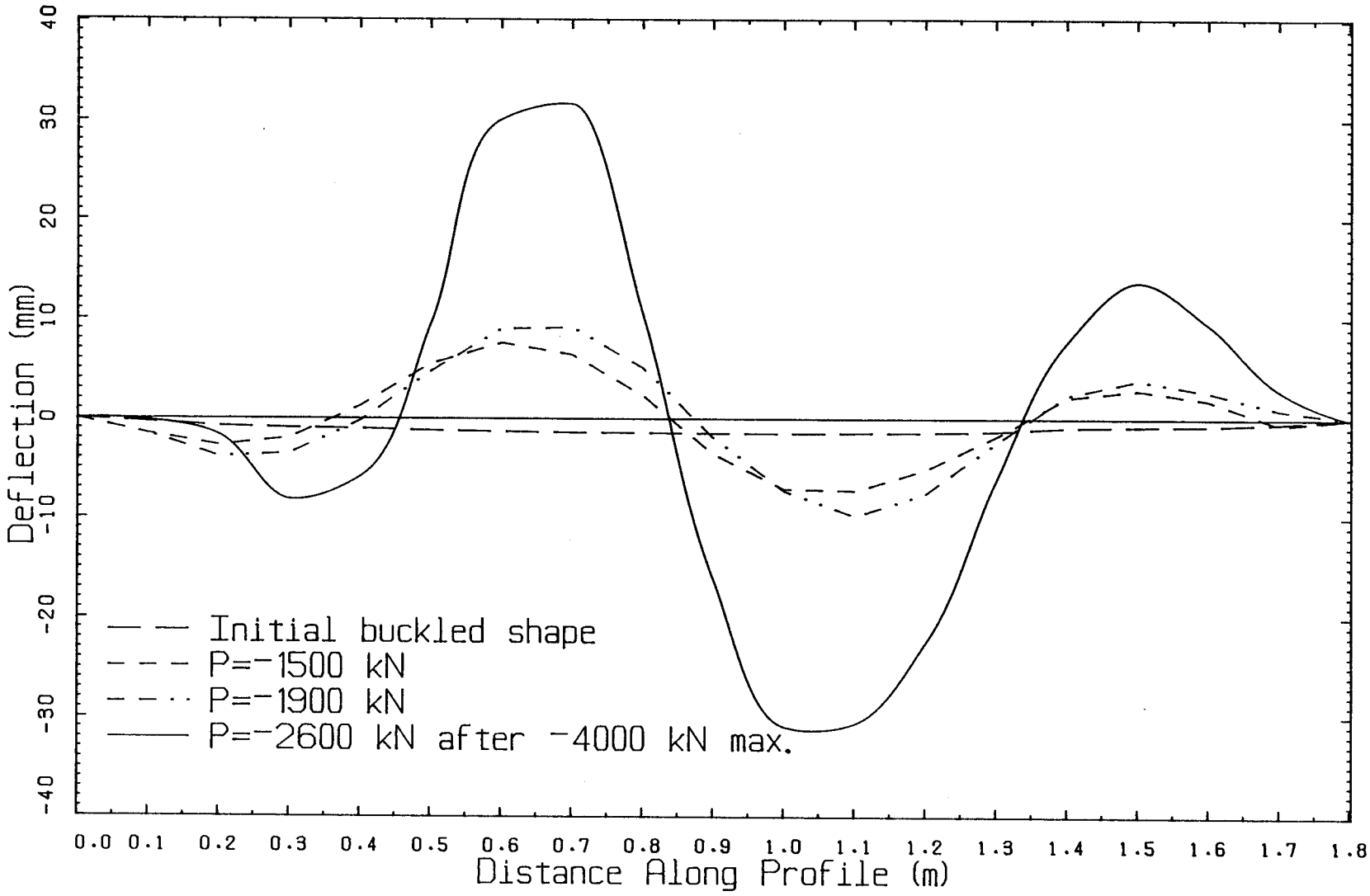


Figure 5.15 Buckle Profiles for Compressive Loads

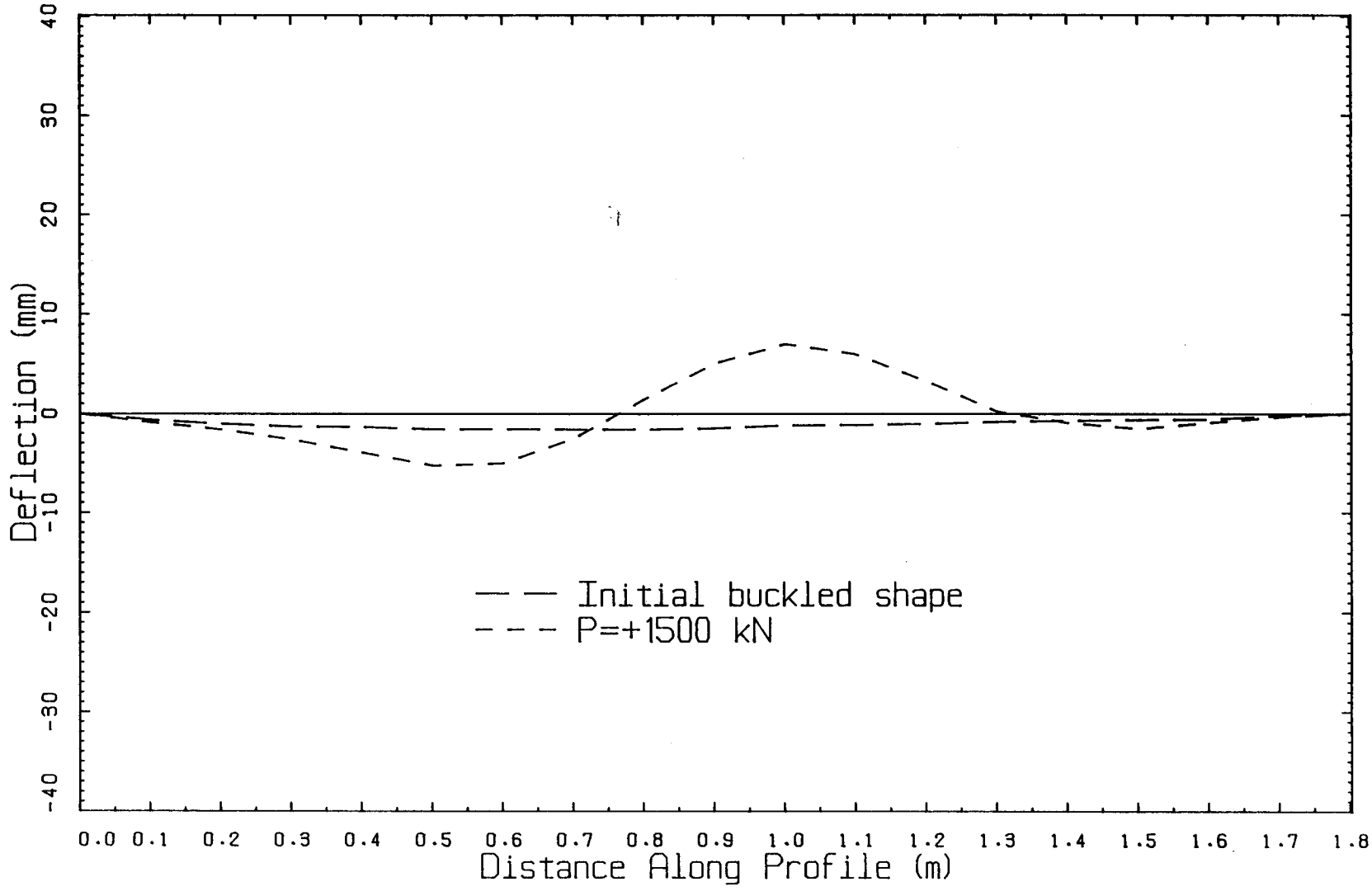


Figure 5.16 Buckle Profiles for Tensile Loads

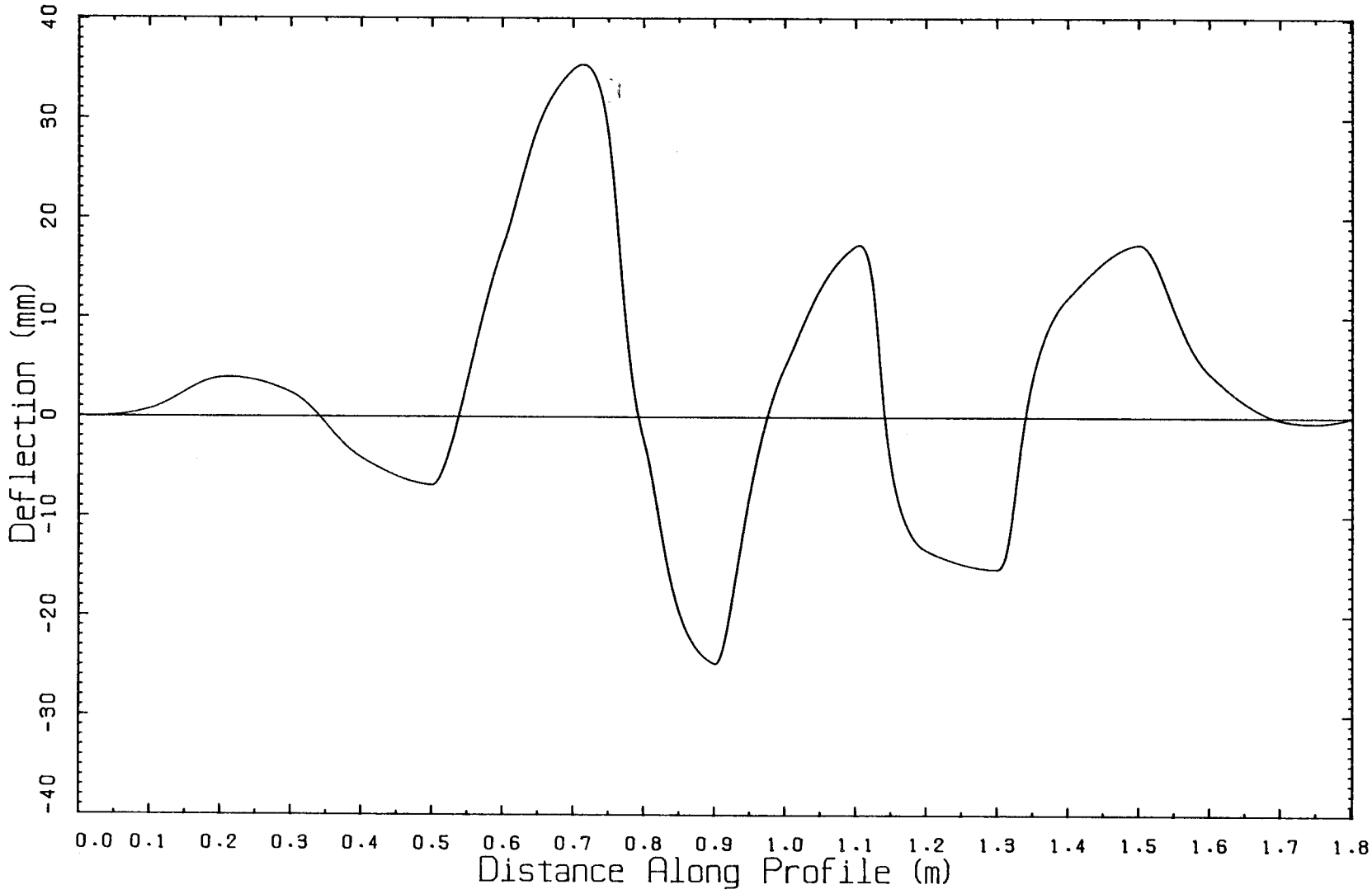


Figure 5.17 Final Buckle Profile

# 6. COMPARISON OF EXPERIMENTAL AND ANALYTICAL RESULTS

## 6.1 Load versus Deflection Behaviour

When comparing the results of an experimental test with the response predicted by any analytical method, it is recognized that the boundary conditions of both the structure and the individual members of the structure can have a significant influence on the behaviour. When testing specimens that utilize actual structural connections, these boundary conditions are hard to define. In the case of the steel plate shear wall test conducted, both the bolted beam-to-column connections and the pinned reaction points introduced areas of uncertainty as to the actual restraint provided. Complicating the problem was the effect of the strains induced as a result of the panel welding. The effects of all of these factors had to be addressed in order to develop a representative load versus deflection response.

The welding-induced strains in the panels were not measured directly. However, by examining the strains induced in the columns and the amount of compressive strain introduced into the panels after the axial preload in the columns had been increased, an estimate of the initial panel strains was obtained. This estimate of the average increase in compressive strain due to the welding process translated into an average tensile force per panel of 654.5 kN. Dividing this force by the total area of the panel (including the fish plates) indicated that the average

stress induced in the panels by the welding of the web plate to the boundary members was about 76.1 MPa. The average compressive strain induced in the panels because of the application of the column preload was measured by the rosette strain gauges. This corresponded to an average stress in the panels of 26.2 MPa. The difference between the two values, approximately 50 MPa, is considered to be a reasonable estimate of the net stress induced in the panels.

Another estimate of the induced panel strains was obtained by comparing the strains measured in the panels after the final column preload with the strains measured in the centre of the east panel when it was observed that the panel was carrying little or no load. These values produce an estimate of the initial welding induced stresses of 25.2 MPa. This estimate is considered to be less reliable than that obtained on the basis of measured column strains.

### 6.1.1 Compressive Loading

The analytical determination of a load versus deflection diagram was done initially for the compressive loading case. The plane-frame model used in the final analysis was slightly different from the one used in the preliminary analysis, having one additional member at the reaction point, Figure 6.1. This model allowed for the physical eccentricity between the centre of the column and the centre of the pinned reaction to be taken into account. The determination of the load versus deflection curve

involved an examination of the various possible joint boundary conditions and the possible states of initial stress in the panels.

The analytically determined load versus deflection curves for the various cases were developed by plotting the difference in the calculated deflections at point B and point D versus two times the given applied load at point A. (These points are identified in Figure 6.1) This is consistent with the measurements taken to obtain the load versus deflection response of the test specimen.

To start the analysis process, a load corresponding to the column preload used in the test frame (1023 kN) was applied directly to the column members in the initial plane frame output file. The initial lateral loading increment used was well below the load at which first yield in the structure would occur. Thus, the application of the column preloads had no effect on the stiffness of the structure. Subsequent plane frame output files were generated, each representing the structural response for each increment of load required to yield one more member in the shear wall model. As noted earlier, the analysis program modified both beam and column section properties that were affected by yielding as a load increment was applied. The output files were then superimposed to generate the complete analytical response.

The first two conditions examined were the cases where the structure had either fully pinned or fully fixed

beam-to-column joints. The yield strength of the panel material used in this analysis was the same value found in the ancillary tests, that is, 242.5 MPa. The two response curves for these conditions are shown in Figure 6.2. The actual response obtained during the test is also shown in this figure. Note that the predicted curves bound the actual behaviour and that the case in which the beam-to-column joints are assumed to be pinned results in a conservative estimate of both the structure stiffness and ultimate load.

A third analytical curve, also shown in Figure 6.2, is an attempt at producing a load versus deflection curve more closely representative of the actual behaviour of the specimen. To develop this behaviour it was assumed that the welding process and the final preloading of the columns resulted in a 50 MPa stress initially present in the panels and that a 1371 kN force was present in the columns. This column load was an average load value derived from the strains measured at the start of the test at the four gauge locations on the columns. The beam-to-column joints were assumed to be fixed connections because it was felt that after the bolted joints slipped the beams and the columns would bear against each other, thereby restraining rotation. The initial 50 MPa stress present in the panels was taken into account in the analysis by simply reducing the panel yield strength from 242.5 MPa to 192.5 MPa.

Another analytical load versus deflection curve was generated for the case where the initial panel stress was

assumed to be 25 MPa. This curve was located between the cases where the panel yield was assumed to be 242.5 MPa and 192.5 MPa. Since the curve did not appear to represent the test data and since the 25 MPa stress level was considered to be less reliable than the 50 MPa value used above, it was not included in the figure.

The equivalent monotonic load versus deflection response, for the load range attained in the cyclic loading phase, was produced by plotting the peak cycle loads and their corresponding deflections. Where the previous peak cycle load was greater, in absolute terms, than the one under consideration, the smaller load was ignored. As can be seen in Figure 6.2, the analytical load versus deflection curve developed assuming an initial 50 MPa stress gives a good prediction of the actual test results.

### 6.1.2 Tension Loading

For the case of tension loading, the configuration of the plane frame model used was different from the one shown in Figure 6.1. The tension bars were inclined at 44.0 degrees in the opposite direction to that shown. Figure 6.3 shows three analytical load versus deflection curves developed for the case of tension loading.

Based on the experience gained in developing the response for the compression loading case, all of the analytical curves shown in Figure 6.3 were developed using the assumption that the yield strength of the panel material

was 192.5 MPa and that the column axial load was 1371 kN. One of the three curves uses the assumption that the beam-to-column joints are pinned and another that the joints are fixed. Upon comparing these two curves with the experimentally obtained load versus deflection curve, it would appear initially that the behaviour is similar to the pinned joints case.

However, a closer examination of the analytical results and a comparison with strain gauge data indicated that the forces measured in the bottom column member were inconsistent with those predicted. The analysis predicted that a tensile force would be developed in the lower column member for this case when a tensile force was applied to the structure. In fact, a compressive force was measured in this member during this loading case. This seemed to indicate that lateral restraint was not being provided at the reactions, thereby requiring the horizontal components of the tension field to compress the column to maintain equilibrium. A calculation based on the assumption that horizontal displacement is possible at the reaction shows that movement of 2.6 mm could occur at point C (Figure 6.1). This corresponds to approximately the difference in the diameters of the pin and clevis hole at that location. Thus, it is reasonable to assume that lateral restraint was not being developed at the reactions.

The structure was then reanalyzed assuming that the support at point C permitted horizontal movement but no

vertical movement. It was also assumed that the beam-to-column joints were fixed until the theoretical slip load was reached, at which point they were changed to pinned joints. This change in restraint was an attempt at duplicating the observed rotations at the top outside corners. The result of this reanalysis is also shown in Figure 6.3. In the higher load ranges, above about 2000 kN, this analytical curve and the experimental curve show very good correlation. The measured load versus deflection response for loads less than 2000 kN was much stiffer than that predicted. This is possibly the result of the welding induced strains in the panels. If the beam-to-column bolted joints had been assumed to have been pinned joints, a conservative estimate of the structure stiffness and ultimate load would have been produced again.

## 6.2 Force Distribution in Boundary Members

The distribution of forces in the boundary members, obtained by calculations using the observed strains at the seven locations on the boundary members (Figure 3.6), is another way of checking the accuracy of the analysis. A comparison of the forces calculated this way and the forces predicted by theoretical analysis is also useful in determining the validity of the boundary conditions assumed.

Figure 6.4 is a plot of the relationship between the overall load applied to the structure and the axial load in the top (column) members. The calculated axial load at the

two locations was quite similar and the theoretically predicted axial load is reasonably close to these curves. Also note that the theoretical response curve does not have the same initial slope under tension and compression loadings. The cyclic loading of the specimen was obtained by reversing the direction of the loads at the fixed loading points. As such, the response of the frame to the loading will not be the same in the two directions. The theoretical response is linear in both loading directions until first yield of a frame or panel member occurs. After this point, the slope of the applied structure load versus the member axial force curve varies as subsequent members yield.

Figure 6.5 shows a comparison between the theoretically predicted axial load and that calculated from measured strains for the lower (column) member for the full range of maximum cycle loads. This member was strongly affected by the loading arrangement, resulting in a dramatic difference in the slopes of the curves in both loading directions. The theoretical and the calculated curves are generally in the same sense for the tension loads, indicating that there was sufficient free movement available in the pins to prevent lateral restraint from being developed. For the compressive loads, it appears that the lateral restraint in the supports did not develop until a load of about 1000 kN. At that point the plots of the observed axial loads change significantly. The lower column member attracted more compressive load than predicted by the analysis for loads greater than 1000 kN.

Figures 6.6 and 6.7 show a comparison between the theoretically predicted axial load in the three vertical (beam) members and that calculated using measured strains for the maximum cycle loads. In all three cases the theoretical curves are similar in slope and magnitude to the calculated values. The slopes of the theoretical curves in the two loading directions again are not identical, as expected.

Comparisons of the calculated moments based on measured strains and the theoretically predicted moments at the monitored locations are shown in Figures 6.8 through 6.11. The comparisons show that the level of correlation between the theoretical and the calculated moments varies considerably. The influence of the size of the members, the fixity of the connections, the size of the connections, the lateral resistance of the supports and the assumptions made in the analysis all affect the level of agreement.

A comparison of the theoretically predicted moments with the calculated moments in the top (column) member, Figure 6.8, shows good agreement for only the lower compressive load levels, the correlation between the theoretical and observed moments for the remainder of the loads applied to the structure is poor.

Figures 6.9 and 6.10 display comparisons between the moments calculated from observed strains and the theoretically predicted moments for the bottom (column) member and the outside (beam) members, respectively. The

general directions of the curves are similar, but the slopes and the magnitudes of the curves differ.

Figure 6.11 shows a comparison of the theoretically predicted moments (equal to zero) and the moments calculated on the basis of observed strains at the centre beam gauge location. The calculated moments indicate that bending of the beam did occur and that the right panel appears to have attracted more load. (Positive bending is simply a result of the sign convention used.)

A correlation between the calculated moments and the theoretically predicted moments is not as critical a criterion as the correlation between the calculated and predicted axial forces. The moments calculated using observed strains are highly sensitive to boundary conditions (effects of joint fixity, joint size, and member size), while the axial load distribution in the members is not influenced by these factors to the same extent. Since the comparisons of the calculated axial loads and the predicted axial loads was favourable in almost all cases, it can be stated that the internal member forces predicted by the inclined tension bar model generally validate the model.

## 6.3 Stress Distribution in Panels

The measured strains in the panels at the nine locations were converted into stresses using the material properties identified by the coupon tests and the conventional plane strain relationship

$$\sigma_x = \frac{E}{1 - \nu^2} (\epsilon_x + \nu \epsilon_y) \qquad (6.2)$$

where:

$\sigma_x$ = stress in the x direction

$\epsilon_x$ = strain in the x direction

$\epsilon_y$ = strain in the y direction

Because the initial state of strain in the panels was unknown, reliable determination of the actual magnitudes and orientation of the principal strains is difficult. This means that an accurate comparison with the predicted strains and orientations should not be expected.

Figures 6.12 through 6.16 show the orientation and the magnitude of the principal stresses, obtained using strain gauge measurements, for a series of applied loads. These applied loads vary between two extreme cases, from an applied tensile load of 3324 kN to an applied compressive load of 3248 kN. At both of these extremes the strains measured in the panels indicate that yielding had occurred at all gauge locations. The magnitudes and orientations of the predicted stresses are also plotted on Figures 6.13 through 6.16. It was considered that at the higher loads the influence of the initial welding-induced strains would be minimized, therefore providing a condition more favorable for comparison.

Figure 6.12 shows the initial state of stress measured in the panels after the final increase in the column preload. These observed stresses, however, are due only to

the final column preload. Since the strain gauges were installed after the installation of the panels, the welding induced stresses are not included in the stresses shown in Figure 6.12. If the welding induced stresses had also been included in the measurements, tensile stresses should have been indicated at all of the gauge locations.

Figures 6.13 and 6.14 show the distribution of the stresses at the tensile and compressive load levels at the load level at which first yield in a panel was determined from the strain gauge data. The yield stress of the panel material used for these comparisons is 192.5 MPa. This value accounts for the approximately 50 MPa tensile stress induced into the panels by the welding process that the measured strain values do not include. This value is also consistant with the yield stress used in the analysis of the structure.

For the tensile loading case, shown in Figure 6.13, the inclination of the tension field appears, on average, to have been larger than that predicted. The gauge locations at the top of the panel produced larger discrepancies than did the bottom gauge locations. For the most part however, reasonable agreement is still evident. Examining Figure 6.14 it can be seen that, for those gauges considered to be operating properly, the inclination of the tension field was close to the predicted angle of 44.0 degrees.

Figures 6.15 and 6.16 show the distribution of the panel stresses at higher loads. The orientation of the tension fields was again reasonably consistent with the

predicted value. The magnitude of the stresses determined at each of the gauge locations is at the yield stress or very close to it. At these load levels, theoretical stresses at all gauge locations should have reached the yield stress level.

In general, the orientation and the magnitudes of the observed stresses in the panels at the higher load levels correlate well with the predicted values. The exception being the group of gauges at location 12, centre of the west panel (see Figure 3.6), which were not functioning properly. Coupling the above observation with the good correlation observed in the comparisons of the observed and the theoretical boundary member forces and the good correlation in the overall structure behaviour, it can be stated that the inclined tension bar model is an accurate method for predicting the response of unstiffened shear wall panels.

## 6.4 Beam-to-Column Joint Rotations

The beam-to-column joint rotations observed during the test are compared with the theoretical beam-to-column joint rotations predicted by the plane frame analysis in Figure 6.17. It must be kept in mind that the measured rotations that are plotted in Figure 6.17 are an average of the rotations found in the two directions of loading. Since the behaviour of the structure was not identical in both loading directions, an accurate comparison of the results is again difficult.

Figure 6.17 shows the measured rotations and the rotations determined by the theoretical analysis for a structure loaded in either compression or tension and for the two possible extremes of beam-to-column joint conditions; fixed or pinned. The measured rotations are located between the predicted rotations for the two sets of boundary conditions. Initially, the slope of the measured joint rotation curve resembles the fixed joint cases. At a load of about 2000 to 2200 kN the response becomes much more flexible. At loads greater than this, it generally resembles the analytical response curves which assume that the beam-to-column connections are pinned. This type of behaviour is to be expected since the connections were designed as bearing connections and the applied loads produced forces in the connections larger than the frictional capacity of the connections. The greater the number of times the joints slipped, the more polished the surfaces became and the lower the rotational resistance. Polishing of the connection plate surfaces was observed after the specimen was dismantled.

## 6.5 Hysteresis Behaviour

The hysteresis behaviour of this shear wall test specimen is similar to the behaviour found by others in previous testing of steel plate shear walls (4,5). Differences in behaviour between the test reported herein and the previous tests are mainly due to the differences in

the buckling load of the panels and the effects of the frame stiffness. Because of these differences, some modifications to the theoretical hysteresis curve previously proposed by Mimura and Akiyana (5) were necessary to describe the experimental results presented earlier.

Comparing the hysteresis plot developed during this test, Figure 5.2, with the hysteresis behaviour of an unstiffened panel as reported by Takahashi, et al. (4), Figure 2.6, obvious similarities can be noted. Both plots display the characteristic degenerating pinched loop behaviour and both plots show that, when panels are reloaded to the same maximum load, the deflections generally increase while the area under the curve decreases. This also seems to agree with the theoretical hysteresis curve developed by Mimura and Akiyana (5). However, expanding the theoretical hysteresis curve developed by Mimura and Akiyana by several cycles, Figure 6.18, shows that the theoretical curve does not degenerate at a rate similar to that observed in the test, Figure 5.2. The deflection theoretically required to redevelop the tension field, CD, is much shorter than the deflection measured in the test. Also, this portion of the theoretical hysteresis curve has a zero slope. This results from the assumption that the boundary members provide no lateral resistance and is consistant with the previous Japanese tests. However, in this test the shear wall frame did contribute to the lateral stiffness of the shear wall and the observed slope in this region of the hysteresis

curve was not zero. This lateral stiffness, however, would still be small when compared to that provided by the tension field of the panel.

The influence of the frame stiffness on the overall stiffness of the structure can be seen in Figure 6.19, the final hysteresis cycle of the test frame. The portion of the curve covering the displacement required to redevelop the tension field has a slope of approximately 93 kN/mm. Also plotted in Figure 6.19 is the stiffness (70.6 kN/mm) of two pin ended columns alone (assuming the steel panel is absent). The beam-to-column connections are assumed to be pinned connections, because by the final cycle these joints had slipped several times resulting in reduced rotational restraint. The slopes of the two lines are reasonably similar with the difference possibly attributed to the uncertainty in the restraint provided by the bolted connections. In the early loading cycles these bolted joints were behaving more like fixed connections resulting in the slope of the curve in the redevelopment phase being greater in the earlier cycles than in the final cycles.

The theoretical hysteresis curve development proposed by Mimura and Akiyana (5) can be modified to incorporate the affects of the frame stiffness and the affects of the low panel buckling strength by making four basic assumptions:

1. The stiffness of the structure during the tension field redevelopment phase can be represented by the elastic stiffness of the framing members alone.

2. When a sufficient number of plastic hinges are produced in the boundary members to form a mechanism, the slope during the tension field redevelopment phase will be zero.
3. If the buckling load for a thin unstiffened panel is very low, then the deflection necessary to produce buckling is also very low and can be neglected.
4. The deflection required to redevelop the tension field is based solely on the amount of yielding experienced by the panels in each direction.

Figure 6.20 illustrates the development of a theoretical hysteresis curve for an unstiffened steel plate shear wall using these assumptions. When load is applied to the structure, the response will follow the monotonic load versus deflection curve past first yield to an arbitrary maximum load at point B. When the structure is unloaded from this point, the load versus deflection curve will unload elastically to point C. Applying load in the other sense, the panel must develop a tension field in the other direction. The deflection required for the tension field to develop is a distance CD' (derivation of this distance to follow). During this rebuckling deflection, the stiffness of the structure is equal to the elastic stiffness of the frame only. Once the tension field has reformed (point D), a linear transition is assumed to apply up to the point of negative yield, E. The formation of the hysteresis loops is then a continuation of the previous processes; yielding to

point F, unloading to point G, reformation of the tension field at point H, and a linear transition back to the point of the previous maximum tension, point B.

The deflection required to redevelop the tension field in any given cycle (distances CD' and GH' in the illustrative example of Figure 6.20) can be derived using the same assumptions made by Mimura and Akiyana, namely, that Poisson's ratio is effectively equal to 0.5 when yielding occurs and that the angle of inclination of the tension field is equal to 45 degrees. (The actual angle of inclination is generally very close to 45 degrees.) This deflection is given by the following expression:

$$\Delta_r = \Delta_1 + \Delta_2 - 0.5\,\Delta_2$$

or,

$$\Delta_r = \Delta_1 + 0.5\,\Delta_2 \qquad (6.3)$$

where:

$\Delta_r$ = deflection required to redevelop tension field

$\Delta_1$ = yielded deflection from previous cycle in the direction of loading

$\Delta_2$ = yielded deflection just completed in the opposite loading direction from that under consideration.

As shown in the equation preceeding Equation 6.3, the deflection required to redevelop the tension field is made up of two deflection components, $\Delta_1$ and $\Delta_2$, but is also influenced by the Poisson effect, in this case $0.5\,\Delta_2$. The

statement is then simplified as given by Equation 6.3. For the first hysteresis cycle in Figure 6.20, the deflections required to redevelop the tension fields are given by:

$$CD' = 0.5\ OC \tag{6.4}$$

$$GH' = OC + 0.5\ OG \tag{6.5}$$

Note that in Equation 6.4 there is no $\Delta_1$ term. This is because for the first loading cycle the yielded deflection from the previous cycle is equal to zero.

Using the relationships developed above, theoretical hysteresis curves were developed for two of the observed loading cycles obtained for the test panel. The theoretical hysteresis curves were developed using the above relationships, the load versus deflection curves generated by the plane frame inclined bar model, and the peak cycle deflections observed in the test. Figure 6.21 provides a comparison between the theoretical hysteresis curve and the actual hysteresis curve for cycle 16. The two curves are reasonably similar, but the theoretical curve encloses about 36 percent less area than does the actual curve. This is to be expected since the joint restraint of the actual frame is greater than the assumed restraint (pinned joints) used in the analytical model. This resulted in a structure that was less stiff during the tension field redevelopment phase. Figure 6.22 compares the theoretical and the observed curves for hysteresis cycle 28. Again, the two curves are

reasonably similar. The slopes of the curves in the tension field redevelopment region correlate better than they did in the previous case, with the theoretical hysteresis curve now enclosing about 20 percent more area than the actual hysteresis curve. The discrepancy is due in part to the differences in the actual monotonic behaviour and the predicted monotonic behaviour.

Because the relationships developed above result in a reasonable prediction of the experimentally obtained hysteresis loops, it is practical to develop predictions of the hysteresis behaviour of other shear walls with different configurations, member section properties, or different connection characteristics. Three such examples follow.

Figure 6.23 is a hysteresis loop developed for a structure similar in configuration to the specimen tested, but having 5 mm thick panels. (A 5 mm thick panel is probably the practical minimum web plate thickness, as governed by handling considerations.) All material properties and member section properties were similar to those used in the analysis of the test specimen. The beam-to-column joints and the support locations were all assumed to be pinned throughout the load history. The angle of inclination of the tension field was calculated to be 43.7 degrees using the new panel thickness. The hysteresis loop was developed based on the deflections taken in cycle 28 of the conducted test and the theoretical load versus deflection curve developed by the plane frame model. As can

be seen from Figure 6.23, the increase in panel thickness increases the ultimate strength of the structure but does not change the basic shape of the hysteresis loop. The stiffness of the frame, 134.2 kN/mm, was comparable to the frame stiffness of the test specimen. This similar stiffness resulted in a similar amount of pinching and a similar enclosed area.

Figure 6.24 shows the theoretical hysteresis loop for a structure identical to the previous case, except that the beam-to-column joints are fixed throughout the load history. The change in the beam-to-column connection resulted in a stiffer and stronger structure, with a considerably increased area enclosed by the hysteresis loop (150%). This is mainly due to the near doubling of the frame stiffness (from 134.2 to 265.2 kN/mm). The horizontal portions of the loop, AB and CD, are due to the formation of a mechanism in the frame. This mechanism will result in an increase in the amount of pinching in the hysteresis loops at higher load levels.

Figure 6.25 shows the theoretical hysteresis curve for a structure of similar configuration to those previously analyzed, except that the panel size is now 2.2 m by 2.2 m. The panel thickness (3.25 mm) and all of the other section properties used are identical to those of the test specimen. The beam-to-column joints and the support points are assumed to be pinned in the analysis. The hysteresis loop exhibits slightly less pinching than the other curves developed. This

is because the stiffness of the frame now constitutes a larger portion of the stiffness of the structure. Taking this trend to the extreme, it is easy to visualize that as the bay width approaches zero the stiffness and ultimate capacity become approximately equal to the stiffness and capacity of two columns acting alone. The hysteresis behaviour will also improve because the bending of Class 1 and Class 2 sections (typical for column members) produces fully developed and stable hysteresis loops. The area enclosed by this hysteresis loop is approximately equal to the area enclosed by the theoretical curve in Figure 6.22.

Now that several of the parameters involved have been examined, it is desirable to examine the hysteresis behaviour of a panel in a configuration typical of a multi-storey building. Figure 6.26 illustrates the plane frame model used to evaluate the hypothetical shear wall structure. The column and beam sections used are the same as used in all previous cases. The panel thickness is set equal to 3.25 mm with a yield strength of 242.5 MPa. The total vertical load applied to the columns, 350 kN per floor, is approximately equal to the column load applied to the test specimen. The applied lateral loads were of equal magnitude for the first and second floors with the lateral load applied to the top floor being one half the magnitude of the load applied to the lower floors. Two shear walls were assumed to resist the total lateral force, Q. All beam-to-column joints were assumed to be pinned joints while

all member nodes along line AB (Figure 6.26) were assumed to be fixed joints. (The lower storey of a typical shear wall would normally consist of a very stiff anchor panel. This is provided so that the tension fields in the panels above can develop fully.) The panels were divided into only seven tension members in order to reduce the quantity of computations involved.

The hysteresis loop developed for the lower storey of this structure, using the maximum deflections recorded during cycle 28 of the reported test, is shown in Figure 6.27. Note that the loop is severely pinched with a considerably smaller enclosed area; only 60 percent of the area enclosed by actual hysteresis loop in Figure 6.22. This is due to the very low frame stiffness (32.11 kN/mm). An identical structure, except having fixed beam-to-column connections, was analyzed and the theoretical hysteresis loop produced shown in Figure 6.28. The area enclosed under this curve is 3.3 times greater than the area under the previous hysteresis loop, Figure 6.27. This is due to the large increase in the frame stiffness achieved by fixing the beam to column connections. Initially the concept of using fixed beam-to-column connections may seem undesirable; however, it must be kept in mind that by fixing only two connections per shear wall stack per floor resulted in a 230 percent increase in the amount of absorbed energy for this arrangement of beams and columns.

## 6.6 Comparison of Hysteresis Behaviours

When examining the hysteresis behaviour of any structural system, it should be compared with what is considered ideal behaviour. Ideal hysteresis behaviour is one that maximizes the enclosed area while minimizing the final deflection. Ideal hysteresis behaviour also displays loops that are stable and non-degenerating, or more simply, these hysteresis loops continue to follow approximately the same load versus deflection path for each subsequent cycle.

The hysteresis behaviour of a moment resisting frame (Figure 2.1) is very close to the ideal behaviour previously described. The amount of area enclosed by the hysteresis loops is very large and the loops are very stable, following the same path for each of the higher loading cycles. This type of hysteresis behaviour is also displayed by the eccentrically braced frame and by the heavily stiffened steel plate shear wall. The hysteresis behaviour of a steel plate shear wall is dependent on the resistance of the panels to buckling. If the panels buckle before yielding occurs, some pinching of the loops will occur.

Pinched hysteresis loops are the typical behaviour of structures that have members that buckle when subjected to compressive loads. Conventional steel cross bracing (Figure 2.2) displays this type of behaviour; the members yielded in tension cannot be recompressed without buckling. This structural system must deflect a larger amount to absorb the same amount of energy (enclosed area) than a system which

displays the same monotonic load versus deflection response but has fully developed hysteresis loops.

Pinched hysteresis loops are also a characteristic of reinforced concrete shear walls. The amount of pinching and the stability of the loops is dependent on the structural details and reinforcement details used. The pinched loops are not due to buckling of members but are the result of the change in stiffness due to the cracking of the concrete and the yielding of the reinforcement.

The observed hysteresis behaviour of the unstiffened steel plate shear wall reported earlier can be compared with the structural systems described above. It is apparent that the behaviour of an unstiffened steel plate shear wall panel is unlikely to achieve the ideal behaviour shown by the eccentrically braced frame or by the moment resisting frame. The behaviour, however, is similar to that displayed by conventional steel cross bracing or by conventional reinforced concrete shear walls.

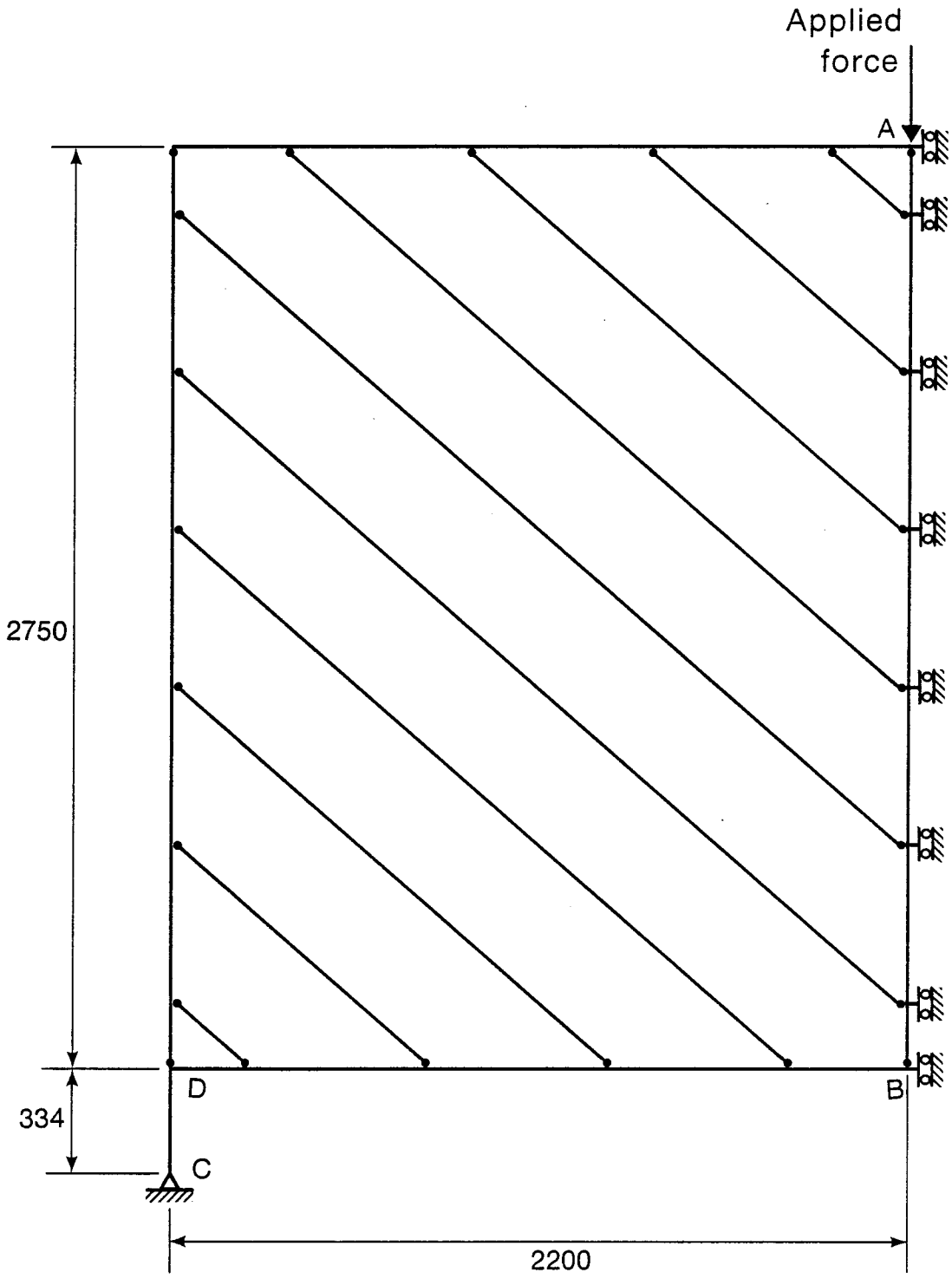


Figure 6.1 Plane Frame Model

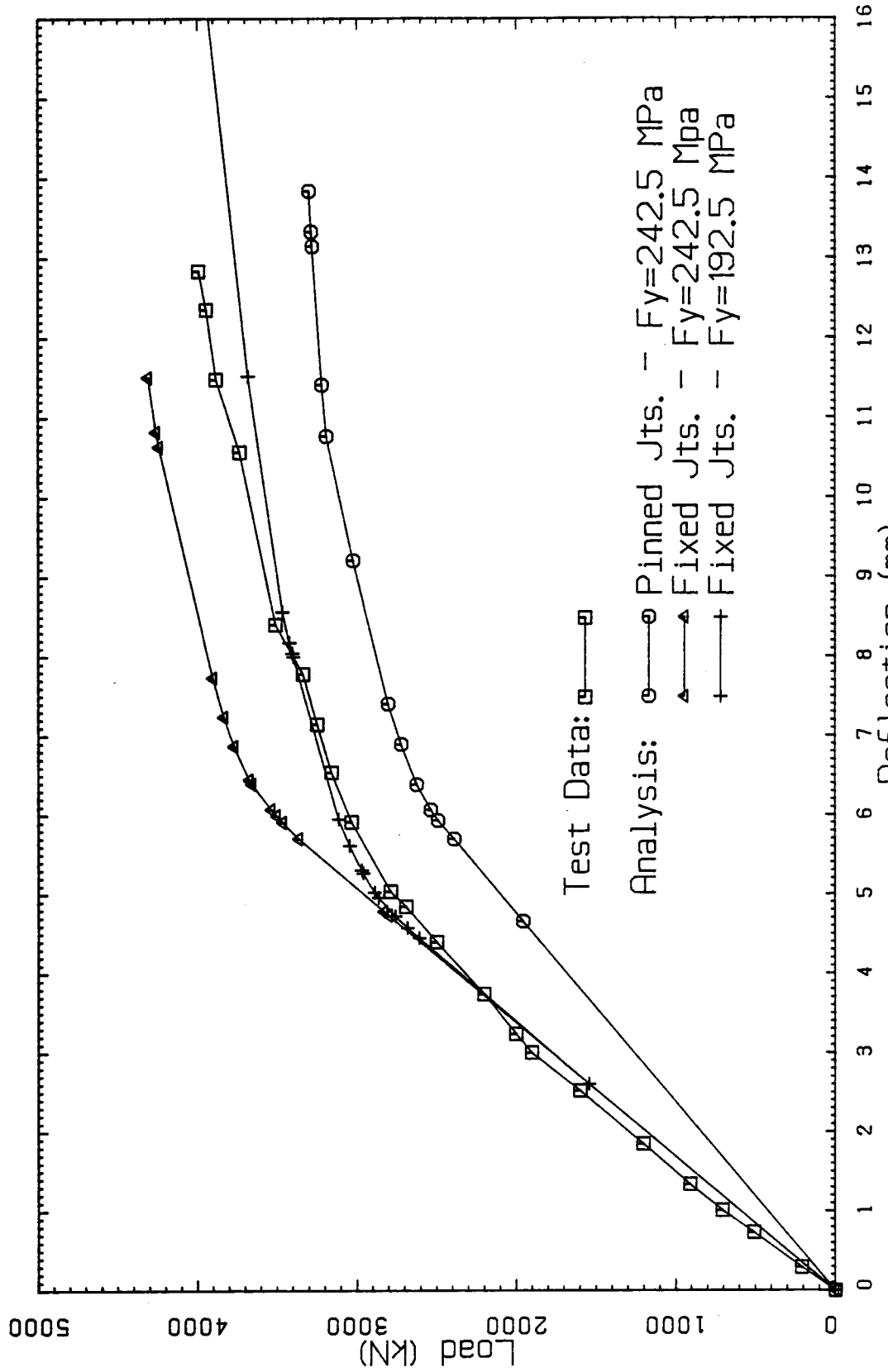


Figure 6.2 Comparison of Theoretical and Observed Compressive Loading Behaviour

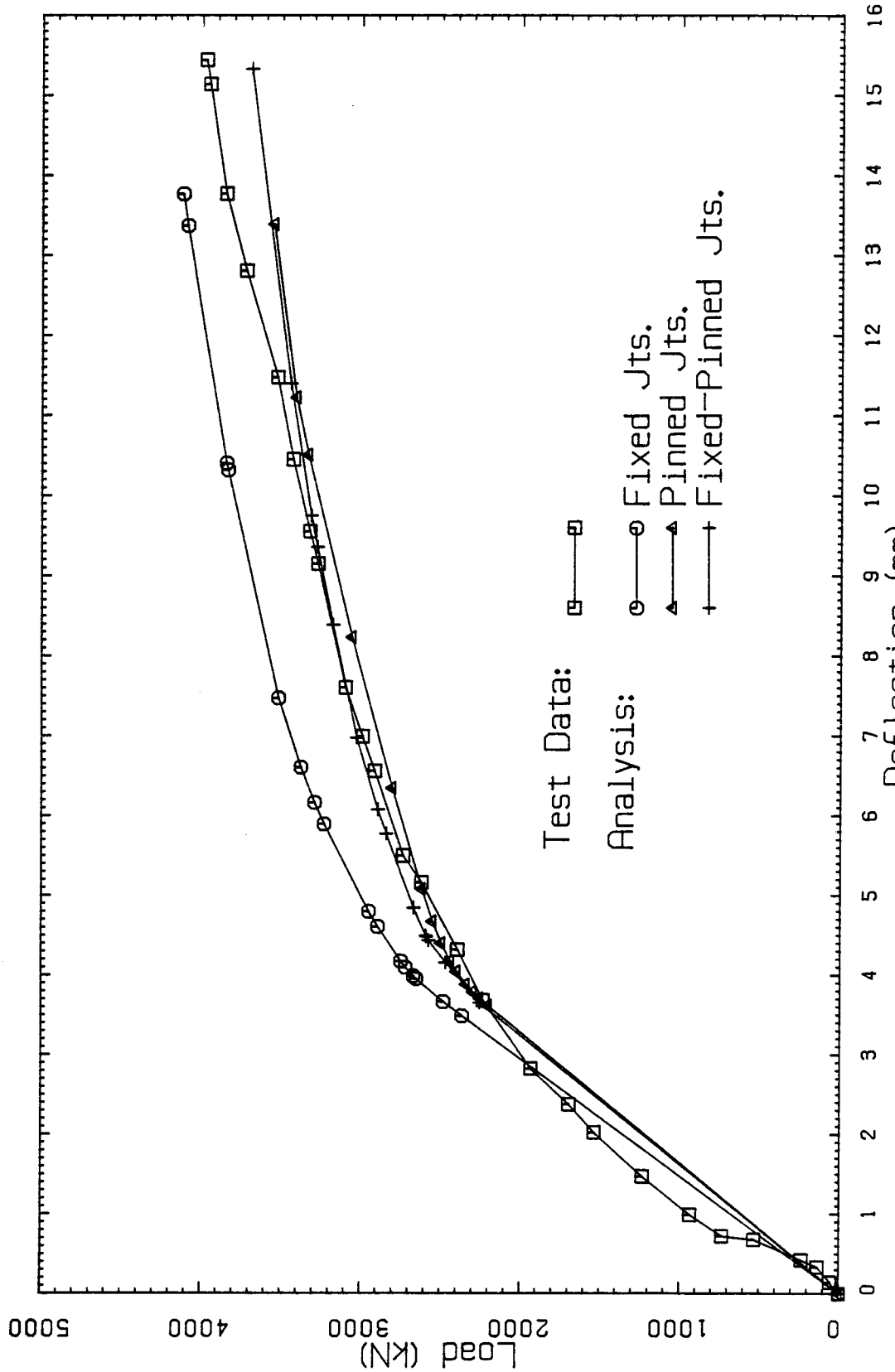


Figure 6.3 Comparison of Theoretical and Observed Tensile Loading Behaviour

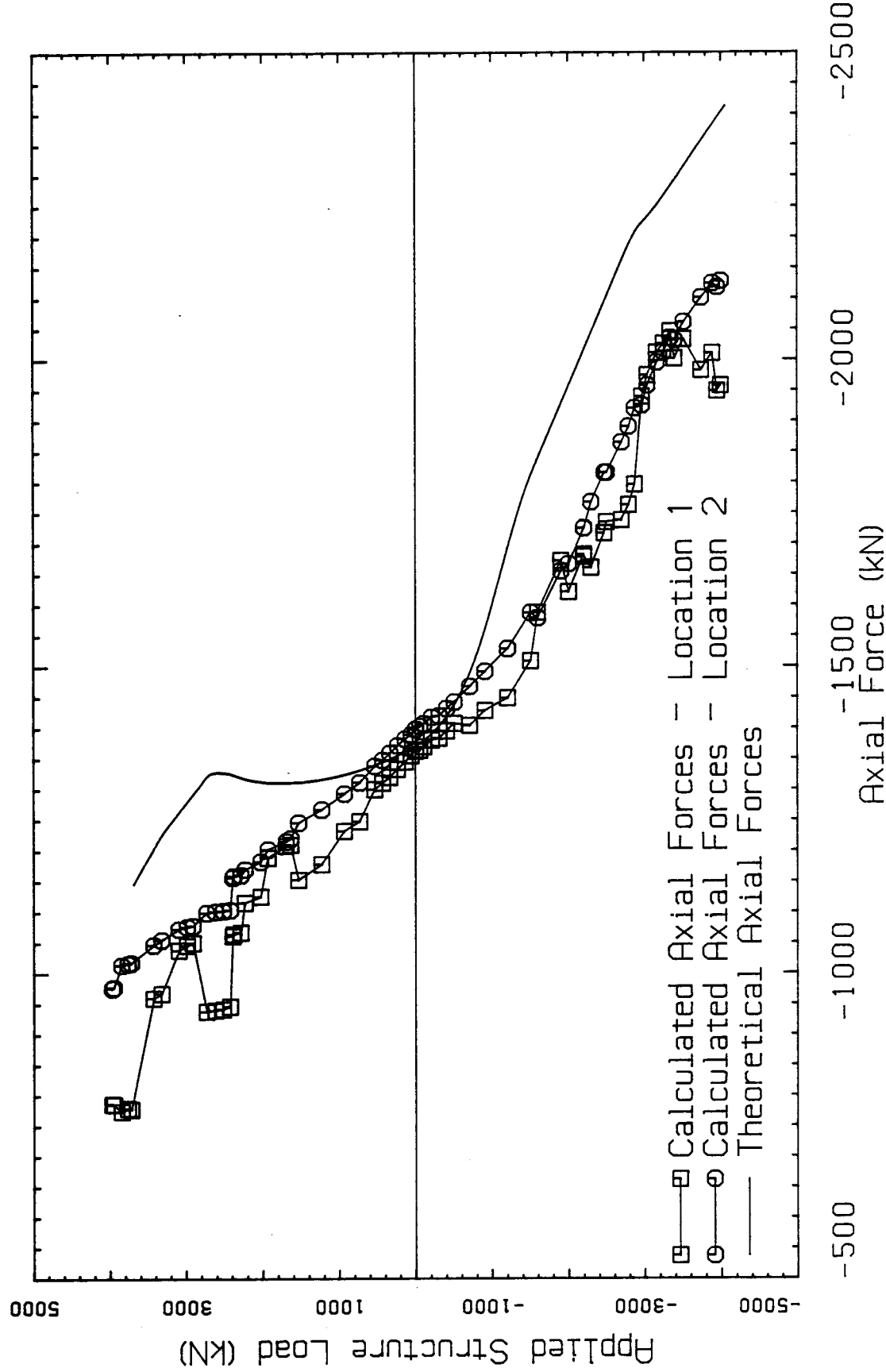


Figure 6.4 Comparison of Observed and Predicted Axial Loads in the Top Column

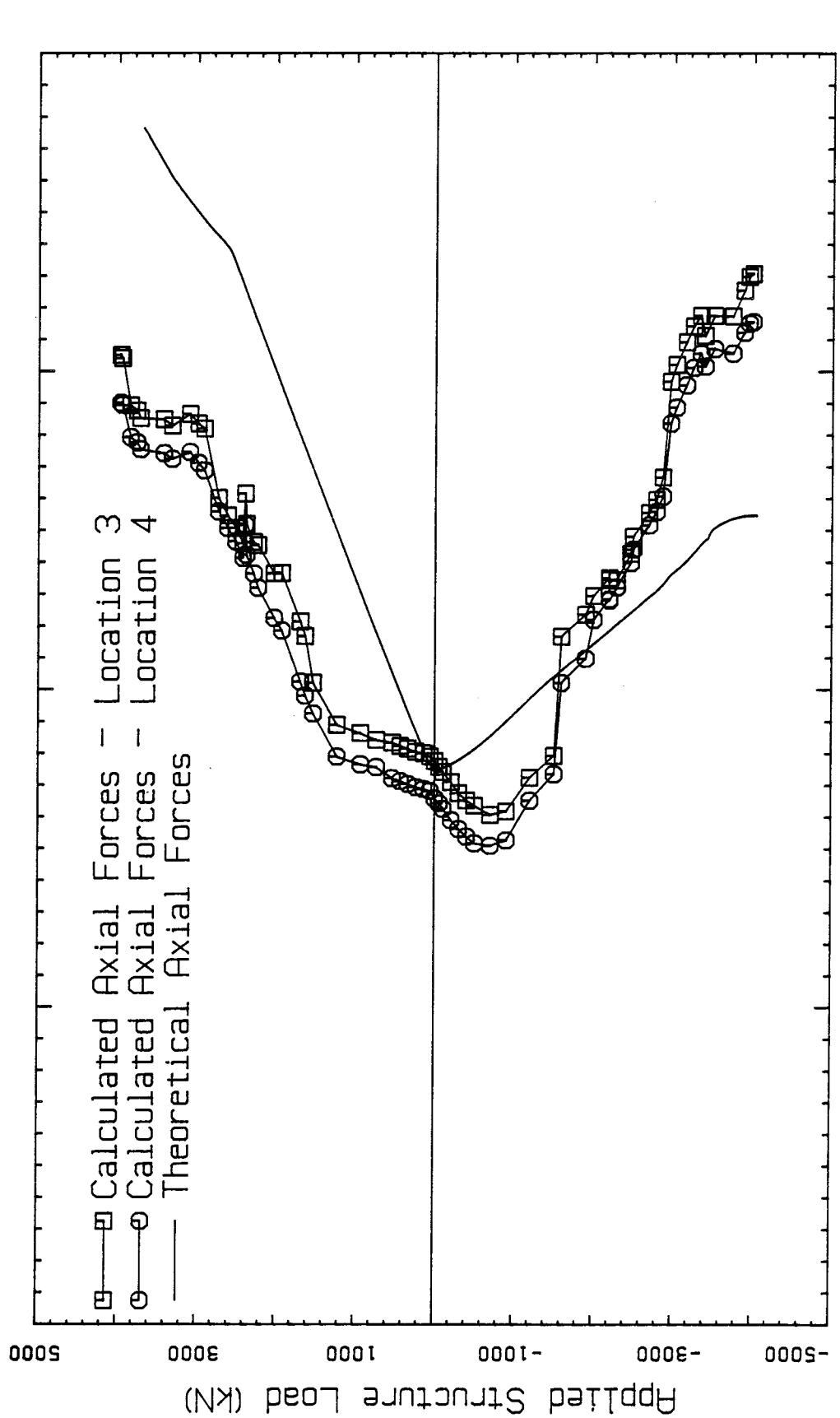


Figure 6.5 Comparison of Observed and Predicted Axial Loads in the Lower Column

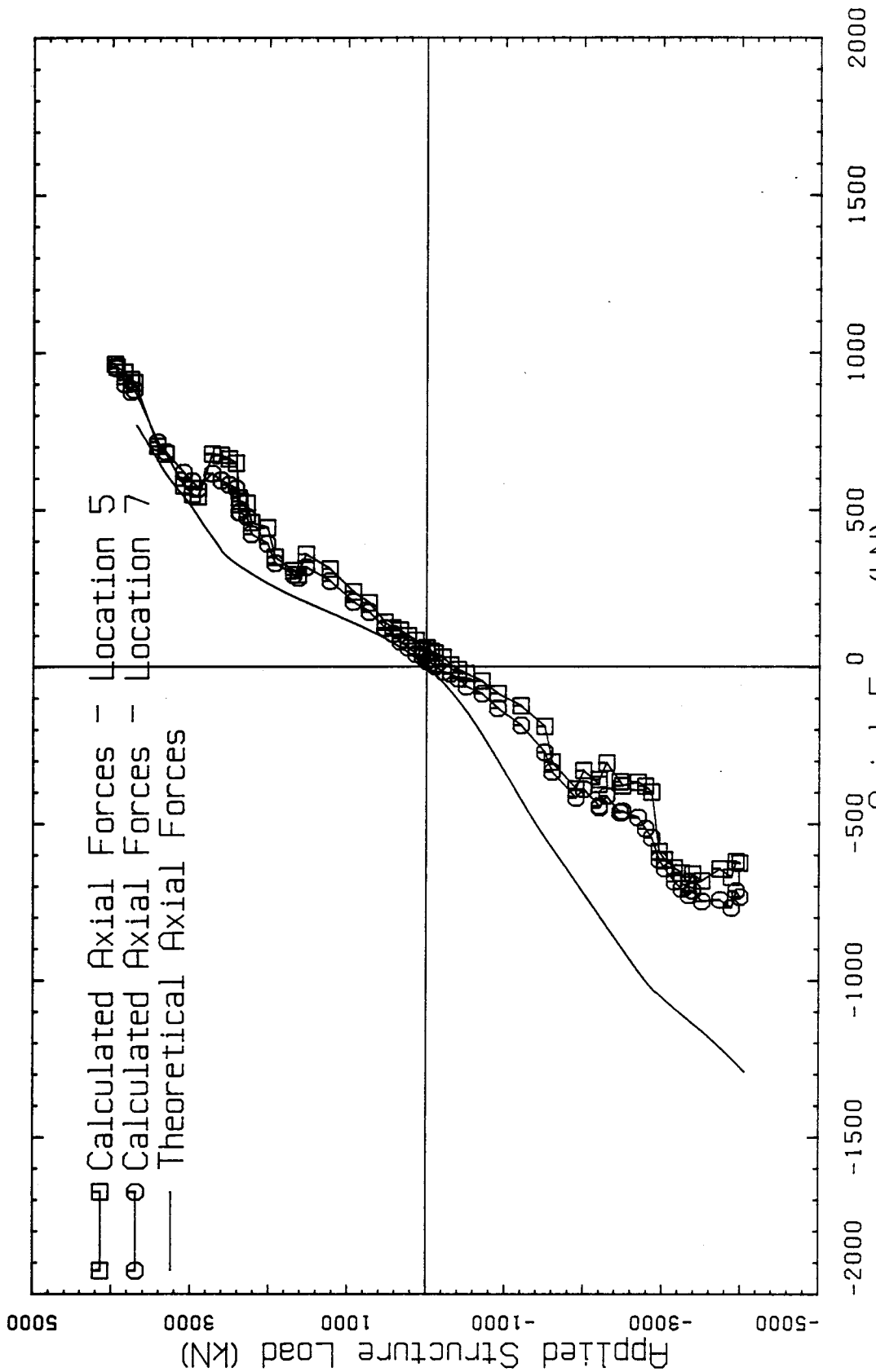


Figure 6.6 Comparison of Observed and Predicted Axial Loads in the Outside Beams

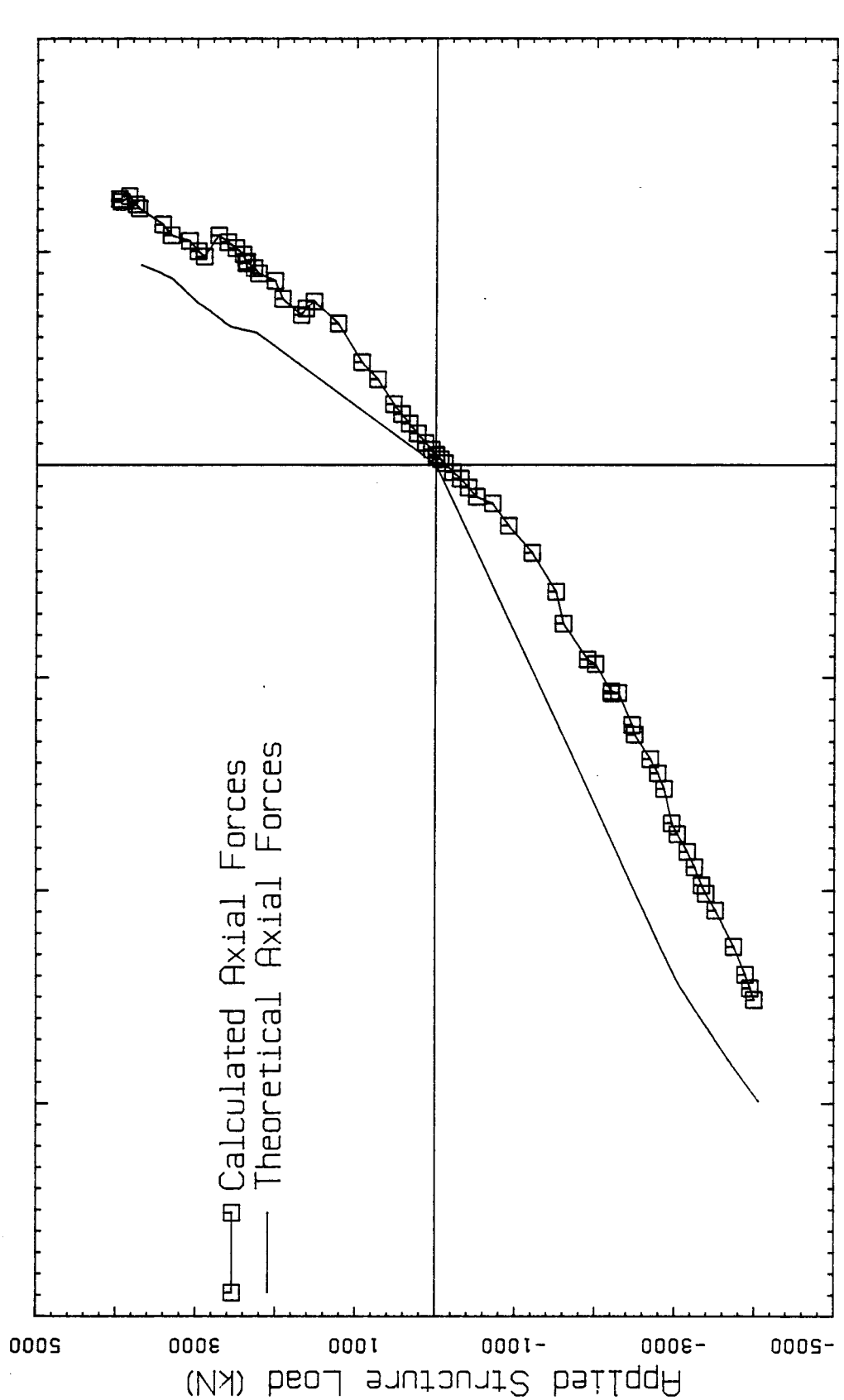


Figure 6.7 Comparison of Observed and Predicted Axial Loads in the Centre Beam

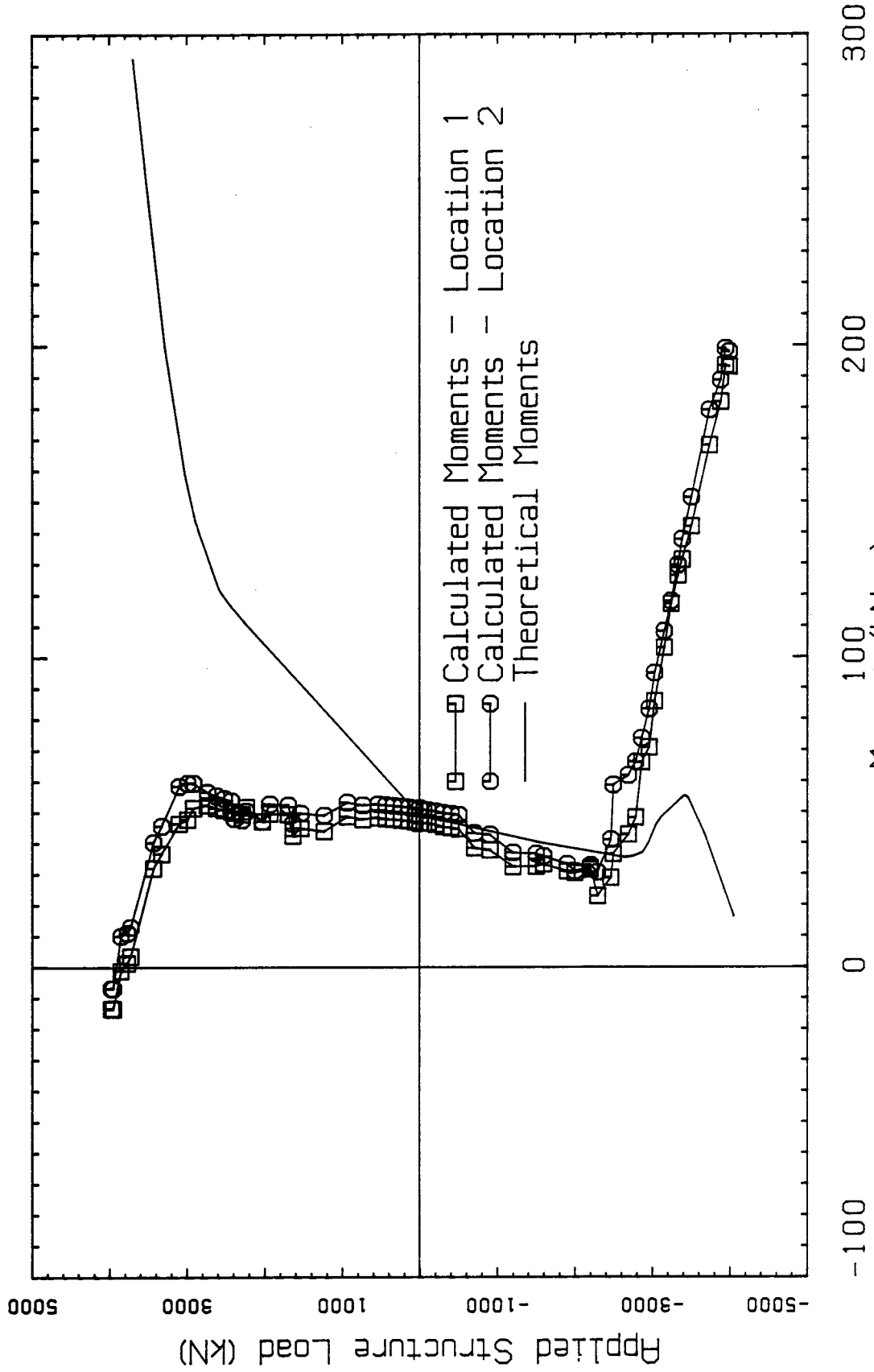


Figure 6.8 Comparison of Observed and Predicted Moments in the Top Column

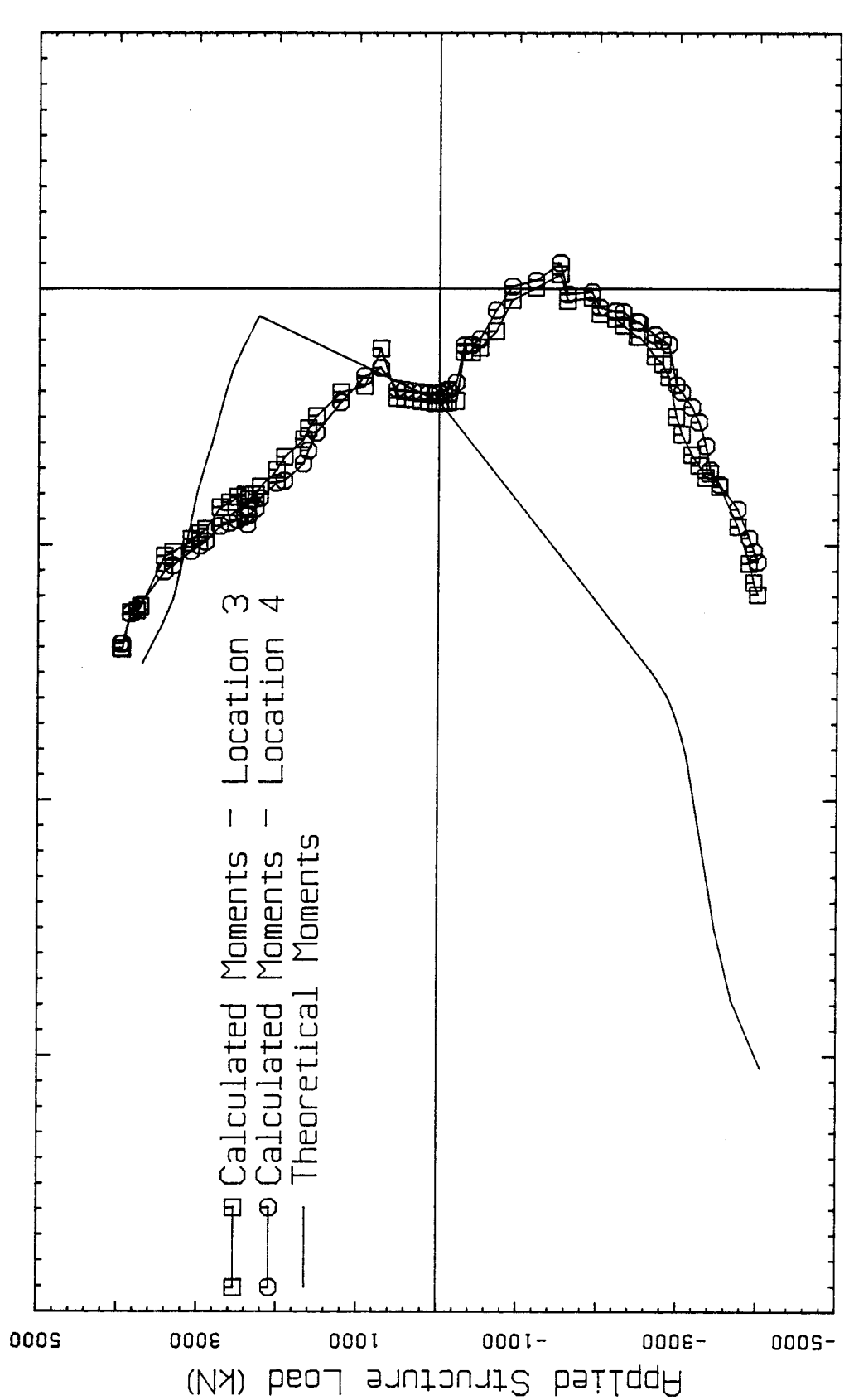


Figure 6.9 Comparison of Observed and Predicted Moments in the Bottom Column

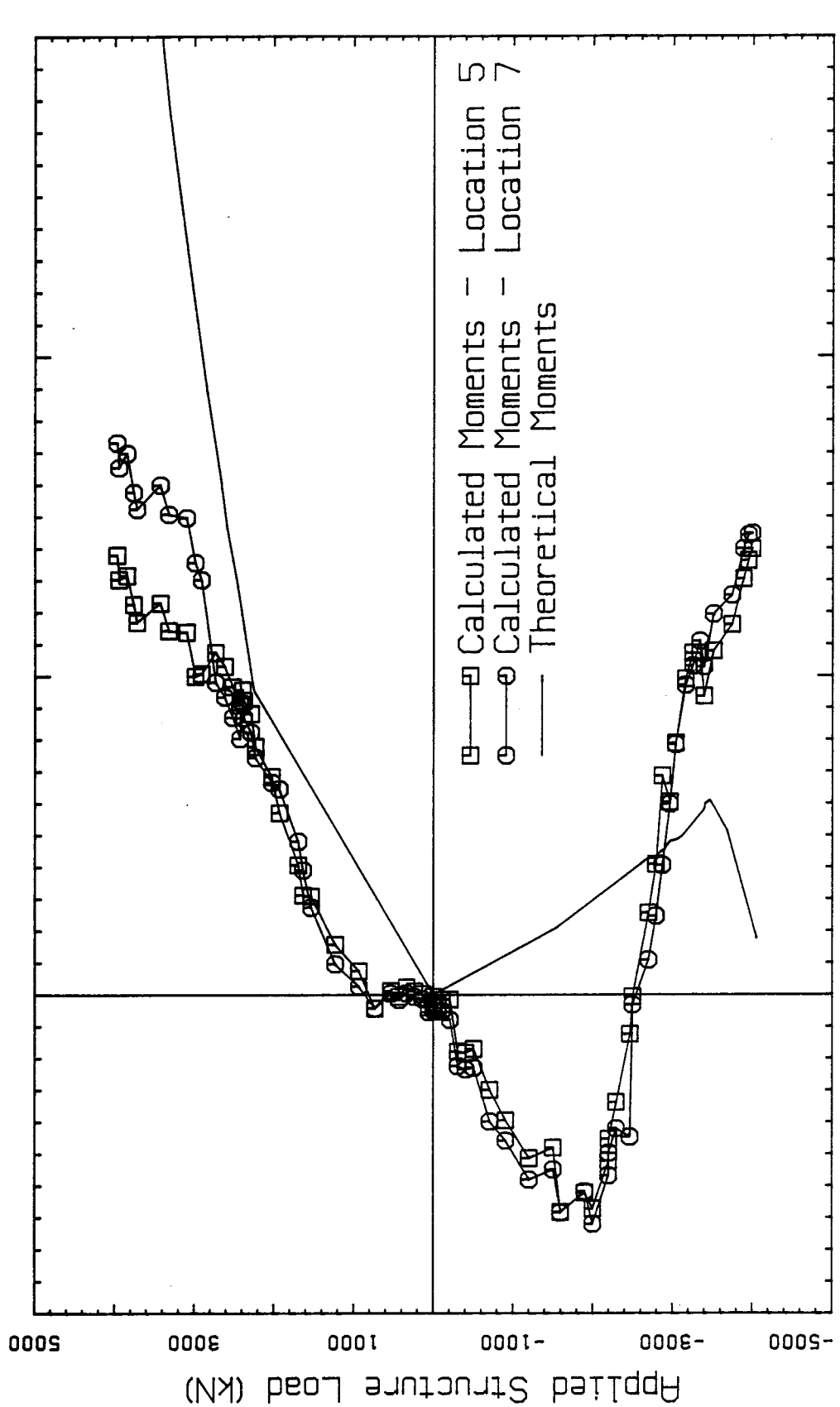


Figure 6.10 Comparison of Observed and Predicted Moments in the Outside Beams

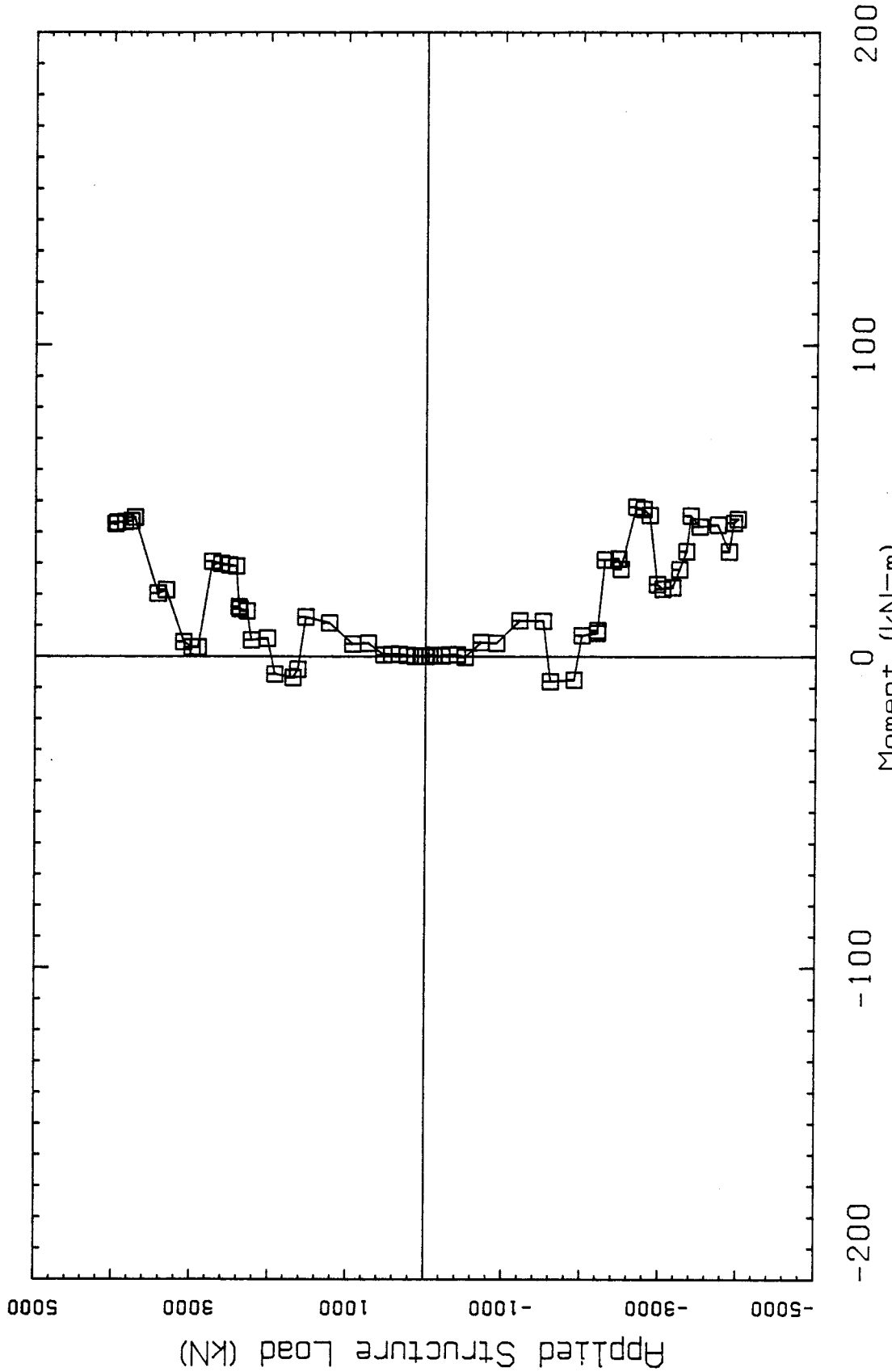


Figure 6.11 Comparison of Observed and Predicted Moments in the Centre Beam

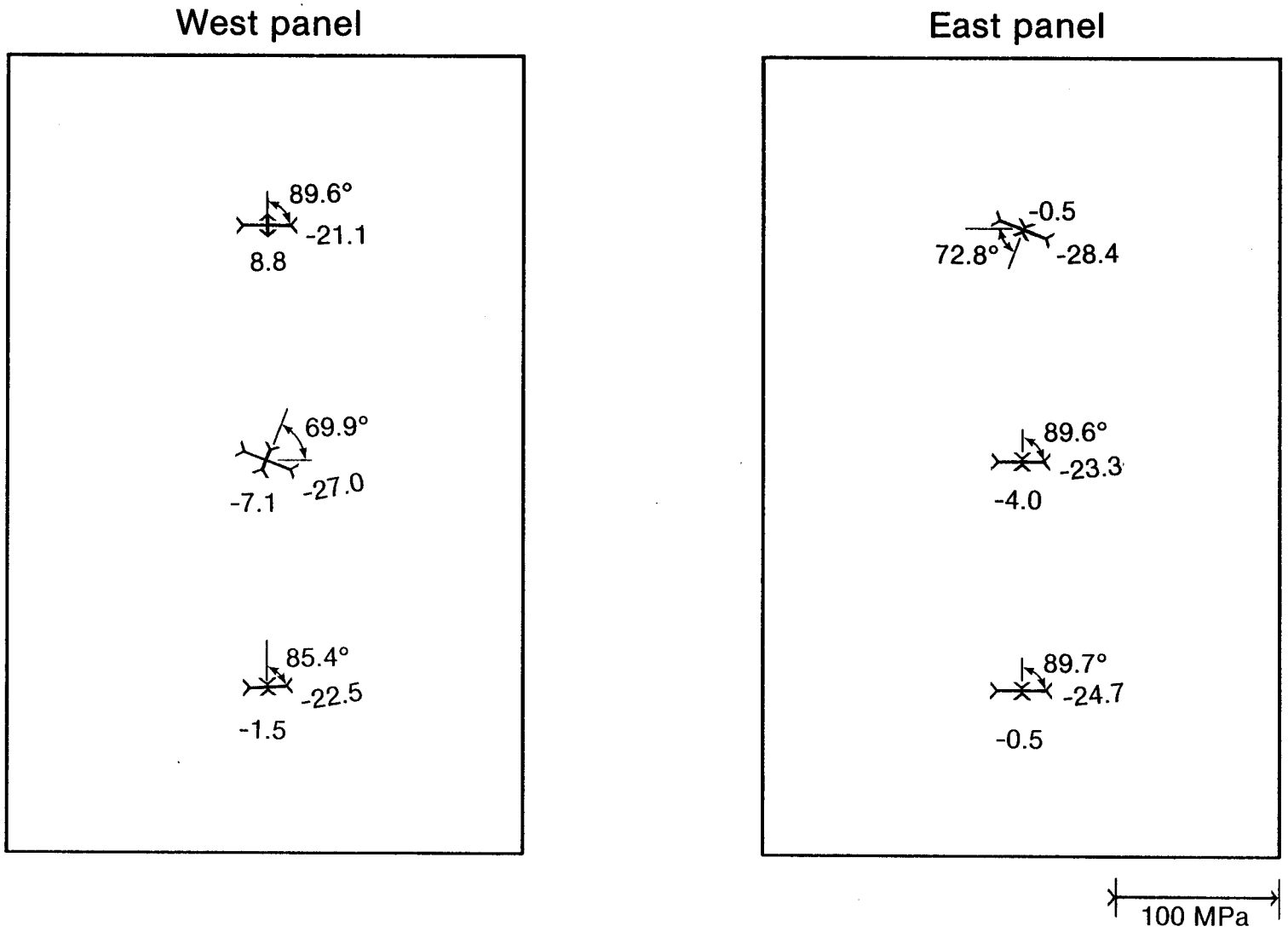


Figure 6.12 Panel Principal Stresses at a Load of 0 kN

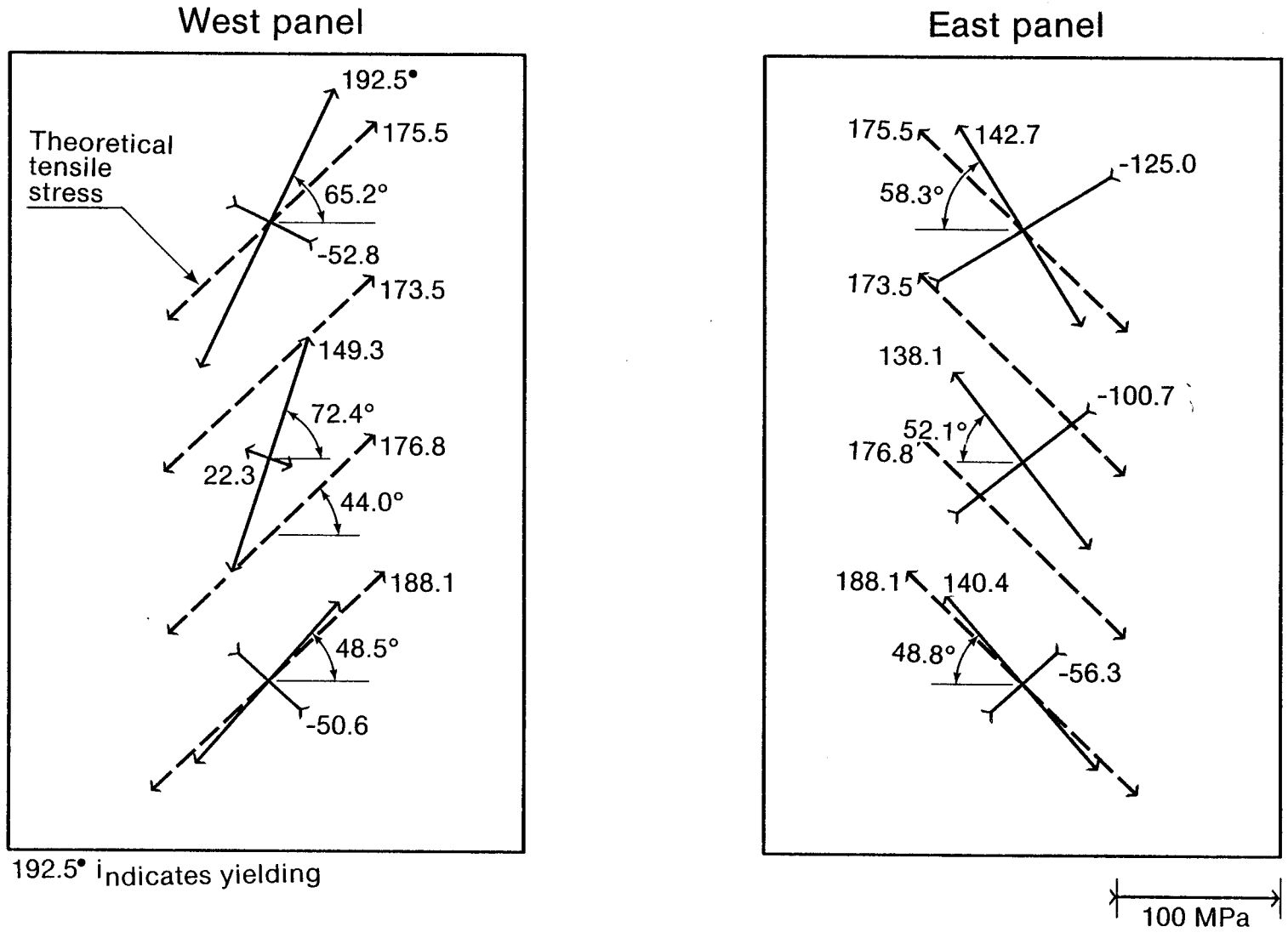


Figure 6.13 Panel Principal Stresses at a Load of +2912 kN

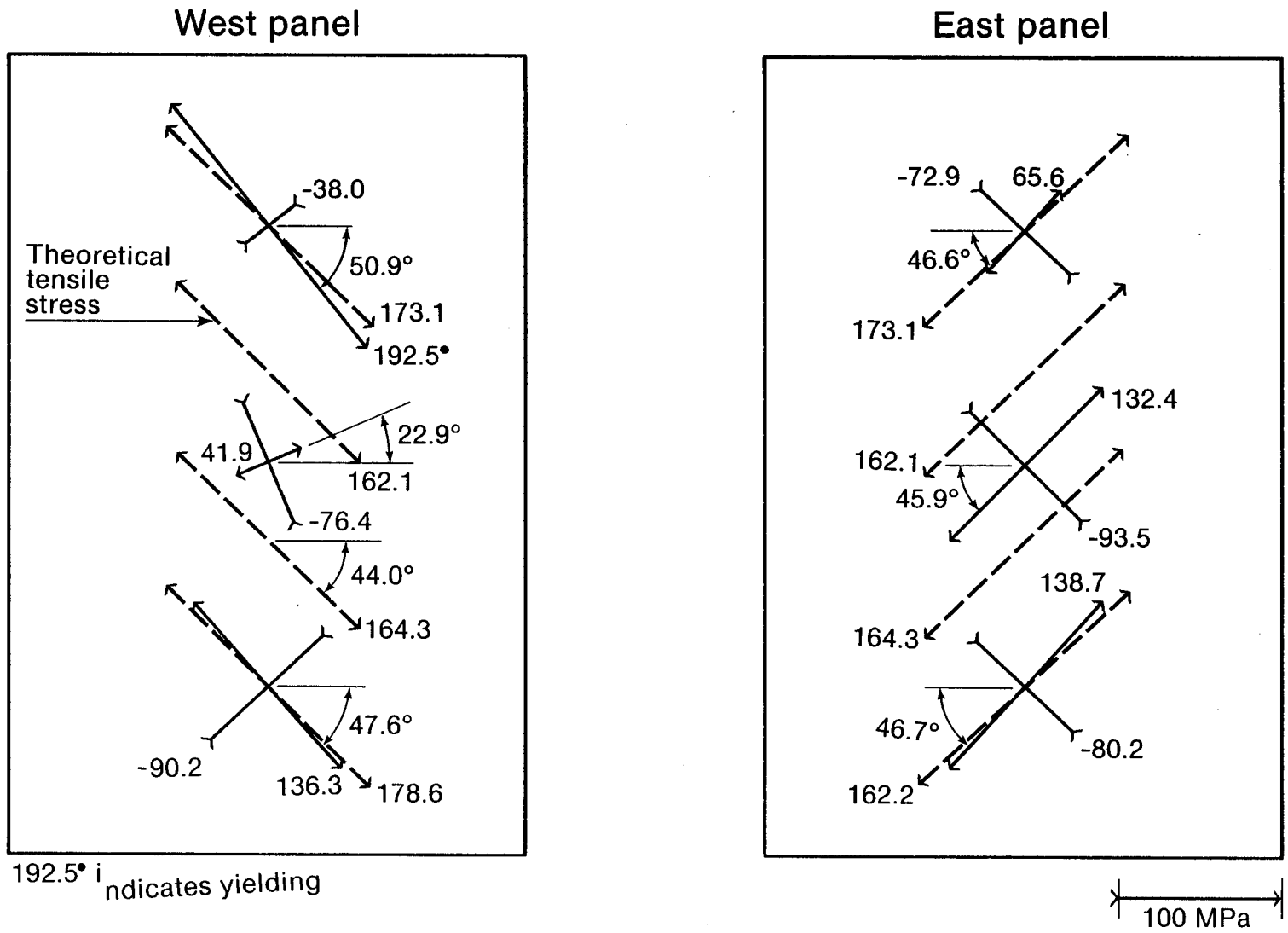


Figure 6.14 Panel Principal Stresses at a Load of -2866 kN

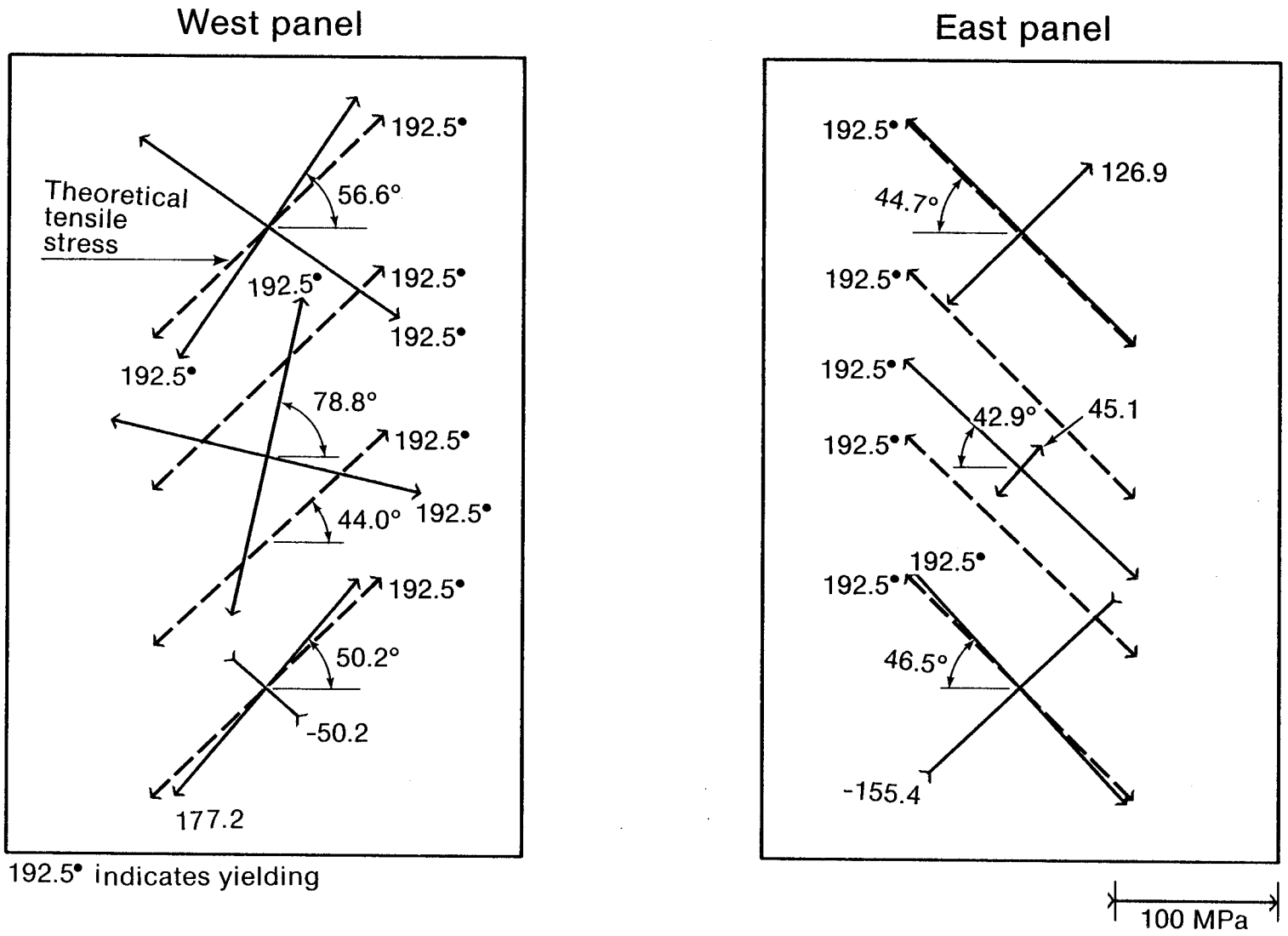


Figure 6.15 Panel Principal Stresses at a Load of +3324 kN

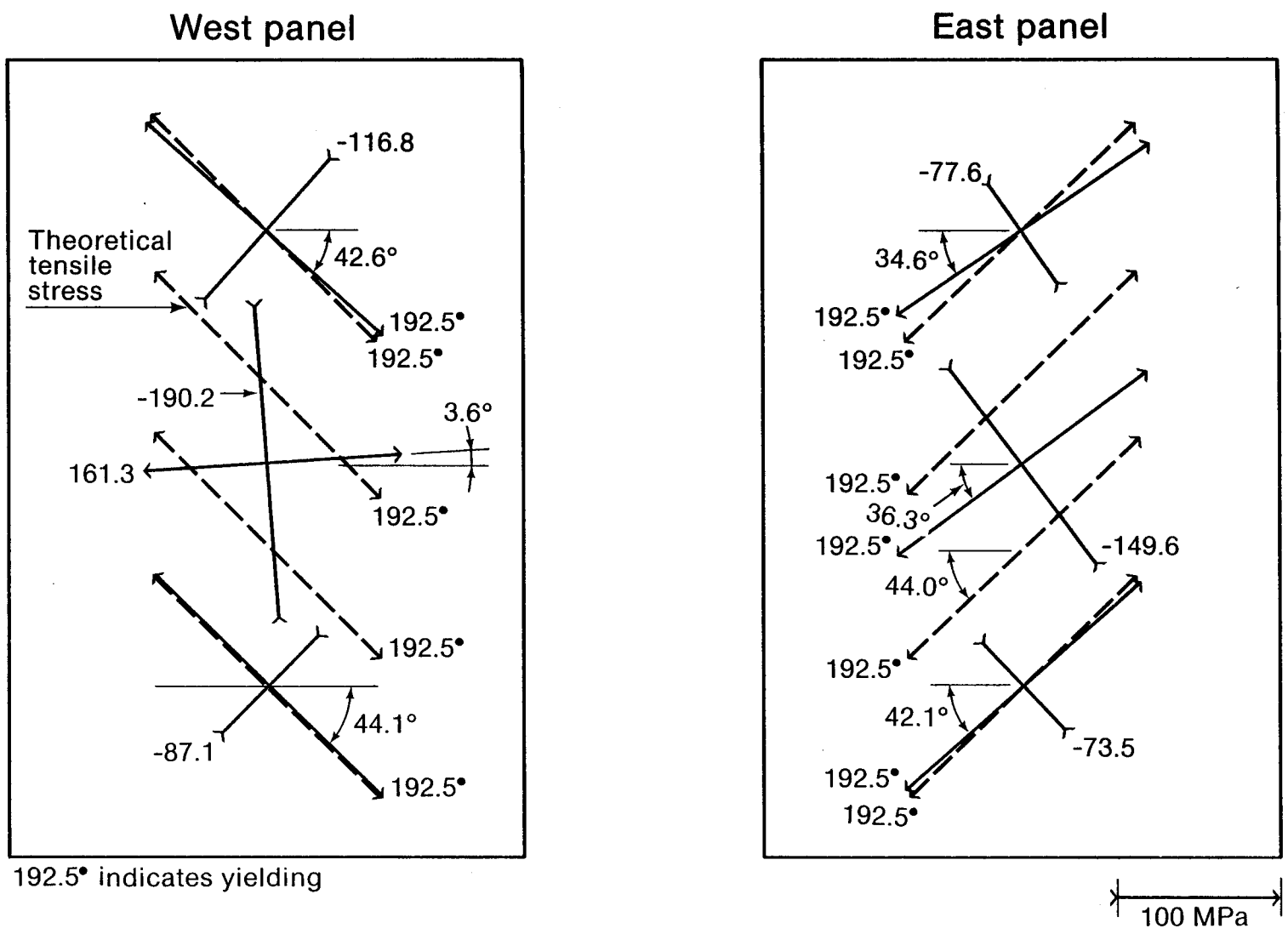


Figure 6.16 Panel Principal Stresses at a Load of -3248 kN

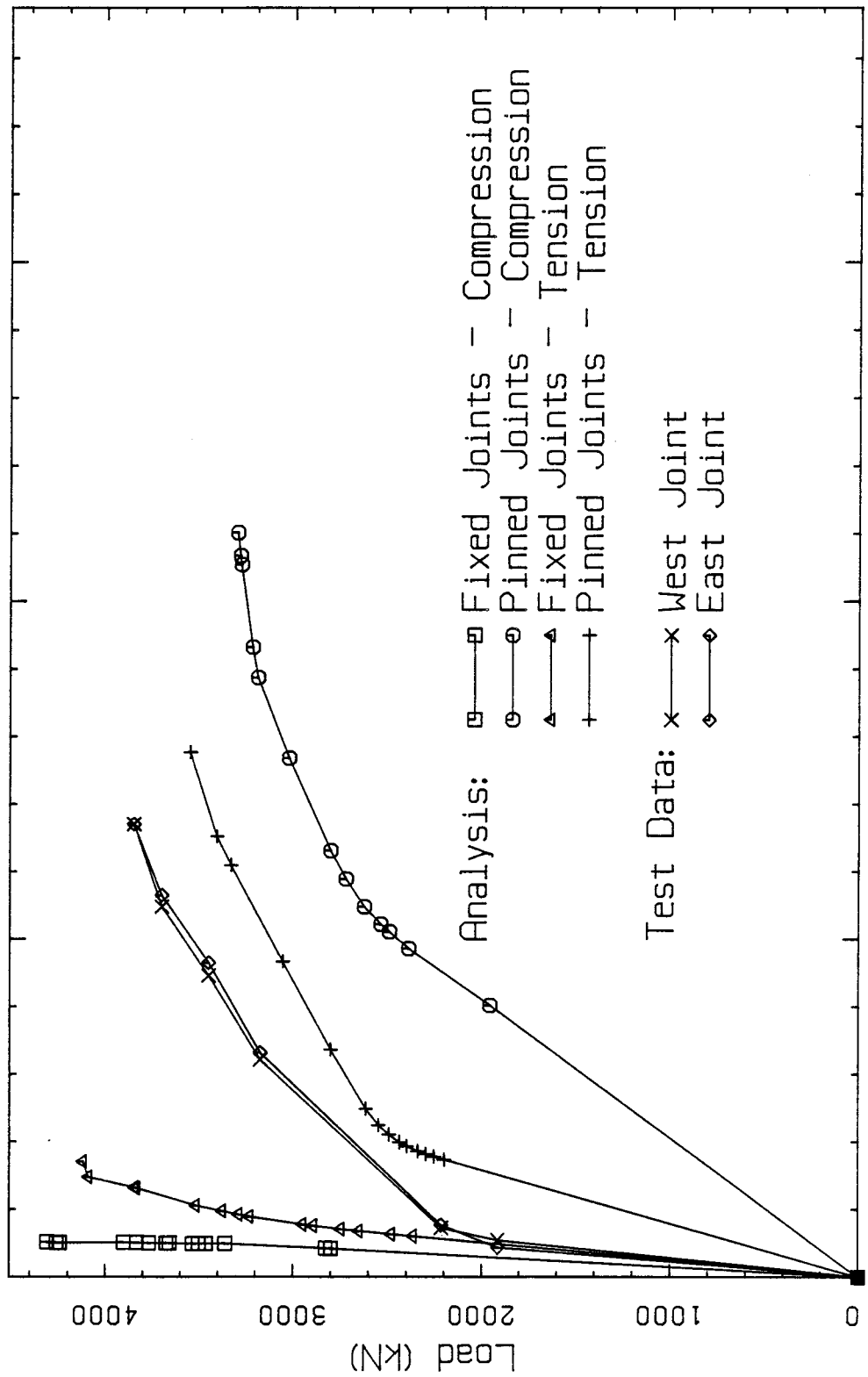


Figure 6.17 Comparison of Observed and Predicted Rotations

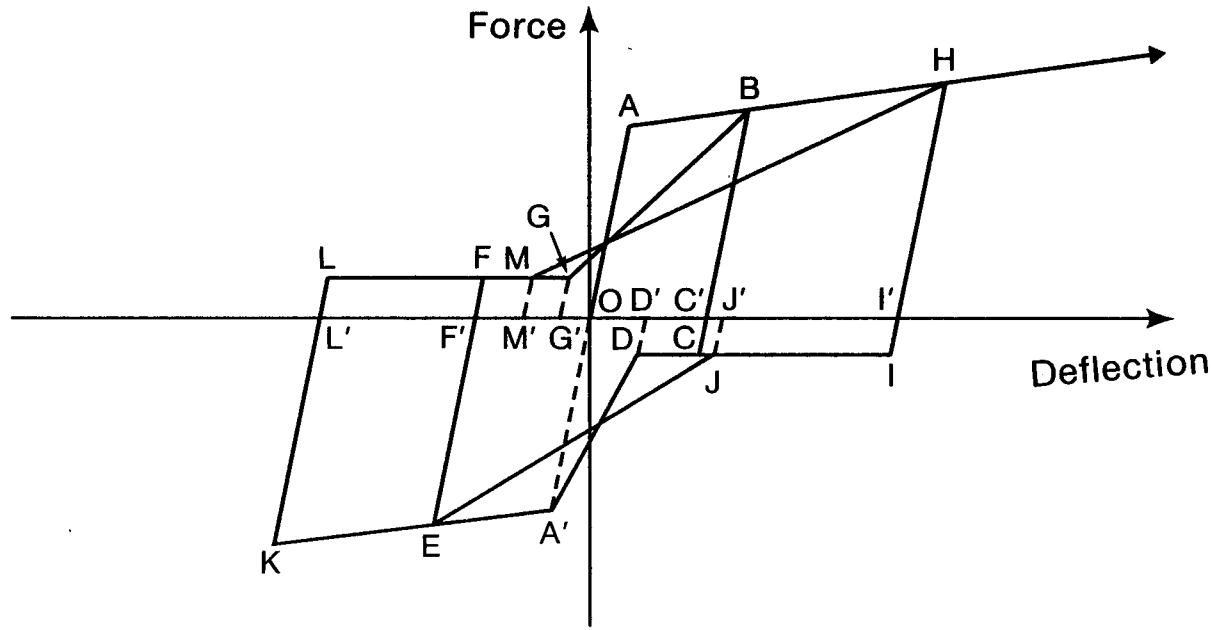


Figure 6.18 Theoretical Hysteresis Curve - Mimura and Akiyana (Reference 5)

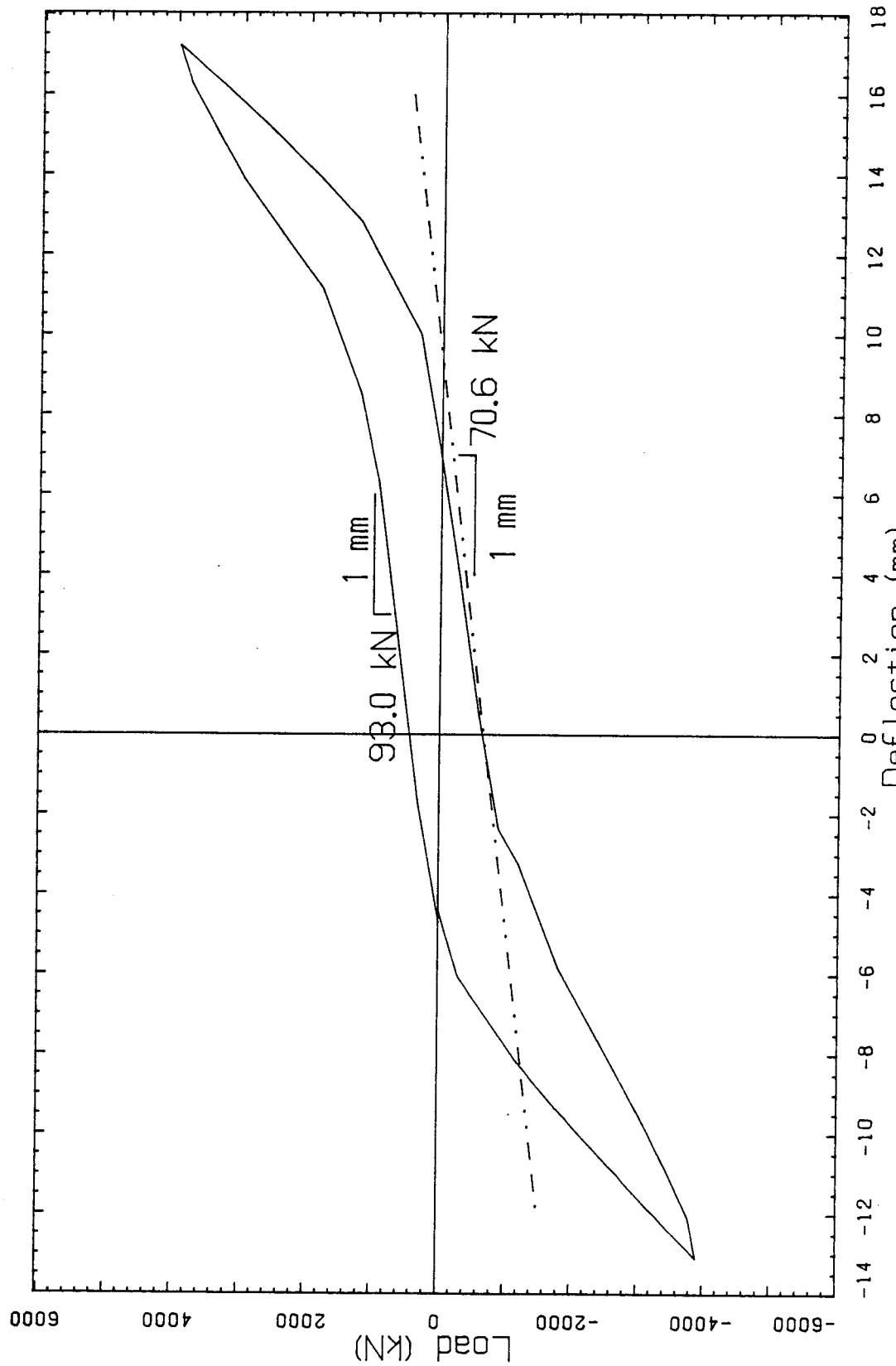


Figure 6.19 Hysteresis Cycle 28

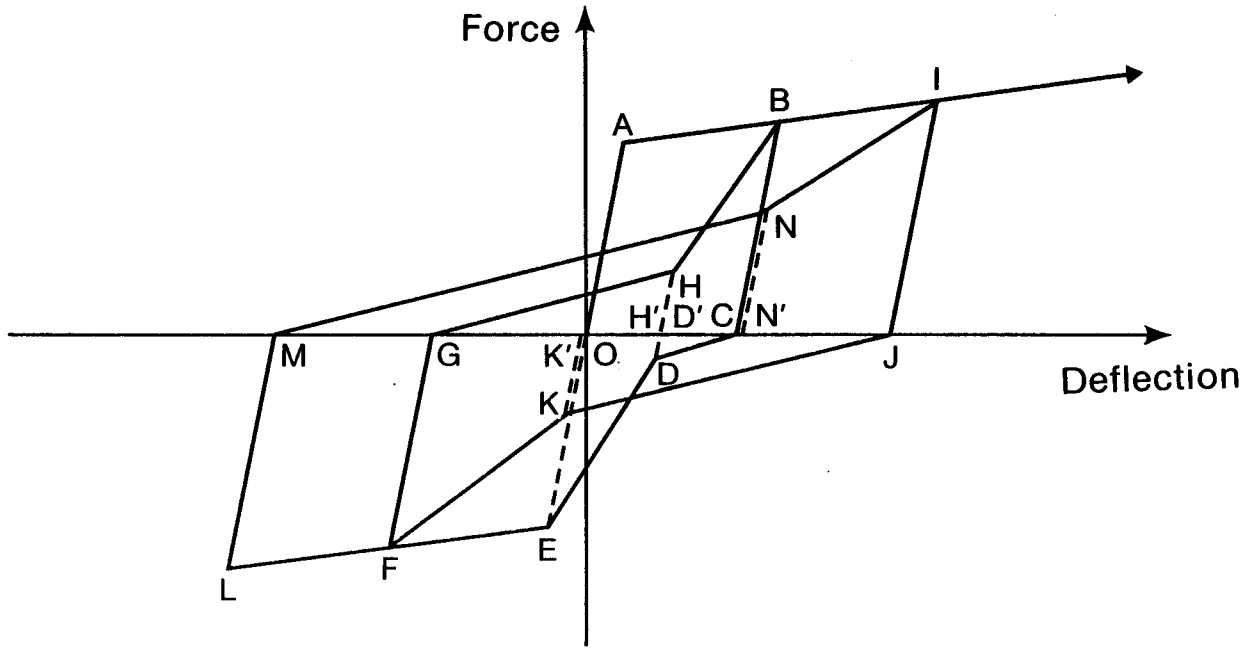


Figure 6.20 Proposed Theoretical Hysteresis Curve

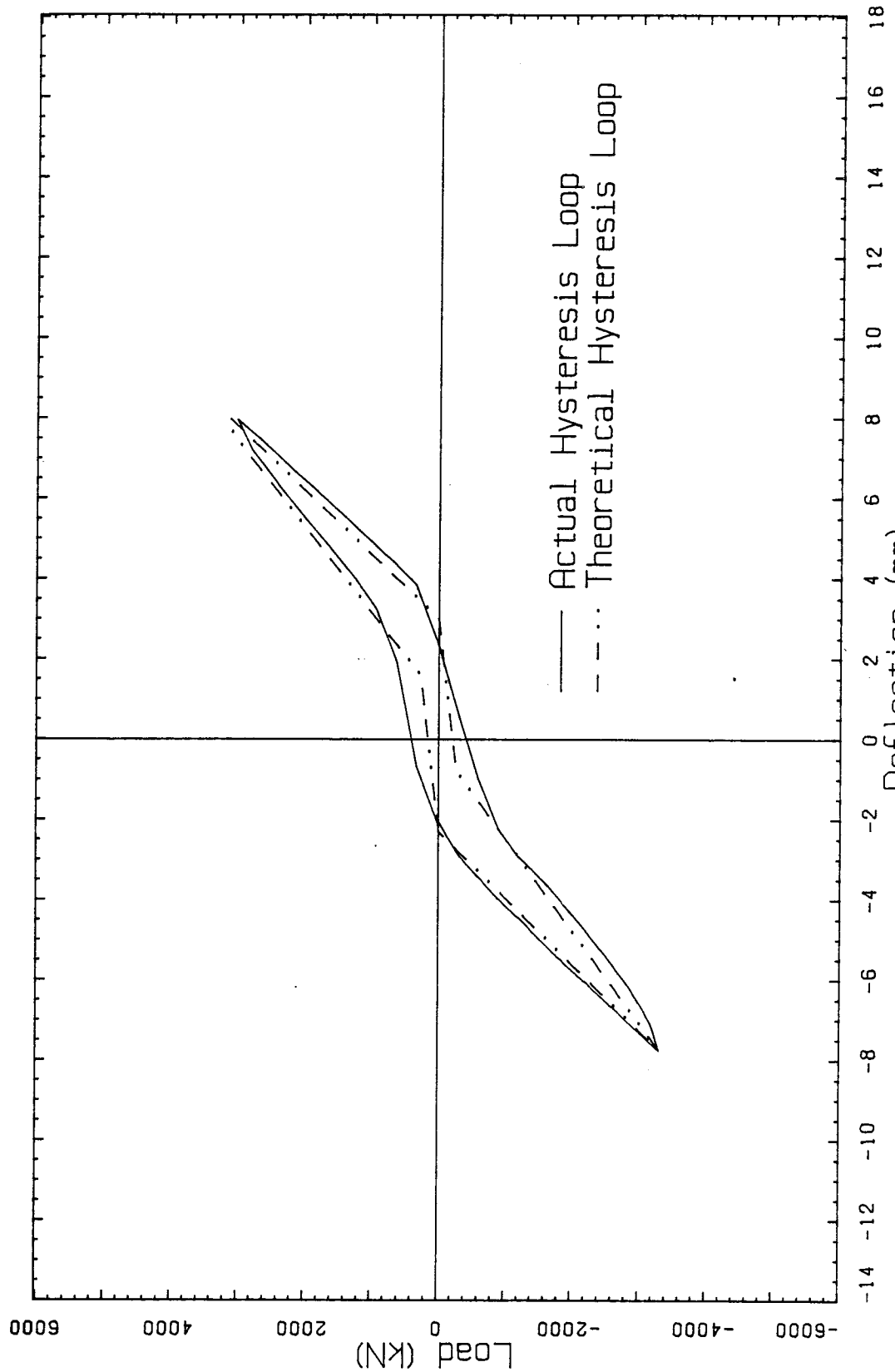


Figure 6.21 Theoretical and Observed Hysteresis Curves for Cycle 16

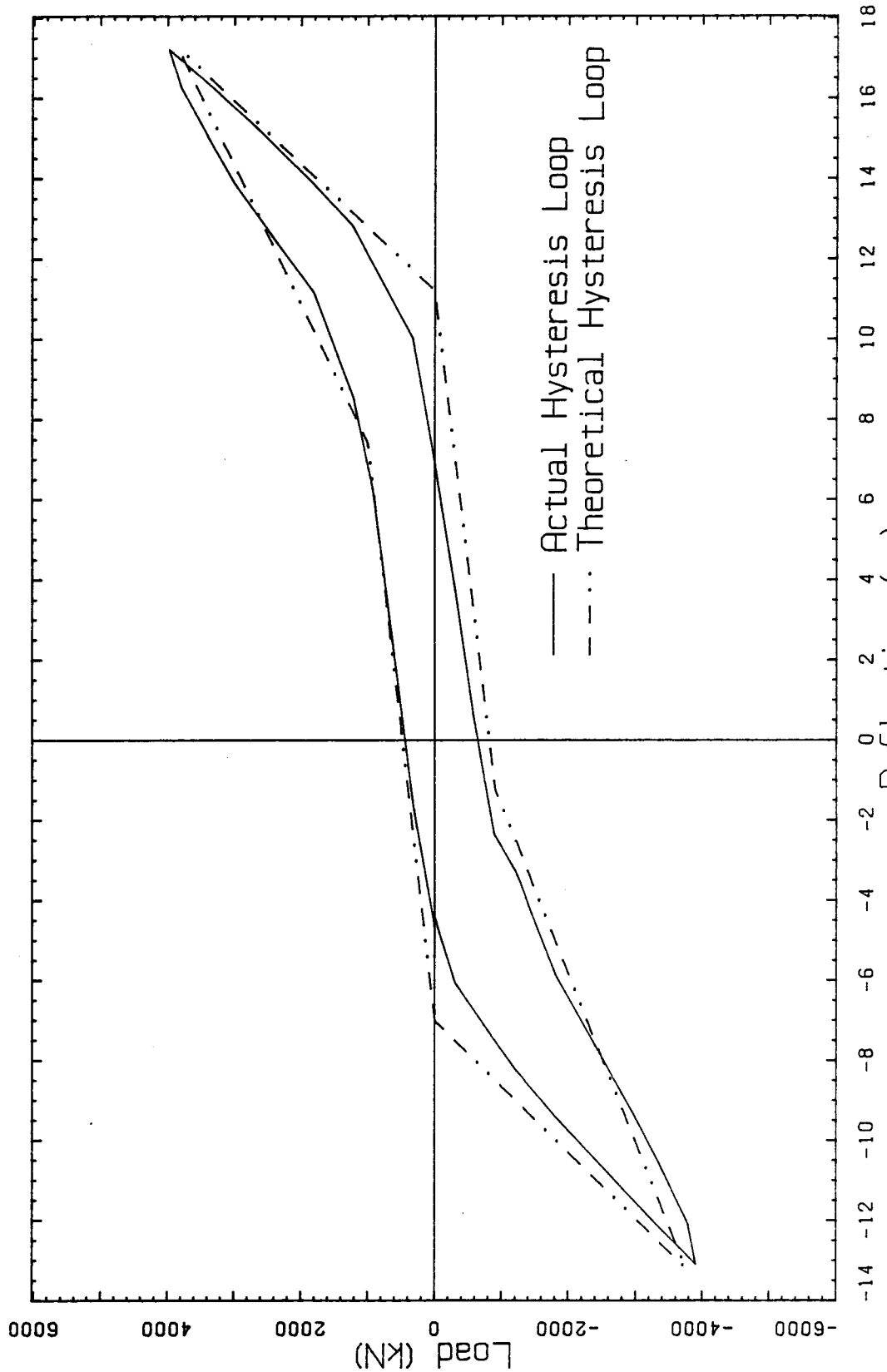


Figure 6.22 Theoretical and Observed Hysteresis Curves for Cycle 28

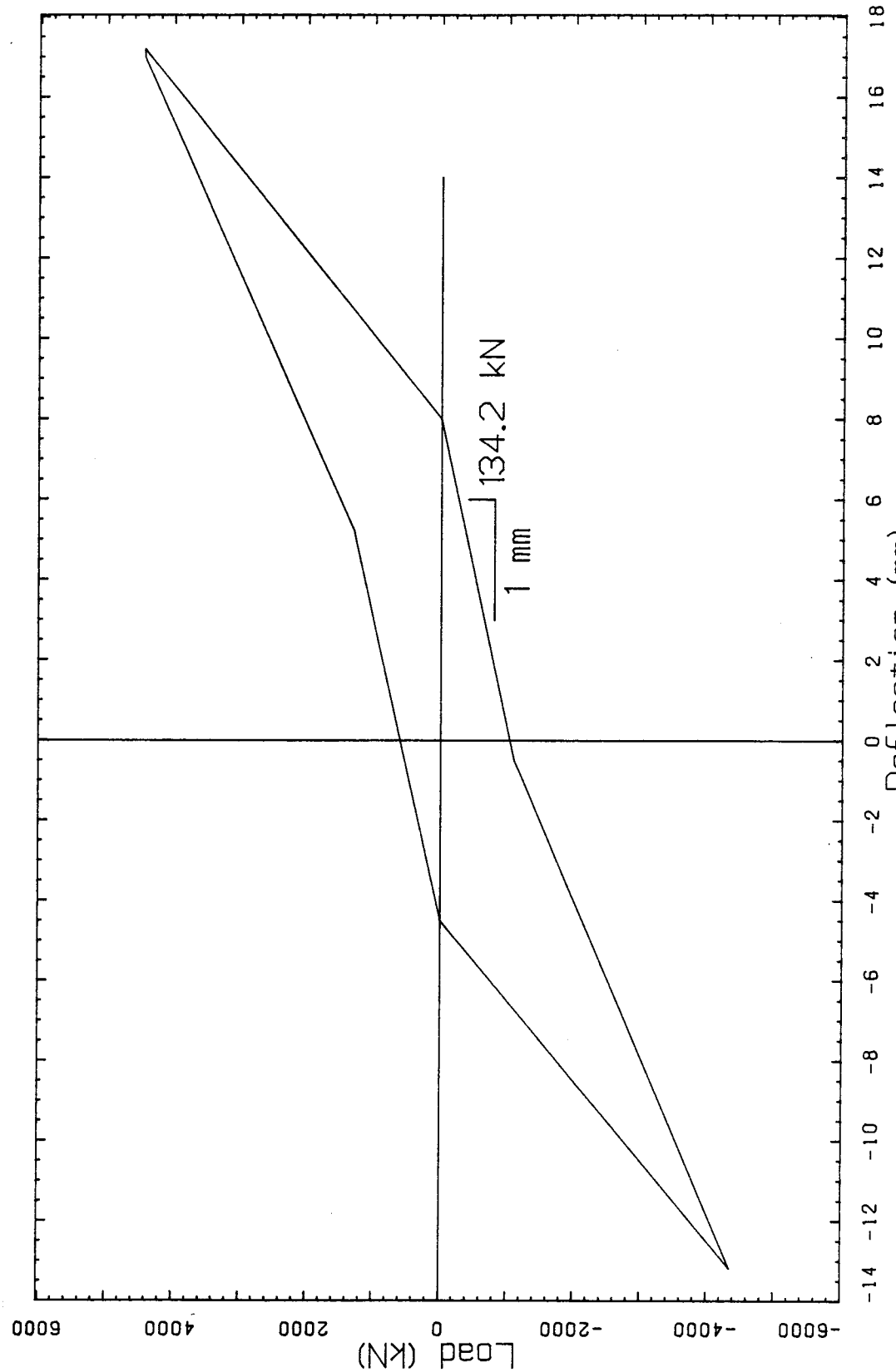


Figure 6.23 Theoretical Hysteresis Loop for a 5 mm Thick Panel and Pinned Joints.

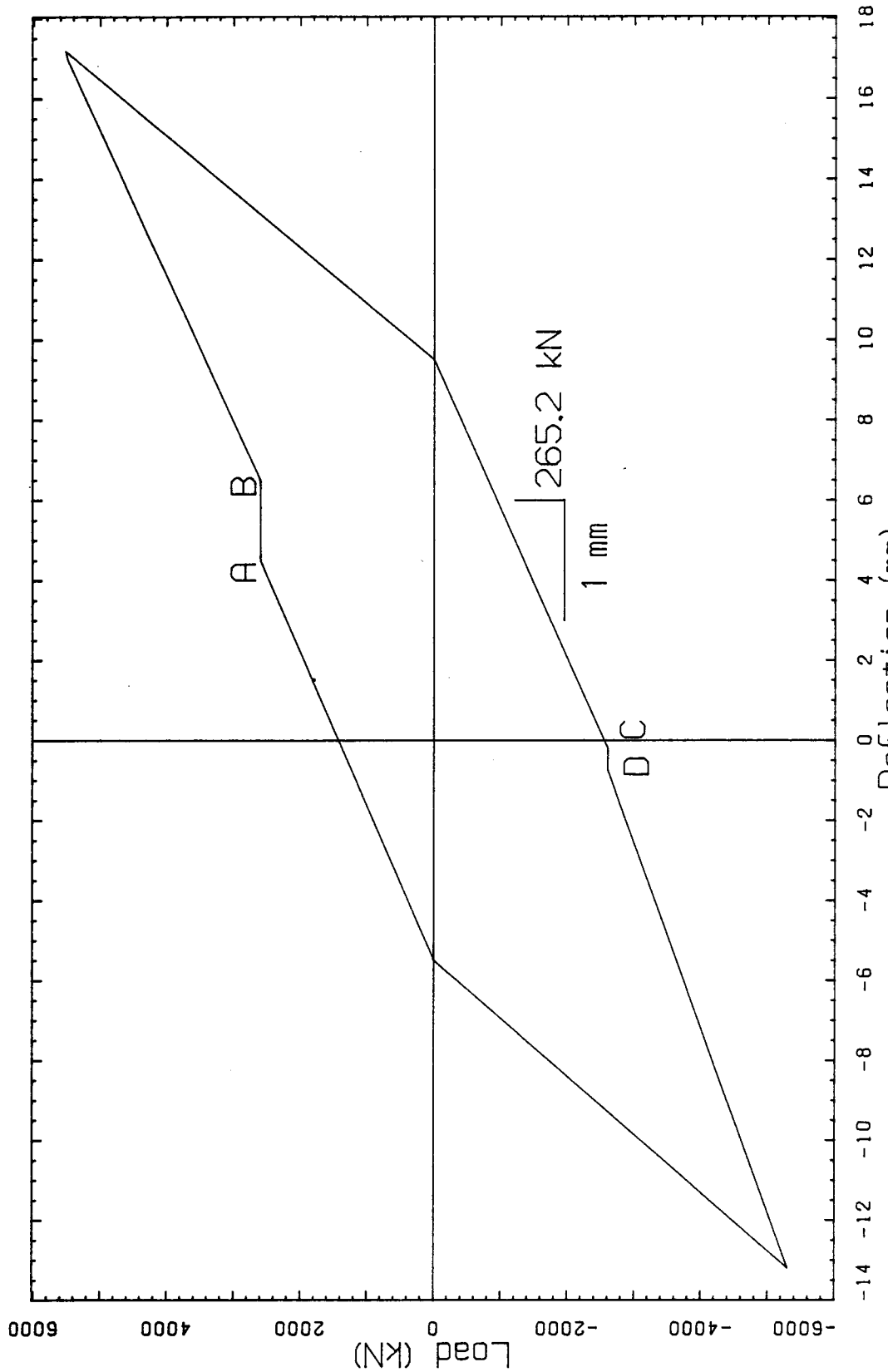


Figure 6.24 Theoretical Hysteresis Loop for a 5 mm Thick Panel and Fixed Joints

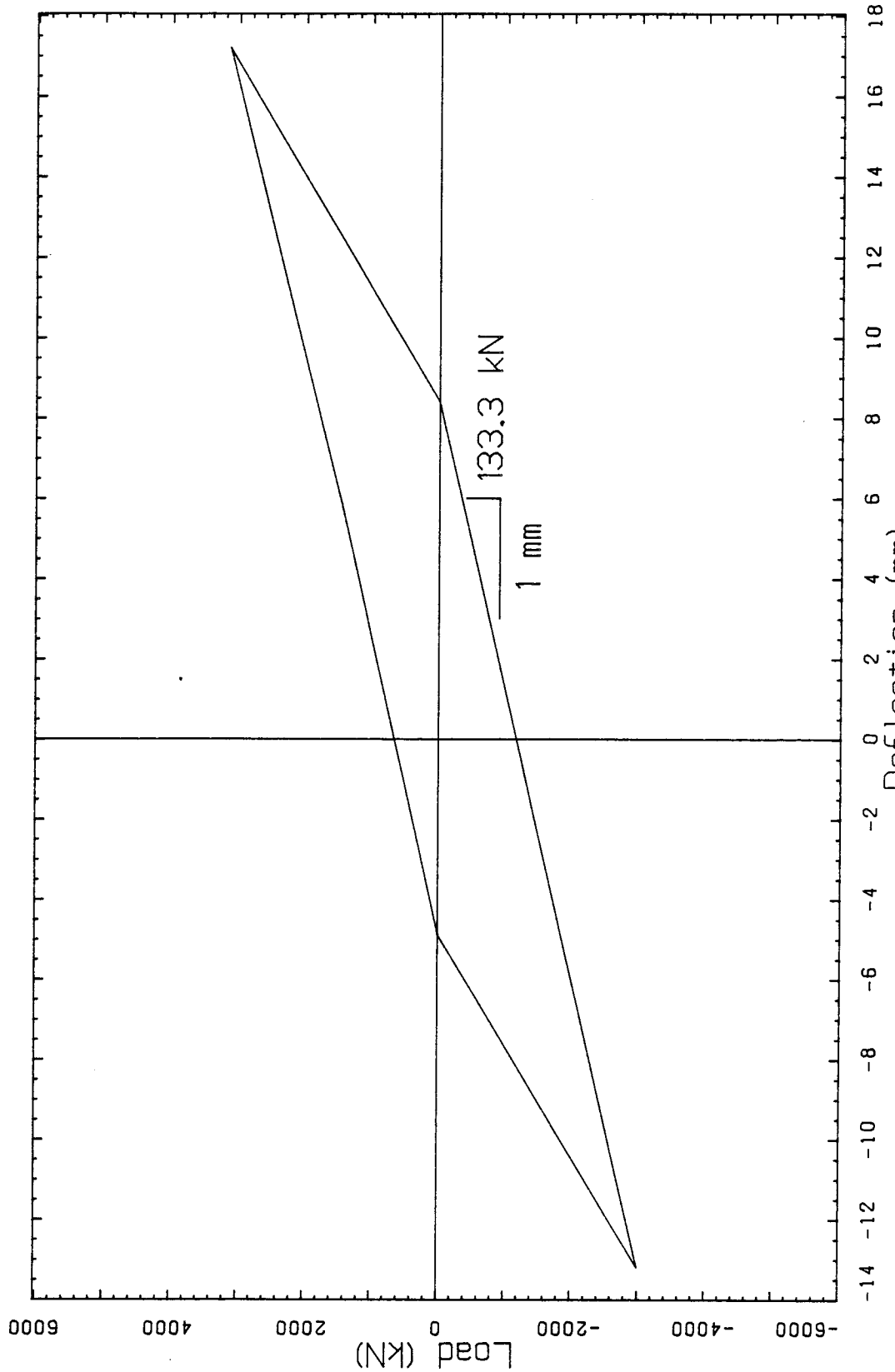


Figure 6.25 Theoretical Hysteresis Loop for a Panel 2.2 m by 2.2 m by 3.25 mm Thick

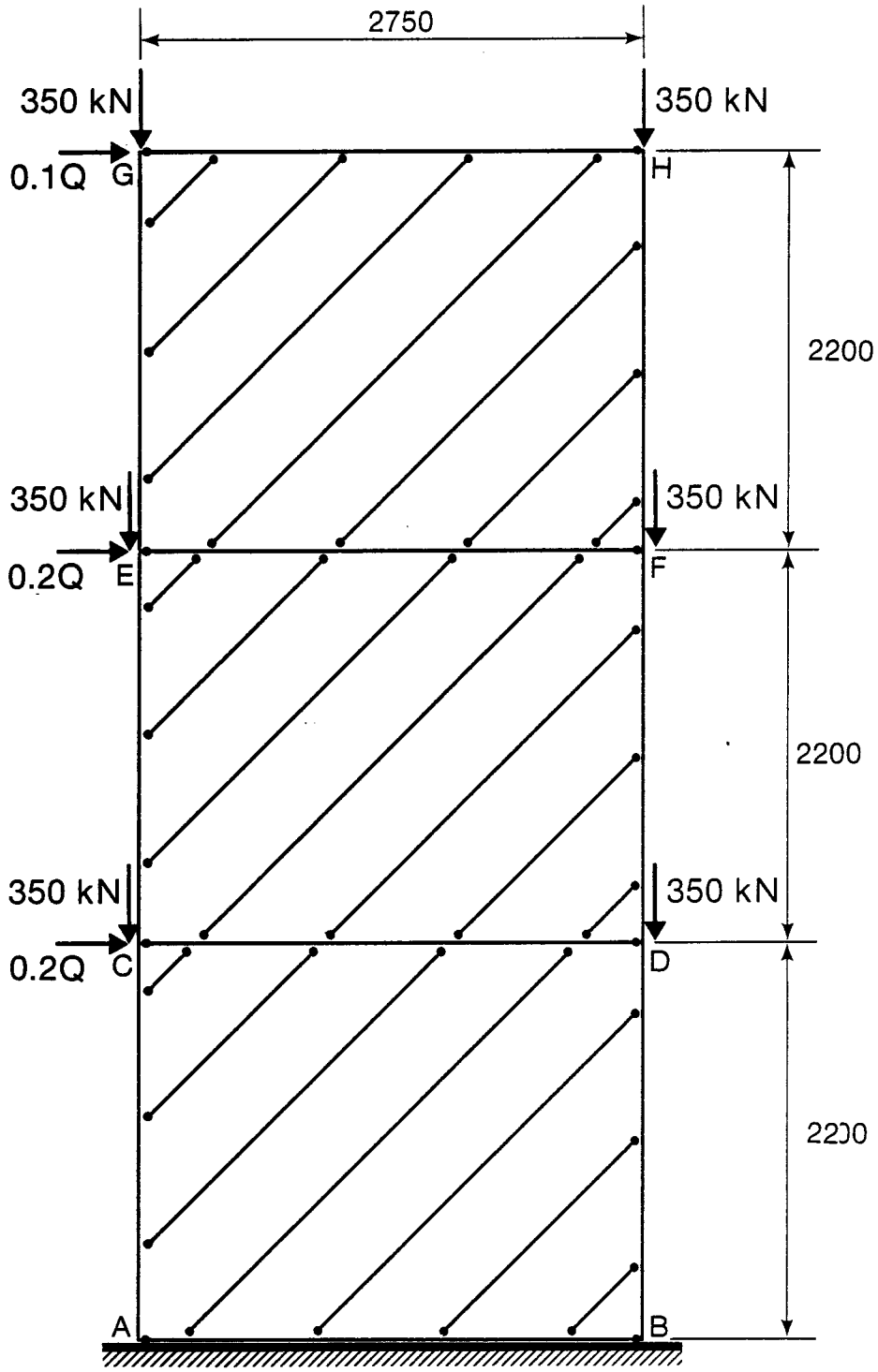


Figure 6.26 Example Three Storey Structure

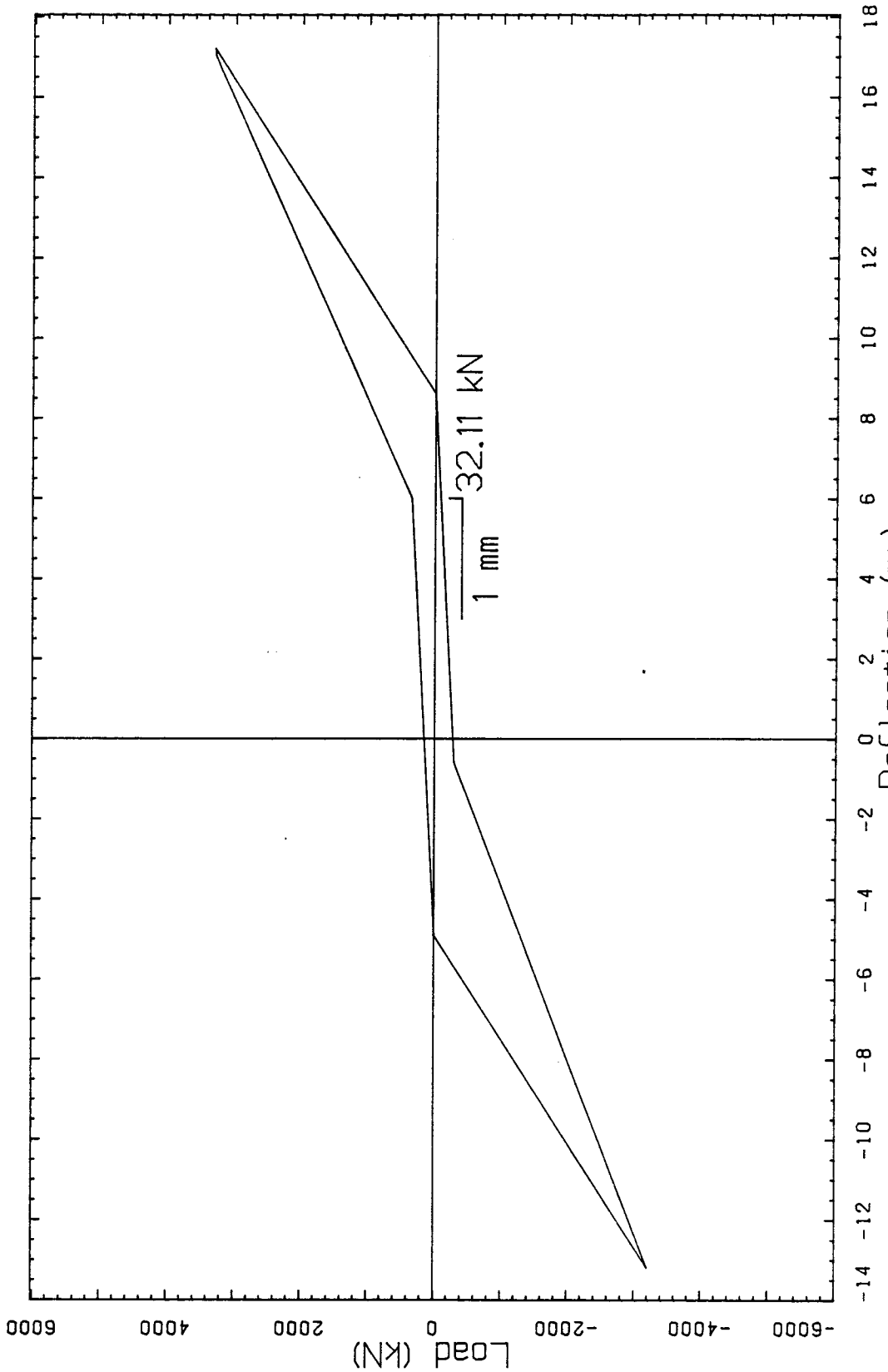


Figure 6.27 Theoretical Hysteresis Loop for the Lower Panel of a Three Storey Structure having Pinned Joints

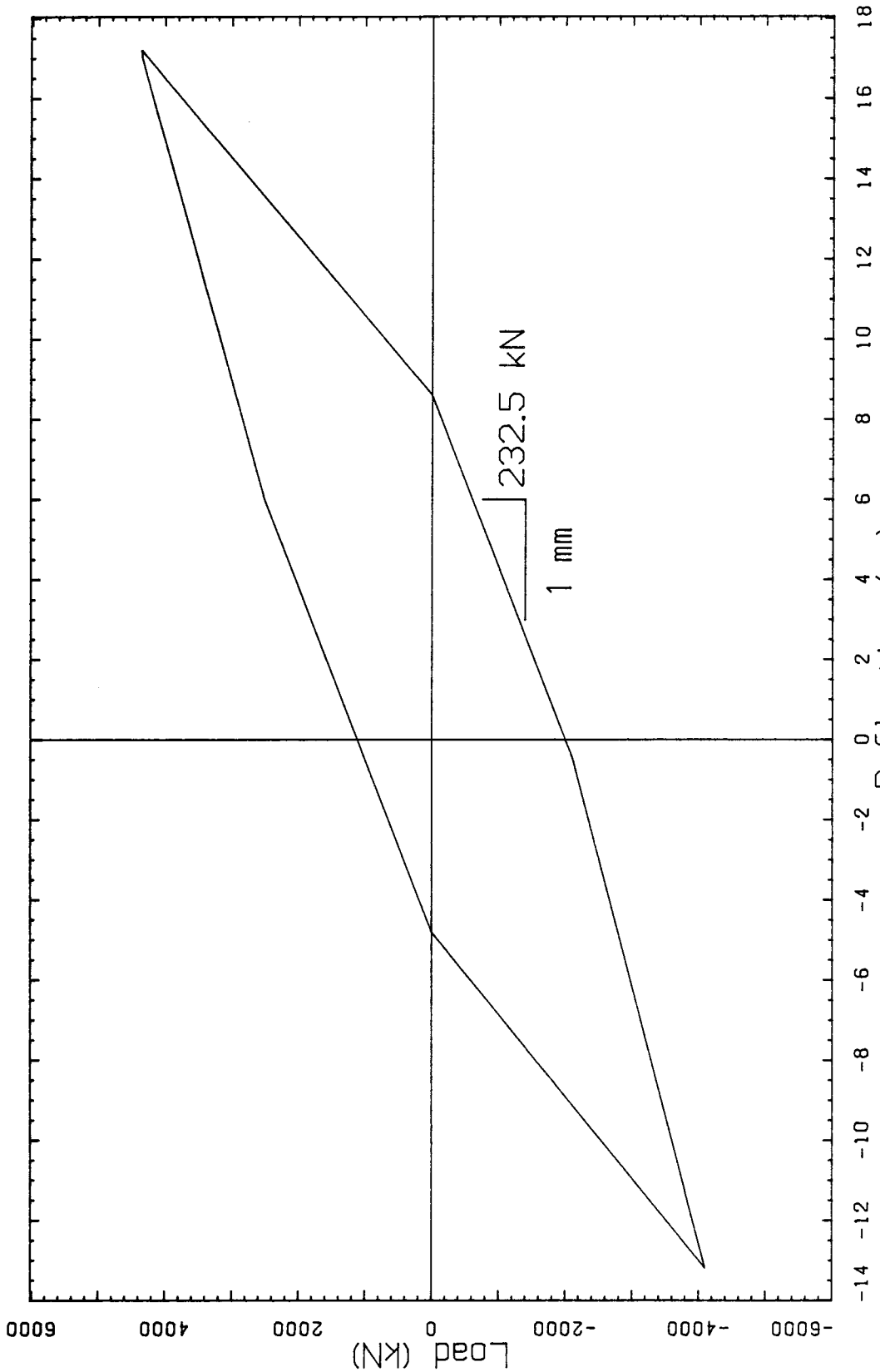


Figure 6.28 Theoretical Hysteresis Loop for the Lower Panel of a Three Storey Structure having Fixed Joints

# 7. SUMMARY, CONCLUSIONS, AND RECOMMENDATIONS

## 7.1 Summary

An experimental testing program was carried out on a nearly full scale unstiffened steel plate shear wall test specimen. The main objectives of the test were to examine the hysteresis behaviour of the specimen and to verify the analytical model for monotonic loading that had been proposed by Thorburn, et al (2). A symmetric specimen consisting of two adjacent panels with opposing tension fields was tested. The beams and columns were joined by bolted connections which were typical of those used commonly in building structures. The specimen was tested in a horizontal position in a configuration resembling a deep beam. The members corresponding to the columns in a vertical shear wall had a compressive preload applied to them by means of two prestressing rods per column. Thus, the axial force present in a prototype structure was simulated in the test specimen. The quasi-seismic loading was applied to the specimen at its midpoint and taken out at the reactions.

The shear wall specimen was subjected to 28 fully reversed loading cycles. During this phase, a maximum load of 4000 kN was applied and a maximum centreline deflection of 17 mm was reached. The hysteresis loops developed were S-shaped, but they were stable. The displacement ductility factor for the last hysteresis curve was between four (compression cycle) and seven (tension cycle). Because the

web plate had been installed in such a way that it was initially very taut and planar, the changes in the orientation of the tension field which occurred with each reversal of the applied load caused very audible pop-throughs to occur. The magnitude of these increased with an increase in the maximum cycle load. As load was increased, weld tearing was observed in several of the corners as a consequence of joint slip and joint rotation. The backing plates used to connect the fish plates at the corners initiated several tears in this region.

The hysteresis curve developed was generally comparable with those associated with conventional cross bracing used in steel frames or with conventional reinforced concrete shear walls. An analytical procedure for producing a theoretical prediction of the hysteresis curve was developed; it provides a good approximation of the behaviour of the unstiffened steel plate shear wall specimen tested.

After the cyclic loading phase was completed, the specimen was loaded monotonically to a maximum load of 6000 kN, the capacity of the testing machine but not the capacity of the specimen. The midpoint deflection exceeded 70 mm.

Strains in the boundary members and in the panels were continuously monitored at several locations during the test. These strains, and the member material properties determined by a series of ancillary tests, were used to calculate the internal forces at the gauged locations. Comparing these forces with those predicted by the inclined tension bar

model generally produced good agreement. The axial loads measured and those predicted produced very good correlation. The orientation of the tension field in the panels and the principal strains, calculated from strain measurements in the panels, were heavily influenced by the initial welding-induced strains. At higher load levels this influence had a lesser effect, with the measured orientation of the tension field in those gauge locations still operational being relatively close to the predicted value of 44.0 degrees.

A comparison of the load versus deflection curves developed using the analytical model with the envelope of the maximum loads versus their corresponding deflections, taken from the hysteresis curve, produced good agreement. The uncertain restraint provided by the bolted connections and the unknown magnitude of the welding induced strains required careful examination of all of the data collected before a representative load versus deflection curve could be produced.

## 7.2 Recommendations and Conclusions

The following recommendations and conclusions can be made from the results of the experimental study conducted on the behaviour of the unstiffened steel plate shear wall test specimen:

1. The inclined tension bar model, that is, the treatment of the buckled panel of an unstiffened shear wall panel

as equivalent to a series of inclined tension members, can be used with confidence to evaluate the strength and ultimate capacity of an unstiffened steel plate shear wall.

2. If the analytical model is developed on the assumption that bolted beam-to-column connections are pinned, a conservative estimate of the ultimate strength and stiffness of an unstiffened steel plate shear wall panel will result.
3. The hysteresis behaviour of an unstiffened steel plate shear wall panel is comparable to the hysteresis behaviour displayed by conventional steel cross bracing or by conventional concrete shear walls. All of these structural systems display an S-shaped, degenerating pinched loop behaviour.
4. The hysteresis behaviour of an unstiffened steel plate shear wall can be predicted with reasonable accuracy by the analytical method described herein.
5. The eccentricity of the fish plate with respect to the centre of the boundary members had no noticeable affect on the performance of the shear wall panels.
6. The connection of the orthogonal fish plates together in panel corners should be done using the minimum thickness of backing plate. This will reduce the possibility of the backing plates shearing the fish plates. Connecting these backing plates to the boundary members or to the fish plates by fillet welds could also prevent the

shearing observed in the test.

7. Designing the panel welds between the panel and the boundary members to carry the ultimate tensile capacity of the plate material appears to produce a very sound structure that can withstand many loading cycles without deterioration.
8. Some effort should be made to minimize welding induced strains in shear wall panels. This could be accommodated by permitting the panels to be installed with an initial out-of-planeness, thereby allowing the welding shrinkage to straighten the panels. It is possible that standard construction tolerances will result in a sufficient amount of initial out-of-straightness to accommodate this welding shrinkage.

### 7.3 Recommendations for Future Testing

The results of one test cannot be interpreted to apply for all cases. Even though the configuration of the specimen used in this study is considered adequate, future research examining other shear wall configurations and details could be done so that the design of the unstiffened steel plate shear wall can be optimized. This research could include:

1. Additional tests examining the hysteresis behaviour of unstiffened steel plate shear walls consisting of different aspect ratios and different member connections. One possible alternative configuration could consist of a multi-storey structure tested in a

cantilever position utilizing full moment resisting connections. This test could examine the possible improved hysteresis behaviour provided by the moment resisting connections in addition to an opportunity to verify the inclined tension bar model and the proposed theoretical hysteresis curve on an alternate configuration. Also, if axial loads were applied to the structure, it would be desirable if they could be applied continuously to failure, since the influence of the axial load acting through the lateral displacement ($P-\delta$) is greatest at the point of maximum lateral deflection.

2. The examination of the effect of joining two unstiffened steel plate shear walls with link beams. These beams would act as the prime energy absorbing units in the structure while the shear walls themselves behaved more or less elastically.
3. The examination of the influence of the initial out-of-planeness of shear wall panels on the magnitude of the welding induced stresses. This could be incorporated in the above mentioned multi-storey test.

## REFERENCES


1. Wagner, H.,"Flat Sheet Metal Girders with Very Thin Webs. Part 1 - General Theories and Assumptions," *National Advisory Commitee for Aeronautics*, Technical Memo No. 604, Washington, D.C., 1931.

2. Thorburn, L.J., Kulak, G.L., and Montgomery, C.J., Analysis and Design of Steel Shearwall Systems, Structural Engineering Report No.107, Department of Civil Engineering University of Alberta, Edmonton, Alberta, May 1983.

3. Timler, P.A., and Kulak, G.L., Experimental Study of Steel Plate Shearwalls, Structural Engineering Report No.114, University of Alberta, Edmonton, Alberta, Nov. 1983.

4. Takahashi, Y., Takeda, T., Takemoto, Y., and Takagi, M., " Experimental Study on Thin Steel Shearwalls and Particular Steel Bracings Under Alternative Horizontal Load", Preliminary Report, IABSE Symposium on Resistance and Ultimate Deformability of Structures Acted on by Well-Defined Repeated Loads, Lisbon, Portugal, 1973.

5. Mimura, H., and Akiyana, H.," Load Deflection Relationship on Earthquake Resistant Steel Shearwalls Developed Diagonal Tension Field",(English Translation) Private correspondence with the Canadian Institute of Steel Construction, Jan. 1980.

6. Popov, E.P., "Seismic Behavior of Structural Subassemblages", *Journal of the Structural Division ASCE*, V.106, No. ST7, July 1980.

7. Oesterle, R.G., Fiorata, A.E., Aristizabal-Ochoa, J.D., and Corley, W.G., Hysteretic Response of Reinforced Concrete Structural Walls, PCA Research and Development Construction Laboratories, Skokie, Illinois, June 1978.

8. Park, R., and Paulay, T., Reinforced Concrete Structures, John Wiley & Sons, New York, 1975.

9. Kuhn, P., Peterson, J.P., and Levin, L.R., "A Summary of Diagonal Tension, Part 1 - Methods of Analysis," *National Advisory Commitee for Aeronautics*, Technical Note 2662, Washington, D.C., 1952.

10. "A Guide to the Structure of B-Class Japanese Buildings", (English Translation) Private correspondence with the Canadian Institute of Steel Construction, Jan. 1980.

11. Troy, R.G., and Richard, R.M.,"Steel Plate Shearwalls Resist Lateral Load, Cut Costs", *Civil Engineering*, ASCE, Vol. 49, Feb. 1979.

12. Baldelli, J.A.,"Shearwalls for Existing Buildings", *Engineering Journal*, AISC, Vol. 20, 2nd Quarter 1983.

13. CSA CAN3 - S16.1 - M84, Steel Structures for Buildings - Limit States Design, Canadian Standards Association, Rexdale, Ontario, 1984.

14. CSA W59 - 1982 Welded Steel Contruction, Canadian Standards Association, Rexdale, Ontario, 1982.

15. ASTM A370-77 Part (1), Standard Methods and Definitions for Mechanical Testing of Steel Products, American Society for Testing and Materials, Vol. 03.01, Philadelphia, Penn., 1977.

16. ASTM E132-61 Part (10), Standard Test Method for Poisson's Ratio at Room Temperature, American Society for Testing and Materials, Vol. 03.01, Philadelphia Penn., 1961.

17. Johnston, B.G., ed.,Guide to Stability Design Critera for Metal Structures, 3rd ed., John Wiley and Sons, New York, N.Y., 1976.

18. Kennedy, S.J., and MacGregor, J.G., End Connection Effects on the Strength of Concrete Filled HSS Beam Columns, Structural Engineering Report No.115, Department of Civil Engineering, University of Alberta, Edmonton, Alberta, April 1984.

19. Derecho, A.T., Iqbal, M., Fintel, M., and Corley, W.G., Loading History for Use in Quasi-Static Simulated Earthquake Loading Test, PCA Research and Development Construction Laboratories, Skokie, Illinois, June 1978.

20. Malley, J.O., and Popov, E.P., Design Considerations for Eccentrically Braced Frames, *Earthquake Engineering Report*, University of California-Berkley, No. UCB/EERC-83/24, Nov. 1983.

*RECENT STRUCTURAL ENGINEERING REPORTS*

Department of Civil Engineering

University of Alberta

114. *Experimental Study of Steel Plate Shear Walls* by P.A. Timler and G.L. Kulak, November 1983.

115. *End Connection Effects on the Strength of Concrete Filled HSS Columns* by S.J. Kennedy and J.G. MacGregor, April 1984.

116. *Reinforced Concrete Column Design Program* by C-K. Leung and S.H. Simmonds, April 1984.

117. *Deflections of Two-way Slabs under Construction Loading* by C. Graham and A. Scanlon, August 1984.

118. *Effective Lengths of Laterally Unsupported Steel Beams* by C.D. Schmitke and D.J.L. Kennedy, October 1984.

119. *Flexural and Shear Behaviour of Large Diameter Steel Tubes* by R.W. Bailey and G.L. Kulak, November 1984.

120. *Concrete Masonry Prism Response due to Loads Parallel and Perpendicular to Bed Joints* by R. Lee, J. Longworth and J. Warwaruk.

121. *Standardized Flexible End Plate Connections for Steel Beams* by G.J. Kriviak and D.J.L. Kennedy, December 1984.

122. *The Effects of Restrained Shrinkage on Concrete Slabs* by K.S.S. Tam and A. Scanlon, December 1984.

123. *Prestressed Concrete Beams with Large Rectangular Web Openings* by T. do M.J. Alves and A. Scanlon, December 1984.

124. *Tests on Eccentrically Loaded Fillet Welds* by G.L. Kulak and P.A. Timler, December 1984.

125. *Analysis of Field Measured Deflections Scotia Place Office Tower* by A. Scanlon and E. Ho, December 1984.

126. *Ultimate Behaviour of Continuous Deep Reinforced Concrete Beams* by D.R. Ricketts and J.G. MacGregor, January 1985.

127. *The Interaction of Masonry Veneer and Steel Studs in Curtain Wall Construction* by W.M. McGinley, J. Warwaruk, J. Longworth and M. Hatzinikolas, May 1985.

128. *Evaluation of Existing Bridge Structure by Nondestructive Test Methods* by L. Mikhailovsky and A. Scanlon, May 1985.

129. *Finite Element Modelling of Buried Structures* by D.K. Playdon and S.H. Simmonds, October 1985.

130. *Behaviour and Ultimate Strength of Transversely Loaded Continuous Steel Plates* by K.P. Ratzlaff and D.J.L. Kennedy, November 1985.

131. *Inelastic Lateral Buckling of Steel Beam-Columns* by P.E. Cuk, M.A. Bradford and N.S. Trahair, December 1985.

132. *Design Strengths of Steel Beam-Columns* by N.S. Trahair, December 1985.

133. *Behaviour of Fillet Welds as a Function of the Angle of Loading* by G.S. Miazga and D.J.L. Kennedy, March 1986.

134. *Inelastic Seismic Response of Precast Concrete Large Panel Coupled Shear Wall Systems* by M.R. Kianoush and A. Scanlon, March 1986.

135. *Finite Element Prediction of Bin Loads* by A.H. Askari and A.E. Elwi, June 1986.

136. *Shear Behavior of Large Diameter Fabricated Steel Cylinders* by J. Mok and A.E. Elwi, June 1986.

137. *Local Buckling Rules for Structural Steel Members* by S. Bild and G.L. Kulak, May 1986.

138. *Finite Element Prediction of Reinforced Concrete Behavior* by S. Balakrishnan and D.W. Murray, July 1986.

139. *Behavior and Strength of Masonry Wall/Slab Joints* by T.M. Olatunji and J. Warwaruk, July 1986.

140. *Bayesian Analysis of In-Situ Test Data for Estimating the Compressive Strength of Concrete in Existing Structures* by G.J. Kriviak and A. Scanlon, July 1986.

141. *Shear-Moment Transfer in Slab-Column Connections* by S.D.B. Alexander and S.H. Simmonds, July 1986.

142. *Minimum Thickness Requirements for Deflection Control of Two-Way Slab Systems* by D.P. Thompson and A. Scanlon, November 1986.

143. *Shrinkage and Flexural Tests of Two Full-Scale Composite Trusses* by A. Brattland and D.J.L. Kennedy, December 1986.

144. *Combined Flexure and Torsion of I-Shaped Steel Beams* by R.G. Driver and D.J.L. Kennedy, March 1987.

145. *Cyclic and Static Behaviour of Thin Panel Steel Plate Shear Walls* by E.W. Tromposch and G.L. Kulak, April 1987.